Raman and X-Ray Fluorescence Spectroscopy Data Fusion for Identification of Pigments in Works of Art




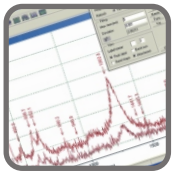
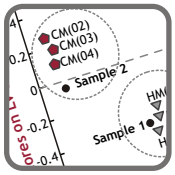

Doctoral Thesis
Pablo M. Ramos

Tarragona, May 2006

Raman and X-Ray Fluorescence Spectroscopy Data Fusion for Identification of Pigments in Works of Art

Doctoral thesis

Raman and X-Ray Fluorescence Spectroscopy Data Fusion for Identification of Pigments in Works of Art

Thesis submitted by Pablo M. Ramos to obtain the degree of Doctor from the Universitat Rovira i Virgili.

Tarragona, May 2006

UNIVERSITAT ROVIRA I VIRGILI

UNIVERSITAT ROVIRA I VIRGILI

DEPARTAMENT DE QUÍMICA ANALÍTICA
I QUÍMICA ORGÀNICA

Dr. Itziar Ruisánchez Capelástegui, Associate professor of the Department of Analytical Chemistry and Organic Chemistry at the Universitat Rovira i Virgili,

CERTIFY: That the Doctoral thesis entitled: ***"Raman and X- Ray Fluorescence Spectroscopy Data Fusion for Identification of Pigments in Works of Art"***, submitted by **Pablo Manuel Ramos** to obtain the degree of Doctor from the Universitat Rovira i Virgili, has been carried under my supervision in the Analytical Chemistry Area of the Department of Analytical Chemistry and Organic Chemistry at the Universitat Rovira i Virgili, and all the results presented in this thesis were obtained in experiments conducted by the above mentioned student.

Tarragona, May 2006

Dr. Itziar Ruisánchez Capelástegui

Science and art belong to the whole world, and before them vanish the barriers of nationality.

Johann Wolfgang Von Goethe

To my beloved Valeria

AGRADECIMIENTOS

Han pasado ya casi cinco años desde que mi amigo Pancho me recomendaba para una beca de doctorado de la Universidad Rovira i Virgili de Tarragona. En primer lugar quiero agradecerle a él, y también a Nano, Lili y Pablo, por alentarme a vivir esta experiencia. Sin su estímulo este proyecto no hubiera sido posible.

Así, con curiosidad y entusiasmo aceptaba el ofrecimiento de hacer un doctorado en Europa. Hoy, al finalizar esta etapa, revivo todas aquellas sensaciones con la incertidumbre que conllevan los nuevos desafíos pero con un entusiasmo aún mayor por la investigación científica. Al profesor Xavier Rius le debo la oportunidad y el espacio para concretar mi sueño, y le agradezco infinitamente por estos cuatro valiosos años de formación como investigador, por contagiarme su motivación por la investigación y por la calidez con que me recibieron él y todo su equipo.

Agradezco de manera especial a mi directora, la profesora Itziar Ruisánchez, por haberme guiado en este proceso, por su respaldo constante y por su disposición a ayudarme en todo momento, brindándome total libertad para desarrollar mis ideas. Le agradezco también el afecto y la confianza depositada durante estos cuatro años.

A todos los integrantes del Proyecto PRAXIS en cuyo marco se desarrolló esta tesis. A su director, el profesor Koen Janssens de la Universidad de Antwerp, por haberme permitido realizar una estancia en su laboratorio y muy especialmente al Dr. Konstantinos Andrikopoulos del Ormylia Arts Diagnostic Centre por sus valiosas enseñanzas, sus consejos y por su amistad a lo largo de estos años.

No puedo dejar de mencionar a Joan, Santi, quienes me ayudaron a dar mis primeros pasos en la quimiometría, mostrando entusiasmo por mi trabajo y una constante disposición para aclarar mis dudas.

Hago también extensivo este agradecimiento a todo el Grupo de Quimiometría, Cualimetria y Nanosensores de la URV. En particular a Marisol, Pilar, Jordi y Alicia por su apoyo, a Ricard por continuo estímulo a mi trabajo, a Enric por su asesoramiento en el uso del software Matlab, a Esther y Alberto por las risas en el laboratorio y a Mariano, Martita e Ignacio por los mates compartidos.

Agradezco a Bella y a Celia por su paciencia y dedicación en la corrección lingüística.

Mucho (todo) debo a mi esposa Valeria por apoyarme y acompañarme en este proyecto. Le agradezco su entusiasmo en mi trabajo, su profesionalismo inspirador en el área del diseño gráfico, su colaboración en todos los gráficos presentados y el diseño de esta tesis.

Les agradezco a mis padres por la educación que recibí y por haber fomentado mi creatividad y a mis hermanos Juan y José su fraternal compañía.

Finalmente agradezco a mis amigos, particularmente a Gabbos por su continua inspiración y por compartir un estilo de vida.

A todas aquellas personas que de un modo u otro colaboraron e influyeron en mi trabajo, gracias. Todos los errores son míos.

ACKNOWLEDGMENTS

Almost five years have already gone by since my friend Pancho recommended me for a PhD fellowship at the Universitat Rovira i Virgili in Tarragona. That's the reason why I want to thank him first, together with Nano, Lili and Pablo, who encouraged me to live this experience. This project wouldn't have been possible without their support.

It was in that mood, full of curiosity and enthusiasm, that I accepted the offer to do the doctorate studies in Europe. Today, when I'm finishing this stage, I experience once more all those feelings and sensations with the uncertainty that new challenges bring about but with an even greater enthusiasm for scientific research. I owe Professor Xavier Rius the opportunity to make my dream come true and I'm deeply grateful to him for these valuable years of training as a researcher, for his sharing with me his enthusiasm for research and for the warmth he and his team showed on my arrival.

I must also thank my thesis director, Professor Itziar Ruisánchez, especially, because she guided me through this process, she supported me constantly and she was always there to help me out while giving me the chance to develop my own ideas at the same time. I also want to thank her for her affection and for the confidence she showed in me over these four years.

I feel I must also mention Joan and Santi, who helped me take my first steps in chemometrics, who were very enthusiastic about my job and who were always there to clarify my doubts.

My thanks, too, to all the members of the PRAXIS Project, who provided the framework for my thesis: to its head, Professor Koen Janssens from the University of Antwerp, for allowing me a stay at his lab, and my special thanks to Dr. Konstantinos Andrikopoulos from Ormylia Arts Diagnostic Centre for his valuable teachings, his advice and his friendship throughout these years.

I also want to thank the whole Group of Chemometrics, Qualimetrics and Nanosensors from the URV. Particularly to Marisol, Pilar, Jordi and Alicia for their support, to Ricard for his continuos encouragement to my work, to Enric for his advice on the use of the Matlab software, to Alberto and Esther for their friendship and pleasant company at the lab and to Mariano, Martita and Ignacio for all those shared *mates*.

I appreciate Bella's and Celia's patience and dedication when editing the language of my work.

A lot –everything, in fact- I owe to my wife, Valeria, for her support to my project. She was especially enthusiastic about my work, her professionalism in the area of graphic design was truly inspiring, she collaborated with every graph presented and with the design of my thesis.

ACKNOWLEDGMENTS

I'm grateful to my parents for the education possibilities they offered me and for fostering my creativity, and I'm grateful to my brothers, Juan and José, for their fraternal company.

Finally, I want to say thank you to my friends, particularly to *Gabbos*, for their continuous inspiration and for sharing their lifestyle with me.

Thank you, too, to all those people who collaborated and influenced my work in one way or another. All the mistakes are my responsibility.

TABLE OF CONTENTS

TABLE OF CONTENTS

SCOPE OF THIS THESIS

SCOPE OF THIS THESIS

Since the mid 1980s, Raman and X-ray fluorescence spectroscopy have become instrumental techniques that can be easily and successfully applied to chemical analysis. In this respect, scientific studies of works of art and the materials used in their creation are one of the fields that have received great impulse.

Several reasons for the spectroscopic investigation of antiquities and art objects can be pointed out. One of them is the interest in the materials and techniques in use during a certain period or region. This knowledge may be utilized for roughly dating the art object (retrieving pigments with a known date of invention may indicate that the artifact dates from a more recent period). Another reason is that this analysis is a useful source of information during a restoration or conservation treatment, and signs of a previous restoration, retouching or even forgeries can be found.

At the beginning of this century investigation in cultural heritage became an important research field that posed great scientific interest, requiring unprecedented interdisciplinary knowledge of a wide spectrum of areas such as history, archaeology, physics, chemistry, engineering, chemometrics and many other disciplines. On the other hand, improvements in the instrumental techniques used have been the goal of many important studies. Even more, in this decade the investigation has been focalized on the development of a new generation of instruments which allows the combination of complementary analytical techniques along with the advantage of portable instrumentation. Both improvements permit a robust and non-destructive chemical analysis of works of art which are difficult or impossible to study in a laboratory (highly valuable masterpieces, large paintings, and wall paintings).

Chemometrics methods are the necessary complement to these instrumental improvements. In order to maximize the robustness of these instruments, automatic and robust data processing tools are needed to obtain the maximum possible information from a work of art.

This doctoral thesis presents a framework to perform data-fusion systems for classification analysis of pigments investigated in the field of cultural heritage. These systems were developed and evaluated within a European Community research project, the main objective of which was to develop a portable micro Raman and micro X-ray fluorescence instrument (PRAXIS).

The general aim of this doctoral thesis is to study different strategies for the implementation of Raman-XRF data-fusion systems, in order to improve classification analysis of pigments investigated in the field of cultural heritage. This study takes into account the nature of the different interferences usually encountered in these types of signals and its elimination by developing dedicated algorithms. Moreover, this study evaluates automation in classification analysis by developing inference systems.

In order to reach that global aim these particular objectives are defined:

1) To study the nature of stochastic events and signal interferences present in Raman and XRF spectroscopy in order to enable the implementation of chemometrics techniques for classification. The methodology used is wavelet transform.
2) To establish the capabilities of a fuzzy logic system for automatic pigment identification.
3) To review the current state-of-art of data-fusion in analytical chemistry and to establish actual data-fusion methodologies onto a Raman-XRF fusion system.
4) To improve data-fusion methodologies by dual-domain analysis achieved by wavelet transform.

Structure

The thesis has been structured in different chapters, each one containing the following information:

- **Chapter 1** is a theoretical chapter; the first part gives an overview of the basic concepts and latest advances in the fields of micro-Raman and micro-X ray fluorescence spectroscopy. The characteristics of a new instrument which combines both techniques are presented along with the improvements achieved in that area. In the second part, the background of chemometrics techniques used in this work is presented.
- **Chapter 2** introduces the framework for the study of ancient pigments. It describes the nature of samples analyzed and gives an overview of the most important pigments used in the creation of works of art throughout the years. Finally, the instruments used in this doctoral thesis for Raman and XRF analysis are described.
- **Chapter 3** deals with the data pre-treatment needed before applying chemometric techniques, both for classification and data-fusion. In that respect, the first part focuses on the principles of wavelet transform as a tool to eliminate signal interferences. This chapter includes a paper in which the development of an innovative method to eliminate noise and background signals from Raman

spectra simultaneously is presented. It has been successfully applied for Raman spectra of ancient pigments.

- **Chapter 4** presents a study of automatic identification of pigments by means of soft computing solutions such as fuzzy logic. A published paper is presented in which fuzzy logic is used to perform an automatic system for pigment identification. This study is extended to a fusion model and X-ray fluorescence analysis data is incorporated in the developed identification system. The ability of fuzzy logic to process imprecise information is described in the last part of this chapter.
- **Chapter 5** deals with three data-fusion architectures and their analysis by means of hard computing solutions as Principal components analysis (PCA) and Partial least squares – discriminant analysis (PLS-DA). The models are implemented for the classification of a set of ancient pigments from Byzantine iconography. Benefits and drawbacks of each method are pointed out and presented in a paper.
- **Chapter 6** incorporates a new innovative strategy for data-fusion. The fusion of data in the wavelet domain is discussed and two approaches are presented for Raman and X-ray fluorescence data-fusion: Mid-level and High level dual domain data-fusion. Both are used and successfully applied for the automatic identification of pigments in classification problems with different levels of difficulty. Two papers are included in which both methods are used for the classification of ancient pigments.
- **Chapter 7** presents a review of the state of the art regarding data-fusion. The different steps necessary to achieve a proper data fusion are discussed.
- Finally, **chapter 8** presents the conclusions of the thesis and suggests some possible issues for future research.

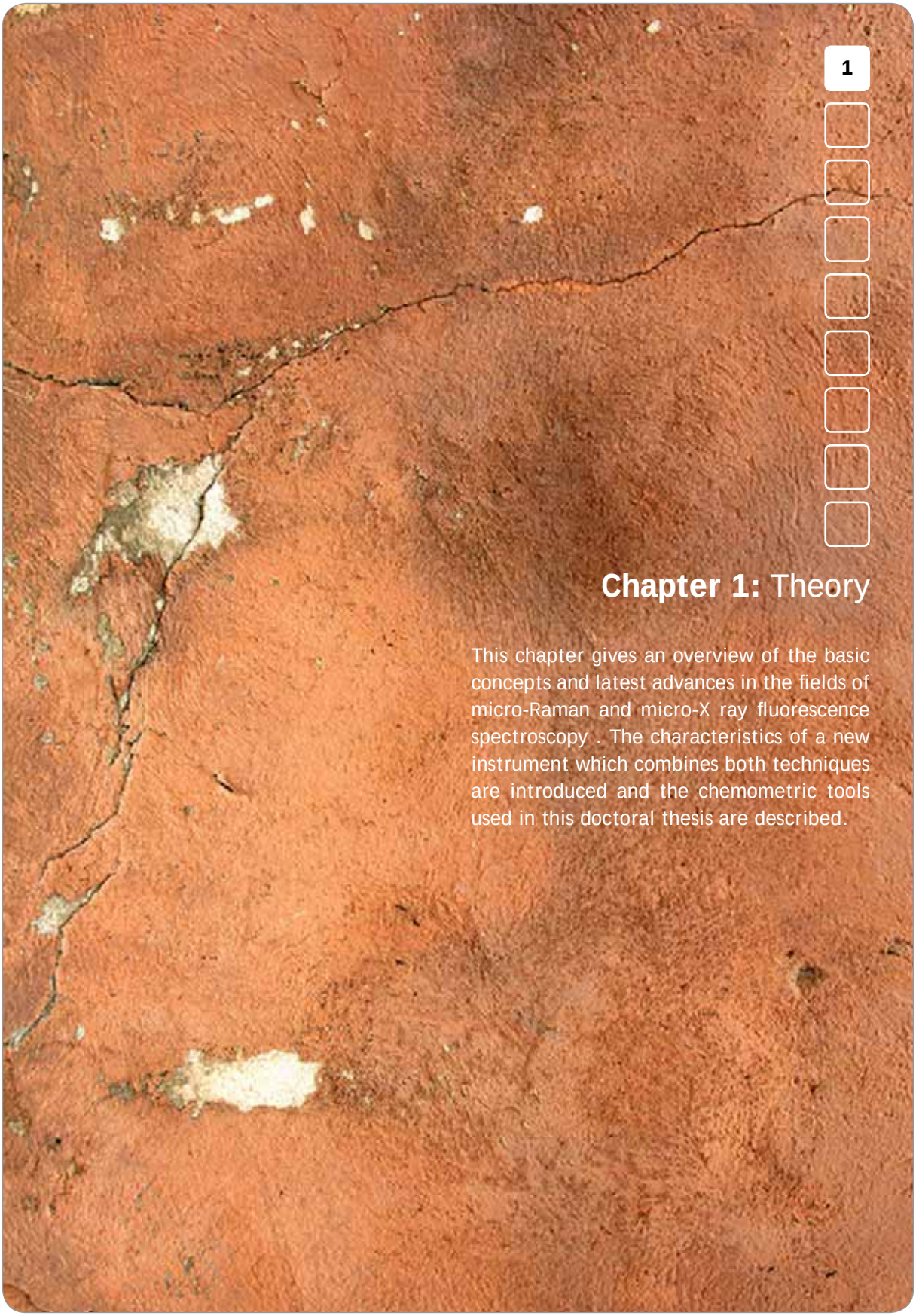

1

Chapter 1: Theory

This chapter gives an overview of the basic concepts and latest advances in the fields of micro-Raman and micro-X ray fluorescence spectroscopy . The characteristics of a new instrument which combines both techniques are introduced and the chemometric tools used in this doctoral thesis are described.

1.1. RAMAN SPECTROSCOPY

1.1.1. Introduction

Raman spectroscopy is a highly specific non-destructive technique for molecular analysis. It can be used for routine qualitative and quantitative measurements of both inorganic and organic materials. The particular advantage of Raman spectroscopy is the possibility of measuring gases, vapors, aerosols, liquids and solids. The measurement conditions can be room temperature, cryogenic and high-temperature observations, including in situ identification and quantification of combustion products in flames and plasmas. In the last few years, this technique has been recognized as a possible method for in situ planetary analysis. Raman spectroscopy is one of the few spectroscopic techniques available for both laboratory and remote measurements, the latter made at a distance from the sample by using optical fibers.

Nowadays, Raman spectroscopy is becoming increasingly important as an analytical tool in conservation science. A growing number of renowned museums own a Raman instrument and some conservation scientists specialize in different applications of this technique.

Raman spectroscopy treats the measurement of radiation scattered from a sample. Raman spectra are usually given as wavenumber (cm^{-1}) shifts from the incident radiation. These shifts in wavenumbers are absolute energy differences between eigenstates of the molecule. Raman spectroscopy probes vibrational transitions indirectly by light scattering. The Raman shifts have the same energy range as the infrared absorptions, and in many cases the same absorptions are

observed. Thus Raman scattering can also be used for qualitative identification of organic compounds using group frequencies and scatter intensities. The selection rules for Raman scattering and infrared spectroscopy are different but the chemical information is similar. In a quantum mechanical view of scattering the incident electromagnetic wave is treated as a perturbation of the eigenstates of the molecule. The perturbation due to the incident radiation produces a time-dependent virtual state, as shown in Figure 1. When the initial and final states are the same, the effect of the perturbation produces Rayleigh scatter and this type of interaction is called inelastic scatter. Raman scatter, which is a result of a transition between eigenstates $\left| m \right\rangle \rightarrow \left| n \right\rangle$, is classified as elastic scatter. A Stoke scatter ν_S is a result of a net energy gain by the molecule, whereas in the Anti-Stokes process ν_A the scatter carries away the excess of energy lost by the molecule.

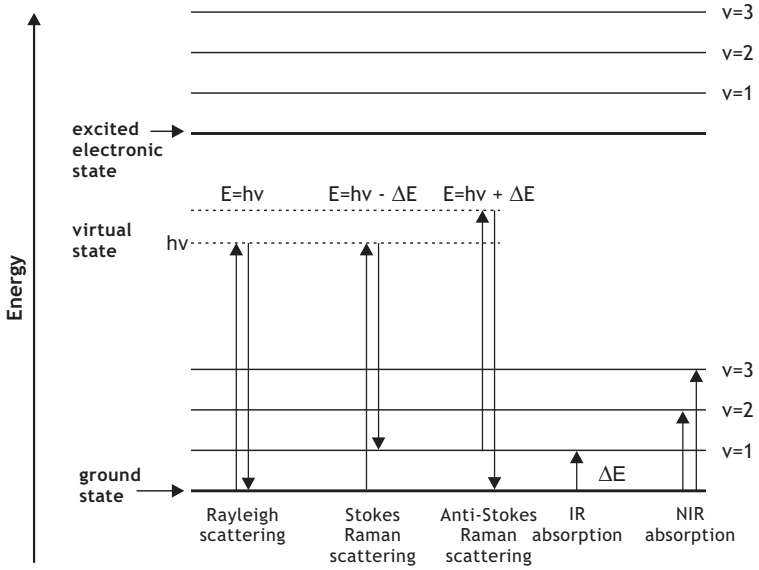

Figure 1.1. Energy level diagram used to illustrate the Raman Scattering process.

The basic types of Raman instruments encountered are dispersive and non-dispersive Raman spectrometers. The dispersive system separates wavelengths spatially, to be scanned across a single detector or monitored by many parallel detectors. The non-dispersive systems do not separate different wavelengths spatially but usually modulate them so that each wavelength has a characteristic modulation frequency. The composite modulated signal is then monitored by a single detector and demodulated by a Fourier transform. While the non-dispersive systems have achieved excellent frequency precision and are better for fluorescence avoidance, the dispersive systems have the advantages of higher sensitiveness and better signal to noise ratio. However the major advantage is the lack of moving parts in the detection components of the system. These properties along with fiber

optics sampling makes dispersive systems ideally suited for in situ measurements and today portable Raman instruments are mainly of the dispersive type.

This work does not attempt to treat Raman theory in depth. Several excellent books and monographs explain these topics in much more detail [1, 2]. Instead, we will focus on the latest developments in instrumentation, especially those concerning micro-Raman spectroscopy.

1.1.2. Instrumental considerations: technological advances

Charged couple device detectors

Charge coupled device (CCD) detectors are part of the renaissance of Raman spectroscopy in 1986, and have replaced nearly all other detector configurations in dispersive Raman spectrometers used for chemical analysis. CCDs are based on storage and manipulation of electrons and holes in a photosensitive semiconductor, usually silicon. The CCD surface is patterned with an array of electrodes; the basic event of importance to photodetection is the generation of an electron/hole pair in silicon by a photon of sufficient energy, each element forming an individual detector element called pixel. Photons in the 200 to 1100 nm range generate photoelectrons in the silicon with a probability that varies with the wavelength and determines the quantum efficiency curve. CCDs offer many advantages such as high sensitivity, low noise with improved signal to noise levels and multichannel acquisition. The basic specification of CCDs is the number and size of pixels in the two dimensional photoactive area. A common format is 256 x 1024 square pixels with 25 μm on each side. A term of importance in CCD detectors is the dark current, which is the spontaneous generation of electron/hole pairs unrelated to incident light intensity. This process is exponentially dependent with the temperature and CCDs must be cooled to reduce dark current. The temperature drop is achieved by liquid nitrogen, air cooling options or thermoelectric coolers.

Fiber-optic sampling

Since Raman spectroscopy measures a frequency shift, the laser wavelength can be chosen to be compatible with fiber optics or other optical components. Raman scattering can be conducted hundreds of meters away from the lab in readily available fibers. For example, fiber optics may be used to carry the laser light to a work of art, such as a wall painting in a historical building, and the collection fibers can bring the scattered light back to the spectrometer. Fiber optics allow both simplified alignment and remote sampling.

Laser rejection filters

In any Raman configuration, a weak signal is observed in the presence of a much stronger Rayleigh scattering or diffuse rejection occurring at the laser frequency. New filter designs based on holograph optics, either improved dielectric filters or semiconducting absorbers, can effectively reject the intense Rayleigh light. The rejection or notch filter is small and simple and permits the use of a small, single-stage spectrograph. The main advantages obtained with these filters are that low noise signals, high sensitivity and many other wavelengths may be studied.

1.1.3. Micro-Raman spectroscopy

Overview of Raman microscopy

The 180º sampling geometry provides means to combine a Raman spectrometer with an optical microscope, thus permitting Raman analysis of very small regions of a sample. The basic optical system of Raman microscopy employs backscattering. The laser beam is focused on the sample by means of a microscope objective. The Raman scattered light is collected within the cone defined by the same objective. This configuration allows to get molecular information from samples with dimensions approximately 1 μm. However, Raman microscopy can be a restricted technique when the samples have either large dimensions to be placed under the microscope, or are too fragile to be taken out of museums or libraries, or are not moveable at all, like wall paintings or heavy monuments. In such cases, fiber optic probes offer more flexibility to solve these inconveniencies by performing *in situ* measurements.

Confocal Raman micro-spectroscopy

The major development in micro-Raman spectroscopy instrumentation is based on the principles of confocal microscopy. The new generation of Raman microscope can offer a powerful non-destructive and non-contact method of sample analysis. The confocal technique provides an efficient way of obtaining interference-free Raman spectra of small samples embedded within strong scatterers or fluorescent transparent media. A confocal microscope has an additional aperture, called confocal hole, which has the effect of decreasing the depth focus. The system isolates the light originated from a small region of the sample coincident with the illuminated spot, and efficiently eliminates the contributions from the out-of-focus zones.

Confocal Raman fiber optic probes

Fiber optic probes offer more flexibility to investigate large samples and to perform in situ measurements. Conventional probes however generally measure at a macroscopic level and are therefore not always well suited for materials where high spatial resolution is required.

The new developments in fiber optic probes combine advantages of both high spatial resolution and ease of handling. In addition, improvements in optical design permit to achieve a resolution very close to that obtained using a confocal microscope, while not compromising the signal collection efficiency. A significant advantage is the reduction of fluorescence background when exploring samples that tend to fluorescence.

1.2. X-RAY FLUORESCENCE SPECTROSCOPY

1.2.1. Introduction

X-ray fluorescence (XRF) spectrometry has become a well established and developed multi-element technique, capable of supplying accurate quantitative and qualitative information on the elemental composition of a variety of materials in a non-destructive manner. The XRF technique has a wide dynamic range, high precision and a minimal requirement for sample preparation. XRF is typically employed for routine and non-routine analysis of environmental, geological, biological, industrial and other types of samples.

In XRF electronic transitions can be induced in the inner shells of the atoms by electromagnetic radiation of suitable energy which is a primary X-ray beam. Such transitions result in the emission of X-rays whose energy and intensity are related to the type and abundance of the atoms concerned by the interaction. X-rays are electromagnetic radiation with wavelengths around 100 pm. There are three photon-atom processes whose influence prevails in the X-ray common practice. The first process is the photoelectric effect in which the photons cause the ejection of an electron leaving a hole in the atom which, when the vacancy is filled by another electron, emits a fluorescence photon that has the energy difference between the electron and the hole level. The second process is the Rayleigh scattering in which the photon changes momentum but not energy. And finally, the third process is the Compton scattering in which both momentum and energy are transferred to the electrons comprising the atom. The desired interaction in XRF is the photoelectric effect, given that the energy of the X-rays detected is a measure for the element's concentration. Micro-XRF (μ-XRF or MXRF), an important variant of XRF emerged in the mid-1980s, based on the spatial confinement of the interaction volume of the primary X-ray beam with the material being analyzed.

1.2.2. Micro X-ray fluorescence spectroscopy

The micro-analytical variant of XRF is based on the localized excitation and analysis of a microscopically small area on the surface of a larger sample, providing information on the lateral distribution of major, minor and trace elements in the material under study. Basically, a beam of primary X-rays with a (microscopically) small cross-section irradiates a sample and induces the emission of fluorescent X-rays from a micro-spot. A suitable detector system collects the fluorescent radiation that carries information on the local composition of the sample. The difficulty in the exploitation of this method refers to the production of X-ray beams

sufficiently intense to allow sensitive microanalysis. Techniques to achieve this have only recently appeared. A standard micro-XRF instrument consists of an X-ray source, a focusing device, a sample holder and a detection system. The first two components define the spectral properties of the primary beam, the sample holder should allow accurate remote control of the sample position and the detection system for the detection of fluorescence radiation. Most of the table-top micro-XRF instruments are equipped with either micro-focus tubes in combination with collimators or straight capillaries, or with high flux tubes with conical capillaries. From the literature, it appears that capillary optics are by far the most popular type of optics for these instruments [3].

This doctoral thesis does not attempt to treat micro-XRF theory in depth. Several excellent books and monographs that explain these topics in much more detail are available [3-6]. We will focus on the latest developments in instrumentation, especially those improvements in micro-XRF.

1.2.3. Capillary optics

Capillary optics is one of the fastest growing X-ray optical technologies because of its capacity of generating high-flux-density beams in the micrometer range and below [7, 8]. There are three types of X-ray mono-capillary concentrators: straight, conical and ellipsoidal (or parabolic).

X-rays entering a capillary under a very small glancing angle propagate inside the capillary by successive reflections almost without losing any intensity.

The development of polycapillary lenses started with the assembly of mono-capillaries forming an ellipsoidal body where each capillary is aiming at the same point. In this way, the capillary lens is able to pick up a large fraction of the radiation from the point source and to guide it towards another point in the lens focal plane. The efficiency of such devices depends on the number of capillaries used, the transmission efficiency of each individual capillary and the thickness of the capillary glass wall. Today, polycapillary lenses are made as monolithic structures which consist of hundreds of thousands of capillaries tightly positioned together in a solid piece of glass.

1.3. A PORTABLE RAMAN X-RAY INSTRUMENT (PRAXIS)

The first Raman-XRF instrument was developed during the PRAXIS project [4, 9]. PRAXIS is a combination of a micro-XRF spectrometer and a micro-Raman spectrometer. The overall objective of this project was to develop and introduce in the market a combined Raman-XRF instrument fitted with a remote measuring head, which allows non-destructive and local analysis of microscopic samples with high elemental sensitivity and outstanding molecular specificity. It can be used as a table-top unit in a laboratory environment (*ex-situ* measurements) and it is also readily transportable and positionable so that it can be used for *in situ* measurements.

The PRAXIS instrument can analyse a small sample area. Typical spot size of the micro-XRF instrument is 25 μm that of the micro-Raman instrument being 5 μm. Further the Raman instrument has a confocal geometry with a depth resolution of approximately 3 – 5 μm. This combination opens the possibility for examination of the distribution of both the inorganic components of the sample and their organic components and the determination of phases or speciation. The basic data generated by this instrument is a hybrid RAMAN-XRF fingerprint (RXF pattern) consisting of the spectral response of a material in the 100-3000 cm^{-1} range of Raman wavenumbers and the 2-25 keV range of X-ray fluorescent energies.

The project PRAXIS is funded by the EU under the Competitive and Sustainable Growth Programme, Project No. GRD1-2001-400000 “A portable Raman X-ray Instrument” contract No. G6RD-CT-2001-00602. The development was performed by a group of different universities and manufacturers.

1.4. CHEMOMETRIC TOOLS

1.4.1. Signal processing: wavelet transform and discrete wavelet transform

The wavelet transform (WT) of a discrete signal [10-14], *f*, can be represented as a linear transformation involving an orthonormal matrix *W* (equation 1).

$$w = W f \tag{1}$$

Where *w* is a vector containing wavelet transform coefficients and *W* is the matrix of the wavelet filter coefficients. Each row of the matrix *W* represents one basis vector out of a collection of possible basis vectors. The basis vectors for a given wavelet function can be derived from a common function called mother wavelet via two operations: translation and dilation.

Signal reconstruction in the case of the orthonormal *W* matrix is described by the simple formula (equation 2):

$$f = W^{t} w \tag{2}$$

Described in mathematics (equation 3):

$$C(a,b) = \int_{-\infty}^{+\infty} f(t)\psi(a,b,t)\,dt \tag{3}$$

Where; *f(t)* is the original signal, and each wavelet ψ is a derivative from the mother wavelet ψ by variation of dilation [15] and translation (b):

$$\psi = \frac{1}{\sqrt{a}}\psi\left(\frac{t-b}{a}\right) \tag{4}$$

With such transform, wavelet coefficients *C(a,b)* can be obtained. For computation, discrete wavelet transform (DWT) is usually employed instead of WT (equation 5):

$$\psi = 2^{-a/2}\,\psi\left(2^{-a}t - 1\right) \tag{5}$$

Fast algorithm

Mallat introduced the fast decomposition algorithm [16], which is widely used to perform the DWT. The vector describing the signal is simultaneously passed trough low-pass and high-pass filters. Outputs are split in two into approximation and detail (or wavelets) coefficients. Approximation coefficients represent a smooth version of the signal at half resolution and detail coefficients contain details of the signal at that level of decomposition. Approximation coefficients can be further

decomposed to form a new vector of approximation coefficients and new details of the signal. With the increase of the decomposition level, less information will be included in the approximation coefficients. The information lost between the approximation coefficients of two successive decompositions is encoded into the detail coefficients. Detail coefficients of the first level of decomposition contain information about the high frequency components of the signal, like noise and spikes [17-23], In the last levels of decomposition, they mainly contain the low-frequency components of the signal. The process can be iterated to level n. At the end, a vector of approximation coefficients and a series of vectors of detail coefficients are accomplished which form the DWT coefficients *w*.

Signal processing by DWT

DWT decomposition provides a basic platform for further signal processing that can be achieved by thresholding the DWT coefficient *w.* There are two main approaches for thresholding, namely soft thresholding and hard thresholding. With soft thresholding, the coefficients that are smaller than threshold value *thr* are set to zero, otherwise reduced by *thr* (equation 6a):

$$\begin{cases} 0, & if\ w_{i,j} < thr; \\ sign(w_{i,j})[abs(w_{i,j}) - thr], & if\ w_{i,j} \geq thr; \end{cases} \quad (6a)$$

With hard thresholding, the coefficients that are smaller than threshold value are set to zero otherwise kept (equation 6b):

$$\begin{cases} 0, & if\ w_{i,j} < thr; \\ w_{i,j}, & if\ w_{i,j} \geq thr; \end{cases} \quad (6b)$$

To eliminate noise (denoising), the detail coefficients in *w* are filtered by thresholding to reduce or remove those elements in *w* that are thought to be atributed to noise.

Multiresolution analysis

One of the main advantages of WT is multiresolution analysis (MRA). It provides a concise framework for explaining many aspects of wavelet theory. MRA allows an efficient algorithm to implement DWT.

WT allows us to represent signals at different scales or resolutions. At the coarse level, only the most prominent large features can be seen, whereas at higher levels finer details are captured. Multiresolution develops representations of a function $f(t)$ at various levels of resolution where each level is expanded in terms of

translated scaling functions $\phi(2^j t - k)$. A sequence of embedded subspaces V_j is created.

$$V_0 \subset V_1 ... V_{J-1} \subset V_j \tag{7}$$

Where *J* corresponds to the highest and 0 corresponds to the lowest resolution level. The signal represented by a function *f(t)* can be approximated by the projection $P_j f$ onto the space V_j:

$$P_j f = \sum_k c_{j,k} \phi(2^j t - k) \tag{8}$$

It is here assumed that $P_j f = f$, for example, the maximum signal resolution is contained in the original function. The wavelet coefficients correspond to the contribution from the projections onto the space of details between two approximation spaces V_j and V_{j+1}. A detail space W_j is spanned by the translated wavelet functions $\psi(2^j\text{-}k)$ and is the difference of detail between two approximation spaces V_{j+1} and V_j:

$$V_{j+1} = V_j \oplus W_j \tag{9}$$

Where $\oplus$ is the direct sum.

The projection $Q_j f$ of *f* onto W_j is:

$$Q_j f = \sum_k d_{j,k} \psi(2^j t - k) \tag{10}$$

and relates to the approximation projections as follows:

$$P_j f = P_{j-1} + Q_{j-1} f \tag{11}$$

which means that

$$P_j f = P_0 f + \sum_{k=0}^{j-1} Q_k f \tag{12}$$

Multiresolution analysis allows to obtain information about how the patterns depend on the frequency contents of the spectral data profiles. It also gives information regarding whether broad or narrow signal components are involved in classification and about the location of these features that originate an observed pattern in the original spectral profile.

1.4.2. Soft computing solutions: fuzzy logic

Soft computing is a consortium of methodologies which works synergistically and provides in either one form or another, flexible information processing capabilities for handling real life ambiguous situations. Its aim is to exploit the tolerance for imprecision, uncertainty, approximate reasoning and partial truth in order to achieve tractability, robustness, low cost solutions and close resemblance to human like decision making.

The theory of fuzzy sets enables the representation and processing of vague propositions and uncertain information. In contrast with the probability theory, the fuzzy-theory is a possibilistic approach, based on the possibility theory.

Fuzzy sets

Fuzzy sets were introduced in 1965 by Zadeh [24-33] as a new way of representing vagueness in everyday life. They are generalizations of the conventional (crisp) set theory. Conventional sets contain objects that satisfy precise properties required for membership. Fuzzy sets, on the other hand, contain objects that satisfy imprecisely defined properties to varying degrees. A fuzzy set *A* of the universe *X* is defined as a collection of ordered pairs

$$A = \{(\mu_A(x), x), \forall x \in X\} \tag{13}$$

where $\mu_A(x)$, $(0 \leq \mu_A(x) \leq 1)$ gives the degrees of belonging of the element *x* to the set *A* or the degree of possession of an imprecise property represented by *A*. The fuzzy sets are normalized to the interval [0,1] and can be represented either discretely or by means of a function.

Every element in the universe of discourse is a member of the fuzzy set in some grade, maybe even zero. The set of elements that have a non-zero membership is called support of the fuzzy set. The function that ties a number to each element *x* of the universe is called the *membership function* $\mu(x)$.

There are two alternative ways of representing a membership function in a computer: continuous or discrete. In the continuous form the membership function is a mathematical function. A membership function is for example bell-shaped, s-shaped, triangular, or trapezoidal. In the discrete form the membership function and the universe are discrete points in a list (vector).

Operations on fuzzy sets

The membership function is obviously a crucial component of a fuzzy set. It is therefore natural to define operations on fuzzy sets by means of their membership

functions. A fuzzy set operation creates a new set from one or several given sets.

Let *A* and *B* be fuzzy sets in a mutual universe.

The intersection of *A* and *B* is

$$A \cap B \equiv \mathrm{a} \min \mathrm{b}$$

The operation min is an item-by-item minimum comparison between corresponding items in *a* and *b*.

The union of *A* and *B* is

$$A \cup B \equiv \mathrm{a}\ max\ \mathrm{b}$$

where max is an item-by-item maximum operation.

The complement of *A* is

$$\overline{A} \equiv 1 - \mathrm{a}$$

where each membership value in *a* is subtracted from 1.

1.4.3. Hard computing solutions: factorial methods

These methods are aimed at projecting the original data set from high dimensional space on to a line, a plane or a 3D-coordinate system.

Principal component analysis (PCA)

The main idea of PCA is to approximate the original matrix *X* by a product of two small matrices [34, 35], the score and loading matrices, according to equation 14:

$$X = T\,L^T \tag{14}$$

where *X* is the original data matrix consisting of *n* rows (objects) and *p* columns (features); *T* is the scores matrix with *n* rows and *d* columns (number of principal components); *L* is the loading matrix with *d* columns and *p* rows; and *T* is the transpose of a matrix.

The projection of *X* down on to a d-dimensional subspace by means of the projection matrix L^T gives the object coordinates in this plane, *T*. The columns in *T* are the score vectors and the rows in L^T are called loading vectors. Both groups of vectors are orthogonal.

The principal components are determined on the basis of the maximum variance criterion. Each subsequent principal component describes a maximum of variance that is not modelled by the former components. According to this, most of the

variance of the data is contained in the first principal component. In the second component there is more information than in the third, etc. Finally, as many principal components as needed are computed to explain a preset percentage of the variance. All redundancy is thereby summarised. This simplifies the graphical interpretation of the data as well as their quantitative use. The resulting PC model is more compact and statistically stable than the individual input data.

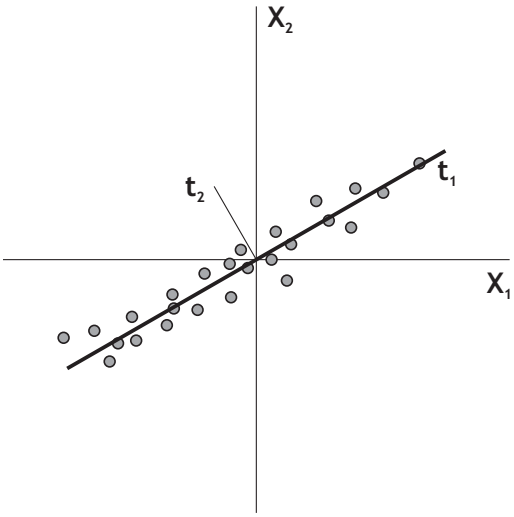

Figure 1.2. PC showing a sistematic patern of variation in a data set.

The principal components can be considered as projections of the original data matrix, *X*, on to the scores, *T*. For this equation 14 must be converted to the scores on the left side by (equation 15):

$$T = X\,L \tag{15}$$

The new coordinates are linear combinations of the original variables.

Because a large fraction of the variance can usually be described by means of one, two or three main components, the data can be visualized by plotting the main components against each other. PCs reveal the systematic, dominant type variations between samples. Usually, each individual PC does not correspond to an individual physical phenomenon. But seen together, the first few PCs usually span the important information space of how the physical phenomena vary. Interpretation of the results of PCA is usually carried out by visualization of the component scores and loadings. The score plot depicts the linear projection of objects representing the main part of the total variance of the data. Correlation and importance of feature variables must be decided from plots of the PC loadings. The loading plot provides the projection of the features on the principal components. From this plot, information about the correlation of feature variables can be deduced.

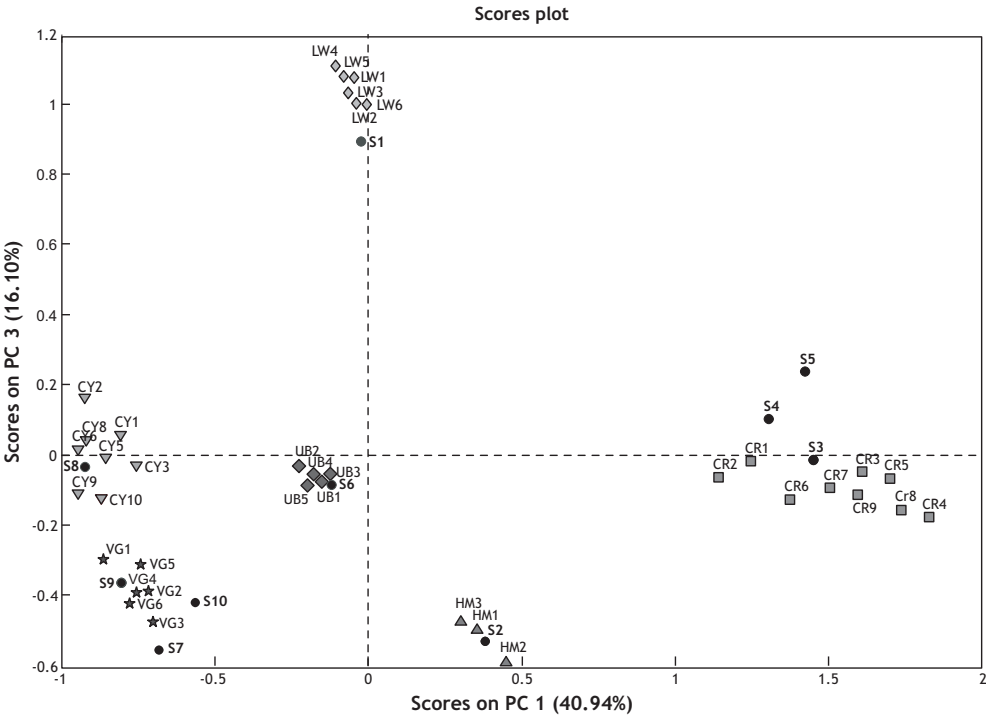

Figure 1.3. PCA score plot showing the sistematic dominant types of variations between samples.

Partial least square regression (PLS)

Comparing with PCA, PLS brings a second table of variables, called Y-variables. The idea is to explore relationships between two data tables, X and Y, or predict one from other. Each PLS latent variable direction of the X-matrix is modified so that the covariance between it and the Y-matrix vector is maximized. The PLS method is based on a bilinear model with respect to the objects and the variables of the X- and Y-matrices [34, 35]. In multivariate data analysis based on soft modelling, we are usually interested in the patterns of variations between the samples, not in absolute numbers. Therefore, it is common practice to mean-centre the variables prior to bi-linear modelling. This means that the input data *X* is first modelled in terms of the mean for the variables, plus an initial residual E_0. This is computed by

$$E_0 = X - 1\bar{x} \tag{16}$$

Both the *X*- and *Y*-matrices are decomposed according to:

$$X = 1\bar{x} + T\,P^T + E \tag{17}$$

The *X*-variables are modelled by the *X*-scores *T*, in terms of *X*-loadings *P* and *X*-residual *E*.

$$Y = 1\bar{y} + T\,Q^T + E \tag{18}$$

The *Y*-variables are likewise modelled by *X*-scores *T*, in terms of *Y*-loadings *Q* and *Y*-residuals *F*. Equivalently; the *Y*-variables may be modelled directly from the *X*-variables via the regression coefficient matrix *B*.

$$Y = 1b_0 + XB + F \tag{19}$$

Where b_0 is the model offset.

The coefficients *B* are estimated as a function of the *X*- and *Y*-loadings P^T and Q^T. The actual values in residuals *E* and *F* in equations and in *B* and b_0 in equation will depend on the number of latent variables used in the model.

The main information lies in the scores *T*, the loadings *P* and *Q* and the estimates of regression coefficients *B*. The rest of the elements are usually rather uninteresting. Either they reflect what does not vary between samples or they contain noise mainly. This means that the many *X*-variables are compressed into a few PCs *T* (latent variables), and both *X* and *Y* are then approximated from *T*. If too few PCs are included in the bi-linear model, the description of *X* and *Y* will be unsatisfactory (underfitting). If too many PCs are included, this is called overfittting. The optimal number of PCs is not that which directly makes fitted residuals *E* and *F* as small as possible. The optimal number of PCs is usually determined from estimates of the prediction error in *Y*.

There are two distinct phases in data-driven predictive modelling. First, the training or calibration phase, where the model for predicting *Y*-variables from *X*-variables is determined based on empirical data *(X,Y)* and prior knowledge. Second, the prediction phase, where the model with known parameters $\bar{x}$, *P*, $\bar{y}$ and *Q* is applied to data from the *X*-variables in new samples, in order to predict the unknown values of the *Y*-variables, or for explorative purposes.

Partial least square regression – Discriminant analysis (PLS-DA)

In PLS-DA [35-37] all the samples are kept inside one common model, and are used for learning how to discriminate between the different classes. The PLS-DA modelling is performed just like any other PLS modelling.

The PLS-DA model consists of building a conventional PLS model, but with class indicator variables as *Y* matrix, and whatever other variables available as *X* matrix, see Figure 1.4. This model allows us to classify even new samples, by predicting to which degree each new sample seems to belong to each class *Y* from their *X*-data.

	X-block	Y-block					
		1	2	3	4	5	6
1. hematite	Chemical variables	1	0	0	0	0	0
2. caput mortum		0	1	0	0	0	0
3. caput mortum violet		0	0	1	0	0	0
4. yellow ochre		0	0	0	1	0	0
5. red ochre		0	0	0	0	1	0
6. burnt sienna		0	0	0	0	0	1

Figure 1.4. Identity matrix for classification of pigments.

Geometrically they are the vectors which allow to view the data points as separable in a multidimensional space and which describe the different classes. These PLS components or latent variables are similar to those from a PC analysis (PCA) of pigment class profiles except that the discriminant PLS components can be thought of as the rotation of the PCA which maximizes the orthogonality of predicted pigment classes (maximum in the sense that 1 is predicted for the correct class and 0 for the wrong class). The bilinear model for the X-block allows visualization of the multidimensional space projections.

1.4.4. Data-fusion

Data fusion is a formal framework in which the means and tools for the alliance of data originated from different sources are expressed [38-44]. It aims at obtaining information of greater quality; the exact definition of 'greater quality' will depend upon the application.

Data fusion is analogous to the cognitive process used by humans to integrate data continually from their senses to make inferences about the external world. It has been widely applied to military situations (battlefield surveillance, tactical situation assessment), commercial purposes (robotics, automated manufacturing, and remote sensing), and the food processing industry.

There is no single optimal architecture for any given data fusion application. For identity fusion Hall and Llinas describe architectures [41], in which multiple sensor observations of a target's attributes are converted to a joint declaration of target identity. These architectures or data fusion techniques can be organized in three levels: 1) data level or low fusion, 2) feature level or mid levelh fusion, and 3) decision or high level fusion.

The low-level fusion consists of combining the signals provided by different techniques before any processing. It implies that the techniques must be similar,

and consequently the signals must be commensurate. The combination of the signals is based on relationships that may exist between techniques. Low-level fusion may be used, for example, for fusing two Raman spectra of the same object, but coming from different ranges of wavenumbers. The combination of the signals may be a simple concatenation of the spectra. Feature extraction is realized on the meta-spectrum conformed by the concatenations of the two Raman spectra.

The mid-level fusion is performed by using the extracted features from each technique. These features are concatenated together into a single feature vector (in the case of spectra) which in turn is input to an identity declaration technique. The output then becomes a joint or fused declaration of target identity based on the combined feature vectors from all the techniques.

The functions of data alignment and association/correlation must still be performed prior to linking the feature vectors from individual techniques into a larger feature vector.

The high-level fusion is performed by using the identity declaration provided by each technique. The identity declarations provided by the individual techniques are combined using decision level fusion techniques such as classical inference, Bayesian inference, or weighted decision methods, among others.

1.5. REFERENCES

[1] R. L. McCreery, Raman Spectroscopy for Chemical Analysis; John Wiley & Sons, Inc: Ohio, United States, (2000).

[2] J. J. Laserna, Modern Techniques in Raman Spectroscopy, 1 ed.; John Wiley & Sons: Málaga, Spain, (1996).

[3] K. H. A. Janssens, F. C. V. Adams and A. Rindby, Microscopic X-ray Fluorescence Analysis; John Wiley & Sons, LTD, (2000).

[4] S. Bichlmeier, K. Janssens, J. Heckel, D. Gibson, P. Hoffmann and H. M. Ortner, X-Ray Spectrometry 30, (2001), 8-14.

[5] G. Vittiglio, S. Bichhneier, P. Klinger, J. Heckel, W. Fuzhong, L. Vincze, K. Janssens, P. Engstrom, A. Rindby, K. Dietrich, D. Jembrih-Simburger, M. Schreiner, D. Denis, A. Lakdar and A. Lamotte, Nuclear Instruments & Methods in Physics Research Section B-Beam Interactions with Materials and Atoms 213, (2004), 693-698.

[6] M. Mantler and M. Schreiner, X Ray Spectrometry 29, (2000), 3-17.

[7] L. Vincze, F. Wei, K. Proost, B. Vekemans, K. Janssens, Y. He, Y. Yan and G. Falkenberg, Journal of Analytical Atomic Spectrometry 17, (2002), 177-182.

[8] K. Proost, L. Vincze, K. Janssens, N. Gao, E. Bulska, M. Schreiner and G. Falkenberg, X-Ray Spectrometry 32, (2003), 215-222.

[9] K. Janssens, Z. Jia, M. V. Gysel and P. V. Espen, PRAXIS: A Combined micro-Raman –micro-XRF Instrument, Euroanalysis XIII, Salamanca, Spain, 6-10 September. (2004).

[10] B. K. Alsberg, A. M. Woodward and D. B. Kell, Chemometrics and Intelligent Laboratory Systems 37, (1997), 215-239.

[11] B. Walczak, Wavelets in Chemistry; Elsevier, (2000).

[12] B. Walczak and D. L. Massart, TrAC Trends in Analytical Chemistry 16, (1997), 451-463.

[13] X. G. Shao, A. K. M. Leung and F. T. Cau, Accounts of Chemical Research 36, (2003), 276-283.

[14] F. Ehrentreich, Analytical and Bioanalytical Chemistry 372, (2002), 115-121.

[15] O. G. A, A. C. Dennis, D. Denvir, J. J. McGarvey and S. E. J. Bell, Analytical Chemistry 73, (2001), 2058-2065.

[16] S. G. Mallat, Pattern Analysis and Machine Intelligence, IEEE Transactions on 11, (1989), 674-693.

[17] F. Ehrentreich and L. Summchen, Analytical Chemistry 73, (2001), 4364-4373.

[18] W. D. Cao, X. Y. Chen, X. R. Yang and E. K. Wang, Electrophoresis 24, (2003), 3124-3130.

[19] C. Perrin, B. Walczak and D. L. Massart, Analytical Chemistry 73, (2001), 4903-4917.

[20] B. Walczac and D. L. Massart, Chemometrics and Intelligent Laboratory Systems 36, (1997), 81-94.

[21] B. K. Alsberg, A. M. Woodward, M. K. Winson, J. Rowland and D. B. Kell, Analyst 122, (1997), 645-652.

[22] C. S. Cai and P. D. Harrington, Journal of Chemical Information and Computer Sciences 38, (1998), 1161-1170.

[23] V. J. Barclay, R. F. Bonner and I. P. Hamilton, Analytical Chemistry 69, (1997), 78-90.

[24] L. A. Zadeh, IEEE Computer 1, (1988), 83-93.

[25] L. A. Zadeh, Technometrics 37, (1995), 271-276.

[26] L. A. Zadeh, Psicothema 8, (1996), 421-429.

[27] L. A. Zadeh, IEEE Transactions on Fuzzy Systems 4, (1996), 103-111.

[28] L. A. Zadeh, Bt Technology Journal 14, (1996), 32-36.

[29] L. A. Zadeh, Fuzzy Sets and Systems 90, (1997), 111-127.

[30] L. A. Zadeh, Computer 21, (1998), 83-93.

[31] L. A. Zadeh, Discovering the World with Fuzzy Logic VOL 57, (2000), 3-28.

[32] L. A. Zadeh, Quo Vadis Computational Intelligence VOL 54, (2000), 123-143.

[33] L. A. Zadeh, IEEE Transactions on Fuzzy Systems 9, (2001), 3-4.

[34] M. Otto, Chemometrics: Statistics and Computer Application in Analytical Chemistry; Wile-VCH: Weinheim, (1999).

[35] H. Martens and M. Martens, Multivariate Analysis of Quality - An Introduction; John Wiley & Sons, LTD, (2001).

[36] M. Barker and W. Rayens, Journal of Chemometrics 17, (2003), 166-173.

[37] U. G. Indahl, N. S. Sahni, B. Kirkhus and T. Naes, Chemometrics and Intelligent Laboratory Systems 49, (1999), 19-31.

[38] V. Steinmetz, F. Sevila and V. Bellon-Maurel, Journal of Agricultural Engineering Research 74, (1999), 21-31.

[39] S. Roussel, W. Bellon-Maurel, J. M. Roger and P. Grenier, Journal of Food Engineering 60, (2003), 407-419.

[40] S. Roussel, V. Bellon-Maurel, J. M. Roger and P. Grenier, Chemometrics and Intelligent Laboratory Systems 65, (2003), 209-219.

[41] D. L. Hall and J. Llinas, Proceedings of the IEEE 85, (1997), 6-23.

[42] I. Bloch, Systems, Man and Cybernetics, Part A, IEEE Transactions on 26, (1996), 52-67.

[43] R. R. Yager, Information Sciences 163, (2004), 175-200.

[44] J. Llinas and D. L. Hall, An introduction to multi-sensor data fusion, Circuits and Systems, 1998. ISCAS '98. Proceedings of the 1998 IEEE International Symposium on, 1998.

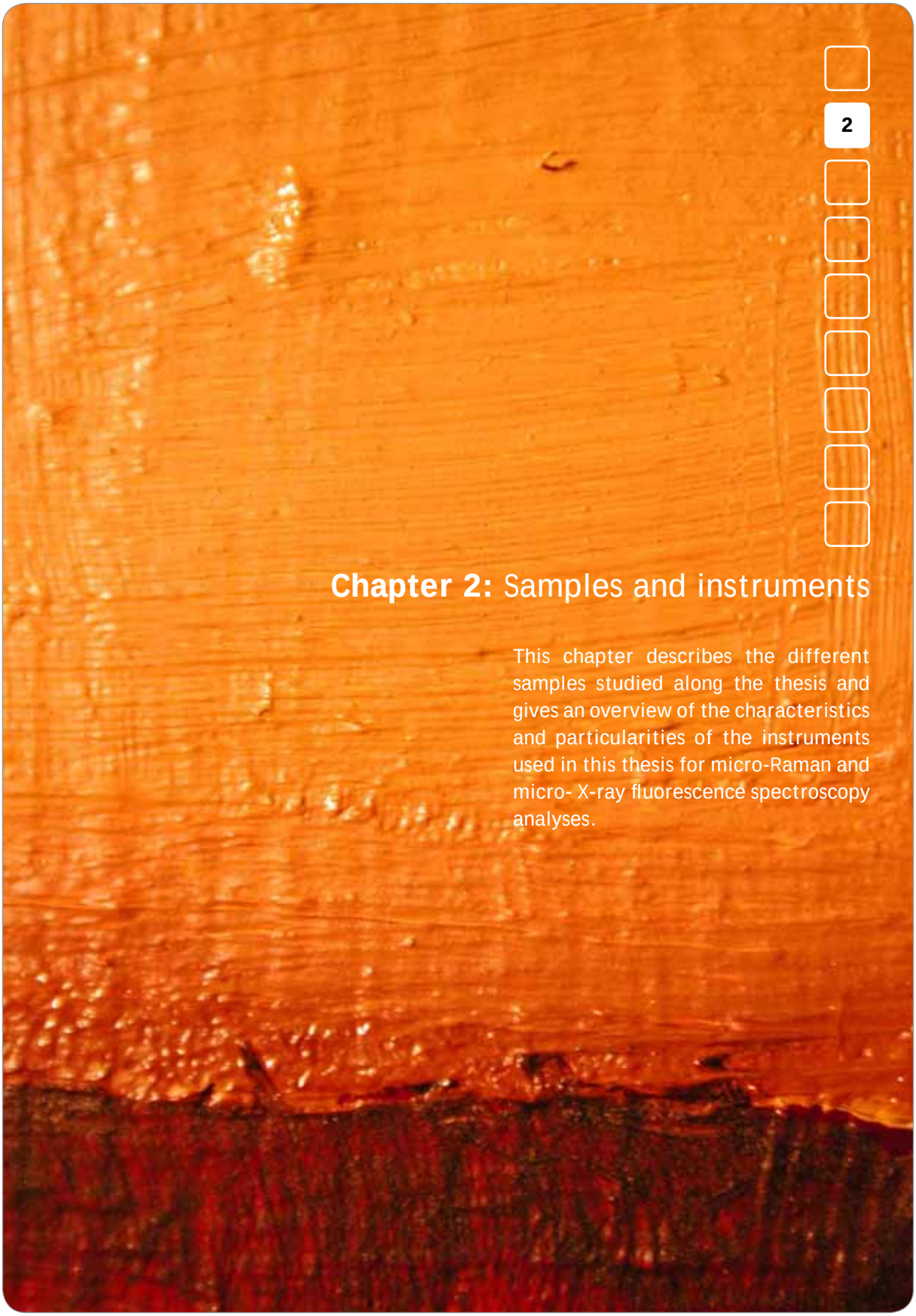

2

Chapter 2: Samples and instruments

This chapter describes the different samples studied along the thesis and gives an overview of the characteristics and particularities of the instruments used in this thesis for micro-Raman and micro- X-ray fluorescence spectroscopy analyses.

2.1. INTRODUCTION

2.1.1. Pigments

Pigments are the primary ingredient of all paints and have been in use since the beginnings of mankind. A pigment is a dry colorant, usually a powder suspended in a substance. This substance can vary from oil, wax, or egg yolk in paintings, plaster in frescoes, or plastics in high technology industry. The paint consists of a pigment ground in a liquid which, once dried into a film, is stuck to the painting surface [1-5].

The first pigments and paintings

From prehistoric times humans have left their impression of the world and have expressed their memories and thoughts in the form of painted images. Over the the ages, these paintings have been made on every possible surface, from rocks to walls to bodies; they have also been used in funeral rituals [1].

Prehistoric painters used the pigments available in their environment, which were the so-called earth pigments and carbon black. The binding agent was water and the pigments stuck to the wall when the binding media dried, adhering the pigment to the wall. The colours were yellow ochre, red ochre, and black.

Natural ochre pigments present a wide range of colours, from yellow to orange, to red to violet. The colour is given by the ferric oxide monohydrate ($Fe_2O_3.H_2O$), better known as rust. Ochre pigments contain varying amounts of octahedral iron oxides, namely hematite (αFe_2O_3) and/or goethite ($\alpha FeOOH$), and white pigments (alumino-silicate as kaolin, quartz as well as calcium compounds as calcite, anhydrite or gypsum) [6, 7]. When the ochre pigment presents high amounts of hematite, the pigment colour is red, whereas ochre pigments with high amounts of goethite give a yellow colour. The words ochre and hematite come from the Greek words *ochros* and *hema*, meaning yellow and blood, respectively [8].

Red ochre is obtained by heating yellow ochre in order to remove the water and obtain the anhydrous ferric oxide. By controlling its heating it is possible to obtain a variety of colours ranging from warm yellows to bright reds. In nature, it is possible to obtain red ochre from volcanic regions where dehydration is caused naturally by thermal activities [1].

The first paintings were made in caves by people who thus decorated their walls. The pigments were sprayed from the mouth and painted onto the surface using the fingers as brushes. Prehistoric dwellers may have discovered that unlike the dye colours derived form animal and vegetable sources, the colour obtained from iron oxide would not fade with the changing environment. Following this line of thought, it is considered

that men travelled long distances to reach new sources of the red pigment. Around the world, in every discovered prehistoric site, there are signs of routes to hematite deposits where man mined. It has been deduced that the main motivation of prehistoric man for mining activities was his need of the red pigment [1, 9, 10].

The excellent colour permanence and the abundance of raw materials made ochre pigments the basic palette of ancient artists, from Egypt to India, and from China to America. Iron oxide pigments are unaffected by alkalies and have been among the main colours available for works of art along the ages [2, 11-13].

The Egyptians began pigment manufacture about 4000 BC. They processed the pigments in order to increase their purity and strength. They also introduced new pigments, one of them was Egyptian blue, which is a very stable pigment and still remains as if fresh in wall paintings performed in those times [14, 15]. This pigment is a calcium copper silicate ($CaCuSi_4O_{10}$). The Egyptians also used malachite, considered the oldest known green pigment, and azurite, which is a greenish blue pigment. Both are chemically similar, containing basic copper carbonate ($2CuCO_3$. $Cu(OH)_2$). They were found in Egyptian tombs and Egyptian women also used malachite for make up. Malachite and azurite are also found in European paints from the 15th and 16th centuries.

The Chinese made their contribution to painting long before Western civilization emerged. They developed vermillion around 2000 years before the Romans used it. Vermillion is a red pigment, obtained by processing a mineral, cinnabar (HgS). The process mainly consists of crushing, washing and heating cinnabar [16, 17].

The Greeks manufactured a white lead pigment which was used until the 19th century [18, 19]. It is still regarded as the whitest of white pigments, and it is basic lead carbonate ($2Pb(CO_3)_2.Pb(OH)_2$). They also developed the use of red lead, which continued to be used until 1990s. Red lead is a form of lead oxide (Pb_3O_4) and is found as minium, a mineral near the river Minius in the northwest of Spain [20, 21]. It is also obtained by heating litharge (PbO) in air.

The Romans made use of the pigments developed by both the Egyptians and the Greeks [22-24]. They introduced a pigment called Tyrian purple, which was obtained from a type of mollusc found in the Mediterranean Sea. Cinnabar was extensively used by the Romans, especially for wall decoration, but also for painting statues and as women's lipstick.

Middle Ages and the Renaissance periods

Throughout the Middle Ages and the Renaissance, mineral pigments (including those from iron oxide) continued to be used by painters. The main characteristic of these periods is the use of clear and well defined bright colours, while brown colours were considered dull. The Italians started to use Umber, which comprises

hydrated iron and manganese oxides and also used raw sienna, an ochre containing silicic acid, and raw umber, which is an ochre containing manganese oxide and iron hydroxide. Raw sienna could be calcined to obtain the richer burnt sienna.

Many developments were done in these times in order to supply the demand of colours by artists. The most important pigment produced in this time was the ultramarine blue. It was made by grinding the mineral lapis lazuli, which is a rock containing the mineral lazulite, mainly found in Afghanistan. Lazulite is a complex sulphur-containing aluminium silicate ($Na_{8-10}Al_6Si_6O_{24}S_{2-4}$). During the Renaissance, the colour blue was associated with purity and ultramarine blue was used to remark this quality in paintings of the Virgin Mary.

Naples yellow was also developed during the Renaissance. This pigment is made of lead antimonate ($Pb(SbO_3)_2$ or $PbSbO_4$).

Although many alternatives were implemented to obtain different colours, malachite and verdigris pigments were still used as greens, orpiment and ochre pigments continued to be used for yellow.

Recent centuries and the development of modern pigments

By the 18th century, synthetic red iron oxide pigments were being made in a laboratory setting. These pigments, which were called Mars red, were found to have all the properties of their natural counterparts, including durability and permanence. By the middle of the 19th century, regular manufacture of synthetic red iron oxide pigments began and has continued to be improved and simplified up to the present. Synthetic yellow iron oxide pigments (mars yellow) have been made since the early 1920s, with major improvements occurring in the 60s and continuing to the present. The development of synthetic brown iron oxide pigments has evolved through the modification of the technology used in producing reds and yellows.

Today, synthetic iron oxide pigments are used extensively by the paint, plastics and other industries [1].

2.1.2. Pigments studied

Most of the reference spectra refer to pigments obtained from one of the most well known collections of artists' pigments produced for fine arts and restorations, that is the Kremer's collection. The materials are further denoted by the name of the producer and the corresponding catalogue number. Table 2.1 shows the list and name of all pigments studied along this thesis.

TABLE 2.1

YELLOW AND ORANGE PIGMENTS

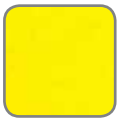

Name
Cadmium yellow

Code-Kremer
21030

Chemical formula
CdS

Source
Inorganic, mineral and synthetic.

Origin and history
Invented in 1846.

Characteristics
Fine, transparent and luminous effect. Excellent permanence.

Toxicity
Not toxic for acute exposure to animals. Chronic effects and carcinogenicity: the standard states that substances containing cadmium are cancer hazard and can cause lung and kidney disease. Cadmium pigments have shown to be significantly less biologically available and less active than other cadmium compounds.

Name
Massicot

Code-Kremer
43010

Chemical formula
PbO

Source
Orthorhombic variety of PbO. The tetragonal variety is the mineral litharge.

Origin and history
Can be dated back as 1300 in medieval Europe. Also called *Cassel yellow* or *Litharge*. May also have been called *Giallorino* in the middle ages.

Characteristics
Yellow to reddish yellow due to minium inclusions.

Toxicity
May cause reproductive disorders. Possible mutagen and carcinogenic to humans. Harmful by inhalation, ingestion and through skin contact.

Name
Naples yellow

Code-Kremer
43130

Chemical formula
$Pb_3(SbO_4)_2$

Source
One of the oldest synthetically produced pigments known.

Origin and history
Used as early as 500 BC.

Characteristics
Opaque lead antimoniate. Identical crystal structure with the mineral, bindheimite. Very heavy and dense. Exceptional covering power. Unaffected by light.

Toxicity
Relative Toxicity Rating: Skin: moderate; inhalation: high; ingestion: high. Skin contact may cause severe skin lesions. Acute inhalation and ingestion may cause antimony poisoning. Lead poison.

Name
Titanium orange

Code-Kremer
43300

Chemical formula
TiO_2
(rutile with Ni and Sb)

Source
Nickel antimony titanium yellow rutile.

Origin and history
Modern pigment.

Characteristics
Inorganic pigment of the very highest light-fastness. Mixing with a little chrome titanium yellow produces the historical Naples yellow tone.

Toxicity
Non toxic.

RED PIGMENTS

Name
Cinnabar or Vermilion

Code-Kremer
10620

Chemical formula
HgS

Source
Mineral cinnabar.

Origin and history
Discovered before the 6th century BC and continued to be used until mid of 20th century.

Characteristics
Homogeneous texture and uniformly opaque.

Toxicity
Can cause skin irritation and allergies. Mercury compounds are especially toxic to humans and can be inhaled or absorbed through the skin. Symptoms of mercury poisoning include psychic and emotional disturbances, followed by seizures, kidney disease, and nerve degeneration.

Name
Red lead or Minium

Code-Kremer
42500

Chemical formula
Pb_3O_4

Source
Mineral and synthethic

Origin and history
The name red lead comes from river Miño (Minius) located in the north west of Spain. One of the earliest pigments artificially prepared and still in use today.

Characteristics
Fairly permanent when mixed with oil. Red lead ground in oil dries the quickest of all pigments.

Toxicity
May have effects on the blood, bone marrow, central and peripheral nervous system and kidneys, resulting in anaemia, encephalopathy, peripheral nerve disease, abdominal cramps and kidney impairment.

Name
Cadmium red

Code-Kremer
21110

Chemical formula
CdS (CdSe)

Source
Synthethic

Origin and history
Made in the 20th century (1930's).

Characteristics
Best substitute for vermillion. It is known to turn brown in outdoor frescos; with copper colors it turns black, as all cadmiums do.

Toxicity
Not toxic for acute exposure to animals. Chronic effects and carcinogenicity: the standard states that substances containing cadmium are cancer hazard and can cause lung and kidney disease.

GREEN PIGMENTS

Name
Malachite

Code-Kremer
10310

Chemical formula
$CuCO_3\ Cu(OH)_2$

Source
Mineral malachite

Origin and history
Most important green up to the 18th century. Discovered in antiquity.
Found in Egyptian tomb paints since the fourth dynasty.
In European paintings it seems to have been of importance mainly in the 15th and 16th centuries.

Toxicity
Moderately toxic.

Name
Green earth cyprus

Code-Kremer
17400

Chemical formula
$K[(Al,Fe(III)),(Fe(II),Mg](AlSi_3,Si_4)O_{10}(OH)_2$

Source
Mineral glauconite or celadonite.

Origin and history
Discovered in antiquity. Frequently used in medieval painting for underpainting of flesh tones. Its use declined after the renaissance.

Toxicity
Non toxic

Name
Viridien

Code-Kremer
44250

Chemical formula
$Cr_2O_3.2H_2O$

Source
Synthethic.

Origin and history
Discovered in 1838 and continues in use.

Characteristics
Bright, clear, emerald. Very good ermanence. Could replace all other greens, both ancient and modern.

Toxicity
Suspected to be carcinogenic.

Name
Chromium Oxide

Code-Kremer
44200

Chemical formula
Cr_2O_3

Source
Synthethic.

Origin and history
It was first used as a pigment in 1812.

Characteristics
It is a dull, opaque, olive-green colour.

Toxicity
In its dry powder form, the chemical is suspected to be carcinogenic and could cause skin or respiratory irritation or allergies.

Name
Verdigris

Code-Kremer
44450

Chemical formula
$Cu(OH).(CH_3COO)$

Source
Prepared by exposing copper to the vapors of fermenting grape skins or in close casks over vinegar.

Origin and history
Known in ancient times as *green of Greece* or *salt green*.

Characteristics
Reactive and unstable, requiring varnishes to protect its color.

Toxicity
Cause eye, skin, respiratory tract irritation and liver damage.

BLUE PIGMENTS

Name
Ultramarine

Code-Kremer
45020

Chemical formula
$Na_{6-10}Al_6Si_6O_{24}S_{2-4}$

Source
Mineral Lapis lazuli, which is a rock mixture containing the mineral Lazurite.

Origin and history
Used from ancient times until today. The earliest occurrence of its use as a pigment was in the 6th or 7th century wall paintings in cave temples at Bamiyan (Afghanistan). Synthetic ultramarine was obtained in 1828.

Characteristics
Natural ultramarine has a high stability to light.

Toxicity
Non toxic

Name
Cobalt blue

Code-Kremer
45700

Chemical formula
$CoO.Al_2O_3$

Source
Synthethic.

Origin and history
It was discovered in 1802 and continues in use.

Characteristics
It is useful in all techniques, as well as being lightproof.

Toxicity
Not listed as a carcinogen by the NTP, IARC, or OSHA; no adverse long-term effects are known. Not known adverse health affects to linseed oil.

Name
Pyrolusite

Code-Kremer
-

Chemical formula
MnO_2

Source
Mineral pyrolusite

Origin and history
Manganese oxide minerals have been used for thousands of years by Ancients People for making pigments and to clarify glass.

Characteristics
It is considered to be among the most permanent pigments in the artist's palette. It can be used in all techniques and combines well with all pigments.

Toxicity
Moderately toxic.

Name
Prussian blue

Code-Kremer
45200

Chemical formula
$Fe_4[Fe(CN)_6]_3$

Source
Synthethic.

Origin and history
Discovered in Berlin by Diesbach about 1704.

Characteristics
It's called the first of the modern pigments, and it was extremely popular throughout the three centuries after its discovery. It is strong in colouring power and very permanent in all techniques except fresco.

Toxicity
Non toxic

Name
Azurite

Code-Kremer
10200

Chemical formula
$2CuCO_3.Cu(OH)_2$

Source
Natural basic copper carbonate.

Origin and history
Employed by 4th Dynasty in Egypt. Was the most important blue pigment in European painting from the 15th to the 17th century. Was widely used in wall paintings in Central Asia and in Japan.

Characteristics
Areas of dark, coarsely ground azurite on paintings can often be recognized by their sandy texture and thickness.

Toxicity
Moderately toxic.

Name
Lead white

Code-Kremer
46000

Chemical formula
$2PbCO_3.Pb(OH)_2$

Source
Mineral hydrocerussite

Origin and history
It is the oldest of the whites still used by modern painters. Discovered in antiquity. It is one of the oldest man-made pigments, and its history dates back to the ancient Greeks and Egyptians.

Toxicity
Causes eye and skin irritation. Causes digestive and respiratory tract irritation. May cause central nervous system effects. May cause blood abnormalities. May cause cancer based on animal studies. May cause kidney damage. May cause reproductive and foetal effects.

Name
Titanium dioxide

Code-Kremer
46200

Chemical formula
TiO_2

Source
Minerals anatase and rutile

Origin and history
It is the white of the 20th century. Discovered in 1821, it was massively produced after 1916..

Characteristics
Good covering. Useful in all techniques. Sometimes, it is cut with large quantities of zinc white to improve its drying time and cohesion with oil.

Toxicity
Non toxic

Name
Lithopone

Code-Kremer
46100

Chemical formula
$BaSO_4.ZnS$

Source
Inorganic origin, mineral and synthetic. Compound of sulphate of Barium and sulphur of zinc.

Origin and history
Invented at the end of the 19th century by Guillame-Ferdinande count of Doudet. At the end of the last century it was used as a surrogate of biacca.

Characteristics
It can be used in tempera and in oil. Not advised for encaustic and fresco.

Toxicity
Ingestion and inhalation: extremely toxic. Zinc sulfide might react with stomach acid to produce hydrogen sulfide

Name
Quartz

Code-Kremer
-

Chemical formula
SiO_2

Source
Often found as impurity in gypsum and cinnabar.

Origin and history
Smoky quartz has been used as gemstones and in ornamental and religious objects for thousands of years.

Toxicity
Cancer hazard (contains material which can cause cancer in humans). Risk of cancer depends on duration and level of exposure. May be irritating to skin and eyes. May affect the heart. May damage the lungs.

Name
Gypsum anhydrite

Code-Kremer
58320

Chemical formula
$CaSO_4$

Source
Mineral calcium sulphate

Origin and history
Gypsum plaster has been used as a building material in Persia for more than 2500 years.

Characteristics
The substance commonly known as alabaster is a fine-grained variety of gypsum (calcium sulphate), much used for vases and ornamental objects.
Uses: plaster, wall board, some cements, paint filler, ornamental stone, etc.
Gypsum has a very low thermal conductivity hence it's use in drywall as insulating filler).

Toxicity
Non toxic

Name
Natural gypsum

Code-Kremer
58300

Chemical formula
$CaSO_4.2H_2O$

Name
Gypsum Bologna

Code-Kremer
58150

Chemical Formula
$CaSO_4.2H_2O$

Name
Alabaster

Code-Kremer
58340

Chemical formula
$CaSO_4.2H_2O$

Name
Chalk Kabania

Code-Kremer
58000

Chemical formula
$CaCO_3$

Source
Mineral calcite

Origin and history
Discovered in antiquity and continues in use.

Characteristics
White pigment of limited hiding power, mainly used for painting grounds. Includes other sorts of calcium carbonate whites. Stable under ordinary conditions. Has an excellent lightfastness, incompatible with alkali-sensitive pigments such as Prussian blue.

Toxicity
Non toxic

OCHRE PIGMENTS

Name
Hematite

Code-Kremer
48651

Chemical formula
Fe_2O_3

Source
Iron (III) oxide mineral

Origin and history
Hematite is among the oldest pigments known to humankind and has been used by every major civilization.

Toxicity
Considered non-toxic.

Name
Caput mortum

Code-Kremer
48700

Chemical formula
Fe_2O_3

Source
Iron (III) oxide mineral and small amounts of iron sulfate.

Origin and history
The Latin term caput mortum literally means dead head. It was known since medieval times, but was mainly used in the 16th century.

Characteristics
Common Names: bruno inglese, caput mortem, caput mortum, caput mortuum, colcothar, colore morello, corpum mortum, Côte d'Azur violet, vetriolo romano bruciato, vetriolo cotto

Toxicity
Considered non-toxic,

Name
Caput mortum violet

Code-Kremer
48750

Chemical formula
Fe_2O_3

Source
Iron (III) oxide mineral and small amounts of iron sulfate.

Toxicity
Considered non-toxic, but the dry powder pigment should always be handle with care so as not to inhale the dust.

Name
Red ochre

Code-Kremer
40020

Chemical formula
Fe_2O_3, clay

Source
Iron (III) oxide mineral consisting of silica and clay owing its colour to iron oxide.

Origin and history
Made into paints by prehistoric peoples who painted with their fingers or with vegetable paint brushes.

Characteristics
Found throughout the world, in many shades, in hues from yellow to brown and faint blue. Good hiding power and excellent permanence in all media.

Toxicity
Not considered toxic.

Name
Burnt sienna

Code-Kremer
40430

Chemical formula
Fe_2O_3, Al_2O_3, MnO_2, clay

Source
Minerals goethite and hematite associated with varying proportions of mineral impurities such as clay, chalk and silica.

Origin and history
Prepared by calcining raw sienna which in the process undergoes a great change in hue and depth of colour. In going from ferric hydrate of raw earth to ferric oxide, it turns to a warm, reddish brown.
It has been used as a pigment since prehistoric times.

Toxicity
Not considered toxic.

Name
Yellow ochre

Code-Kremer
40010

Chemical formula
$Fe_2O_3 .H_2O$, clay

Source
Iron (III) oxide mineral consisting of silica and clay owing its colour to iron oxide.

Origin and history
Made into paints by prehistoric peoples who painted with their fingers or with vegetable paint brushes.

Toxicity
Not considered toxic.

2.2. INSTRUMENTS

2.2.1. Polycapillary-based micro X-ray fluorescence spectrometer

Preliminary micro-XRF spectra were collected using a polycapillary based XRF spectrometer which consists of a Kevex PXS4 mini-focus Mo-tube x-ray tube (70 W maximum power, 250 mm anode spot), an XYZ sample translation/rotation stage, an optical microscope and an Si(Li) detector. The distance from the impact point of the electrons on the anode to the Be window of the tube is ca 2.0 cm; the emerging x-rays are focused by a polycapillary lens which is contained in a cylindrical brass holder; the latter is mounted on a five-axis gimbal lens holder (Newport M-LP-05B).

The receiving end of the capillary is placed at a distance that maximizes the transmission through the lens. Fluorescent radiation is detected with a 30 mm^2 Canberra Si(Li) detector (180 eV resolution at Mn K) having a 2.5 cm diameter end-cap. In this case, a polycapillary lens manufactured by the Institute for Low Energy Physics (Beijing Normal University, Beijing, China) was employed. These measurements were performed at the department of chemistry of the Antwerp University, Belgium.

2.2.2. Micro-Raman spectroscopy

Preliminary Raman spectra were collected by a micro-Raman system 1000 from Renishaw. The experimental set-up was kept constant in all spectra recordings of the reference samples. The excitation radiation, produced by a HeNe laser (632.8nm), was directed in an Olympus metallurgical microscope and it was focused on the sample by a 50x long working distance microscope objective. The laser power on the sample was ~2mW. Rayleigh scattering was appropriately rejected by a couple of Notch filters. A 2D CCD detected the Raman signal while the resolution of the monochromator was about 5cm^{-1}. The continuous scan method (in which the angle of the grating continuously changes as each data point is read from the CCD detector) was used and extended spectra covering the -100 - 1800cm-1 spectral range were recorded. The lower wavenumber limit was selected to confirm instrument calibration. In addition, the spectral range was kept constant in all measurements so that the number of data-points per wavenumber was the same in all the recorded spectra. These measurements were performed at Ormylia arts diagnosis centre, Greece.

2.2.3. PRAXIS: combined micro-XRF and micro-Raman instrument

PRAXIS instrument combines Raman and XRF methods in one instrument [25-28]. By using optical elements it is possible for both of them to concentrate the excitation radiation to a small sample area that allows a position sensitive analysis with a spatial resolution in the range of 5 – 50 µm.

That opens possibilities for the analysis of the chemical composition of all elements heavier than Mg with the help of X-ray fluorescence and additionally the analysis of phases and the identification of complex molecules by Raman spectroscopy. During the PRAXIS project two prototypes were developed. All the measurements involved in the present study have been done with the first prototype, located at the chemistry department of the Antwerp University. The second prototype was finished at the end of the project and only some trials with modern pigments have been done which are not included in the present thesis.

In the first prototype, the measuring components are mounted on a head on top of a cabinet. The measuring head contains:

- The x-ray tube (max. 50 kV, 30 W, anode material can be Rh, Mo, W) with a polycapillary lens to concentrate the emitted x-rays to a small spot on the sample. The spot size is approximately 25 µm.
- An SSD x-ray detector for an energy dispersive detection of fluorescence radiation.
- A Raman-head that focuses the laser radiation to the sample capturing the Raman scattered radiation and filters the laser radiation from that response along with a high-mag microscope.
- Two wavelengths for Laser excitation can be used (633 and 785 nm).
- A fiber optic connection of the measuring head to the spectrometer and a compact axial optical spectrometer for these two wavelengths
- The spectral range is 130 cm^{-1} – 3270 cm^{-1} for 633 nm and 130 cm^{-1} – 2240 cm^{-1} for 785 nm.
- The resolution is approximately 3 cm^{-1} /pixel for 633 nm and 2 cm^{-1} /pixel for 785nm.
- A chamber for sample positioning with an X-Y-Z stage (the minimum step size is 1 µm if the stage is X-Y and 1.25 µm for Z.
- An endoscope with low magnification for sample examination.
- Another component is a PC that controls the instruments using a Windows-based program to perform Raman and XRF analyses.

2.3. REFERENCES

[1] J. R. Barnett, S. Miller and E. Pearce, Optics & Laser Technology Colour and Design in the natural and man-made worlds 38, (2006), 445-453.

[2] E. Manzano, A. G. Bueno, A. Gonzalez-Casado and M. del Olmo, Journal of Cultural Heritage 1, (2000), 19-28.

[3] P. Vandenabeele, L. Moens, H. G. M. Edwards and R. Dams, Journal of Raman Spectroscopy 31, (2000), 509-517.

[4] M. Perez-Alonso, K. Castro, I. Martinez-Arkarazo, M. Angulo, M. A. Olazabal and J. M. Madariaga, Analytical and Bioanalytical Chemistry 379, (2004), 42-50.

[5] M. Castillejo, M. Martin, M. Oujja, D. Silva, R. Torres, C. Domingo, J. V. Garcia Ramos and S. Sanchez Cortes, Applied Spectroscopy 55, (2001), 992-998.

[6] U. Casellato, P. A. Vigato, U. Russo and M. Matteini, Journal of Cultural Heritage 1, (2000), 217-232.

[7] M. Elias, C. Chartier, G. Prevot, H. Garay and C. Vignaud, Materials Science and Engineering: B 127, (2006), 70-80.

[8] D. Bikiaris, S. X. Daniilia, S. Sotiropoulou, O. Katsimbiri, E. Pavlidou, A. P. Moutsatsou and Y. Chryssoulakis, Spectrochimica Acta Part a-Molecular and Biomolecular Spectroscopy 56, (2000), 3-18.

[9] J. L. Mortimore, L. J. R. Marshall, M. J. Almond, P. Hollins and W. Matthews, Spectrochimica Acta Part a-Molecular and Biomolecular Spectroscopy 60, (2004), 1179-1188.

[10] D. Hradil, T. Grygar, J. Hradilova and P. Bezdicka, Applied Clay Science 22, (2003), 223-236.

[11] H. G. M. Edwards, L. Drummond and J. Russ, Spectrochimica Acta Part a Molecular and Biomolecular Spectroscopy 54, (1998), 1849-1856.

[12] J. M. Erlandson, J. D. Robertson and C. Descantes, American Antiquity 64, (1999), 517-526.

[13] R. J. H. Clark and P. J. Gibbs, Journal of Raman Spectroscopy 28, (1997), 99&.

[14] M. Uda, S. Sassa, S. Yoshimura, J. Kondo, M. Nakamura, Y. Ban and H. Adachi, Nuclear Instruments and Methods in Physics Research Section B: Beam Interactions with Materials and Atoms 161-163, (2000), 758-761.

[15] L. Burgio and R. J. H. Clark, Journal of Raman Spectroscopy 31, (2000), 395-401.

[16] J. Zuo, X. C. Zhao, R. Wu, G. F. Du, C. Y. Xu and C. S. Wang, Journal of Raman Spectroscopy 34, (2003), 121-125.

[17] R. J. H. Clark, P. J. Gibbs, K. R. Seddon, N. M. Brovenko and Y. A. Petrosyan, Journal of Raman Spectroscopy 28, (1997), 91&.

[18] L. Burgio, R. J. H. Clark and K. Theodoraki, Spectrochimica Acta Part a-Molecular and Biomolecular Spectroscopy 59, (2003), 2371-2389.

[19] L. Burgio, R. J. H. Clark and S. Firth, Analyst 126, (2001), 222-227.

[20] H. G. M. Edwards, F. Rull, P. Vandenabeele, E. M. Newton, L. Moens, J. Medina and C. Garcia, Applied Spectroscopy 55, (2001), 71-76.

[21] H. G. M. Edwards, S. E. J. Villar and K. A. Eremin, Journal of Raman Spectroscopy 35, (2004), 786-795.

[22] D. C. Smith and A. Barbet, Journal of Raman Spectroscopy 30, (1999), 319-324.

[23] S. E. J. Villar and H. G. M. Edwards, Analytical and Bioanalytical Chemistry, (2005).

[24] G. A. Mazzocchin, F. Agnoli, S. Mazzocchin and I. Colpo, Talanta 61, (2003), 565-572.

[25] K. Janssens, Z. Jia, M. V. Gysel and P. V. Espen, PRAXIS: A Combined micro-Raman –micro-XRF Instrument, Euroanalysis XIII, Salamanca, Spain, 6-10 September. (2004).

[26] K. Janssens, J. Sekula, M. Becucci, E. Castellucci, B. Roussel, J. Ostwald, J. Schmalz, A. Bjeoumikhov, N. Langhoff, P. Ramos, I. Ruisánchez and K. Andrikopoulos, Design Of A Combined Micro-Xrf/Micro-Raman Spectrometer, 2nd international conference on the application of Raman spectroscopy in art and archaeology, Ghent, Belgium (2003).

[27] K. Janssens, W. D. Nolf, O. Schalm, B. Vekemans, E. Castellucci, B. Roussel, S. Charonov, J. Schmalz, J. Tilgner, M. Haschke, N. Langhoff, P. Ramos, I. Ruisánchez and K. Andrikopoulos, Praxis: A Combined μ-Xrf/μ-Raman Spectrometer For Use In The Cultural-Heritage Area, 2005 Denver X-ray conference, Colorado Springs, Colorado, USA (2005).

[28] K. Andrikopoulos, S. Daniilia, B. Roussel and K. Janssens, Journal of Raman Spectroscopy submitted, (2006).

3

Chapter 3: Signal processing

This chapter briefly describes the techniques commonly used for signal processing in order to improve the signal-to-noise ratio. This signal processing stage entails de-noising and baseline correction. Wavelet transform is described as a tool for signal de-noising along with its possibilities to remove low frequency signal components. The performance of this methodology as a new tool to remove noise and background components simultaneously is presented in the paper: *Noise and background removal in Raman spectra of ancient pigments using wavelet transform*.

3.1. SIGNAL PROCESSING IN RAMAN AND XRF SPECTRA

The main goal of signal processing is the improvement of signal-to-noise ratio. Ideally, any procedure for signal enhancement should be preceded by a characterization of the noise and the deterministic part of the signal [1].

In Raman spectroscopy the most common tools for signal enhancement are *smoothing by moving average* and *polynomial smoothing*, in the time domain and Fourier transform (FT), in the frequency domain [2].

Filtering and smoothing are related and complementary. Filtering is more complicated because it involves a forward and backward Fourier transform. However, in the frequency domain the noise and signal frequencies are distinguished, allowing the design of a filter that is modelled for these frequency characteristics.

Polynomial smoothing can be seen as a trial error operation. It improves the signal-to-noise ratio but the best smoothing function has to be empirically found. Also, frequency characteristics of the signal can be slightly modified. However, because of its computational simplicity, polynomial smoothing is the preferred method of many instrument manufacturers.

Baseline correction or background removal is performed principally by *multi-point baseline* or *interactive polynomial baseline*. Both algorithms calculate the best fit polynomial to the spectrum baseline and then subtract it from the spectrum.

In XRF, this task is commonly named spectrum evaluation and its purpose is to remove background noise and resolve peak overlaps. This is usually done by least-squares fitting of a mathematical model to the spectral data and results in a list of elemental X-ray intensities per spectrum [3]. These corrections are important when small peaks (of trace elements), situated in the immediate vicinity of very intense lines (of major elements), are to be correctly fitted.

The background in XRF spectra is the result of many processes and therefore can have a complex shape [3]. Hence, it is not impossible to predict this shape by means of an empirical approach. Usually, the background shape is estimated a priori and is subtracted from the spectrum before the actual fitting. Another option is to describe the background shape by a suitable mathematical function, usually a polynomial, and optimize its coefficients together with the other parameters of the fitting model [4, 5].

3.2. WAVELET TRANSFORM

In spectroscopic measurement, the raw spectra are a combination of true readings and noise. In order to extract the true readings (deterministic part of the signal), a digital processing method such as filtering is commonly employed. Methodologies frequently used in micro-Raman and micro-XRF were commented in the previous section. Since 1989, the development of wavelet theory has had a remarkable impact on analytical chemistry. Wavelet filters have been introduced into this area of chemistry for signal de-noising and data compressing. In the last years, wavelet transform (WT) has been used to distinguish important properties from the acquired data, pattern recognition, quantification, background removal, multiscale regression and derivative calculations [1, 6-26].

Generally, WT is superior to Fourier transform (FT) in many aspects. In Fourier analysis, only sine and cosine functions are available as filters. However, many wavelet filter families have been proposed. Furthermore, there is a well-known drawback in FT, since the filters are localized in the frequency domain and the time-information is hidden after transformation. It is impossible to know where a particular feature of the signal takes place. A small frequency change in FT produces changes everywhere in the Fourier domain. On the other hand, wavelet functions are localized both in frequency (or scale) and in time, via dilations and translations of the mother wavelet, respectively. Both time and frequency information are maintained after transformation.

3.2.1. Noise and background removal in Raman spectra of ancient pigments using wavelet transform.

Pablo M Ramos and Itziar Ruisánchez.

Journal of Raman Spectroscopy 36, 2005, 848-856.

Journal of Raman Spectroscopy 36 (2005), 848-856

NOISE AND BACKGROUND REMOVAL IN RAMAN SPECTRA OF ANCIENT PIGMENTS USING WAVELET TRANSFORM

Pablo Manuel Ramos and Itziar Ruisánchez

Department of Analytical Chemistry and Organic Chemistry. Universitat Rovira i Virgili. Campus Sescelades, C/. Marcel·lí Domingo, s/n 43007 Tarragona, SPAIN

Abstract

The wavelet transform is applied to Raman spectra to remove heteroscedastic noise from ancient pigments such as azurite and ultramarine blue. Wavelets from the Daubechies, Coiflet and Symmlet families are evaluated. Two different thresholding strategies on the detail coefficients are applied; the first is a one-dimensional variance adaptive thresholding and the second is a block threshold de-noising. The block thresholding strategy removes the noise and preserves the band shapes best. Background removal during the de-noising process is also investigated and results are very good when the block thresholding strategy is used to suppress background at the optimal level of the de-noising process.

Keywords: Wavelet transform; Heteroscedastic noise; Background; Ancient pigments.

Introduction

Today Raman spectroscopy is widely recognized as a powerful non-destructive technique for characterizing materials. It is particularly well suited to identify ancient pigments in cultural heritage studies [1] because it provides a fingerprint of the material being analysed. Analysing spectra is often difficult because of the presence of noise and background signals. It is also difficult to apply chemometric techniques to this type of data [2, 3] in the presence of non-stationary noise and non-constant varying spectroscopic background.

In Raman spectra from ancient pigments, the major contributor to background noise is the intrinsic fluorescence of the pigment components and binding materials. Considerable effort has been made to improve the spatial resolution of the technique so that small grains of pigment can be analysed with little or no interference from surrounding areas. However, pigment fluorescence is still present, and is usually several orders of magnitude more intense than the weak Raman scattering so the spectrum is completely dominated by fluorescence. Another source of noise to be considered is the detector, as is the case when a charge coupled device detector is used [4]. In the study of pigments, however, noise is usually more sample dependent than detector dependent. One important

cause may be unspecific absorption or radiation by colour or black samples.

Noise removal is an important operation in data processing but today there is no general de-noising strategy. De-noising strategies, including parameter selection, are strongly dependent on the problem ahead. They depend on the signal-to-noise ratio, on the shape of the signals and their superposition, on the resolution of complex overlaid signals, and on the justification or violation of model assumptions regarding noise distribution.

Wavelet transform (WT) is a relatively new de-noising technique which in recent years has been increasingly recognized for its relevance to analytical chemistry [5] and today it is a high-performance signal and image processing technique [6, 7].

Wavelets are functions that are localized in both the time and frequency domains. Because of this property, both the time and frequency characteristics of the signal are captured in WT. A considerable number of WT methods have been applied to the processing of analytical signals [6, 8-13], some of which have proved to be useful for Raman de-noising, spike removal [14], and background removal [15-19]. However, as far as we know, there are no previous studies in the literature on the use of wavelets in Raman studies of pigmented materials.

The aim of this study is to investigate the performance of the WT for the signal de-noising of Raman spectra from pigments studied in the field of cultural heritage. Our main interest is to prove that wavelets can efficiently remove noise around the bands of interest without damaging their shape and area. We use new improvements in WT analysis to achieve the best result, and investigate simultaneous de-noising and background removal.

Theory

Wavelet transform

Wavelet transform (WT) is analogous to (FT), in which sine and cosine are the basis functions. Wavelets are a family of basis functions which are effective at extracting both time and frequency-like information from a time-varying signal. Figure 1 presents the most commonly used wavelet families. The WT splits a signal into localized contributions (details and approximations) labeled by scale and position parameters. The multiresolution wavelet transform algorithm [16, 20] is a procedure that decomposes a signal into orthogonal resolution components at different scales. Each of the contributions at a different scale (or resolution level) gives information about the different frequencies contained in the original signal. In Figure 2, the fine scale features are captured by detail coefficients at fine resolution levels (labeled D_i, where *i=1,2,3…n*). The smooth component is captured by approximation coefficients (A_n). For more wavelet transform theory and applications, two excellent tutorials explain the algorithms in detail [21, 22].

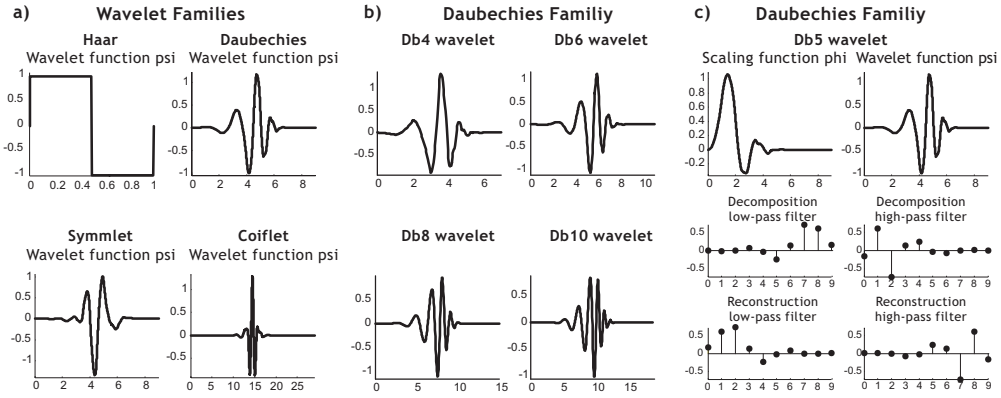

Figure 1. a) Wavelets: Haar (Daubechies 1), Daubechies, Symmlet and Coiflet. **b)** Wavelets from the Daubechies family. **c)** Decomposition and reconstruction, high-pass and low-pass filters for the Daubechies 5 wavelet

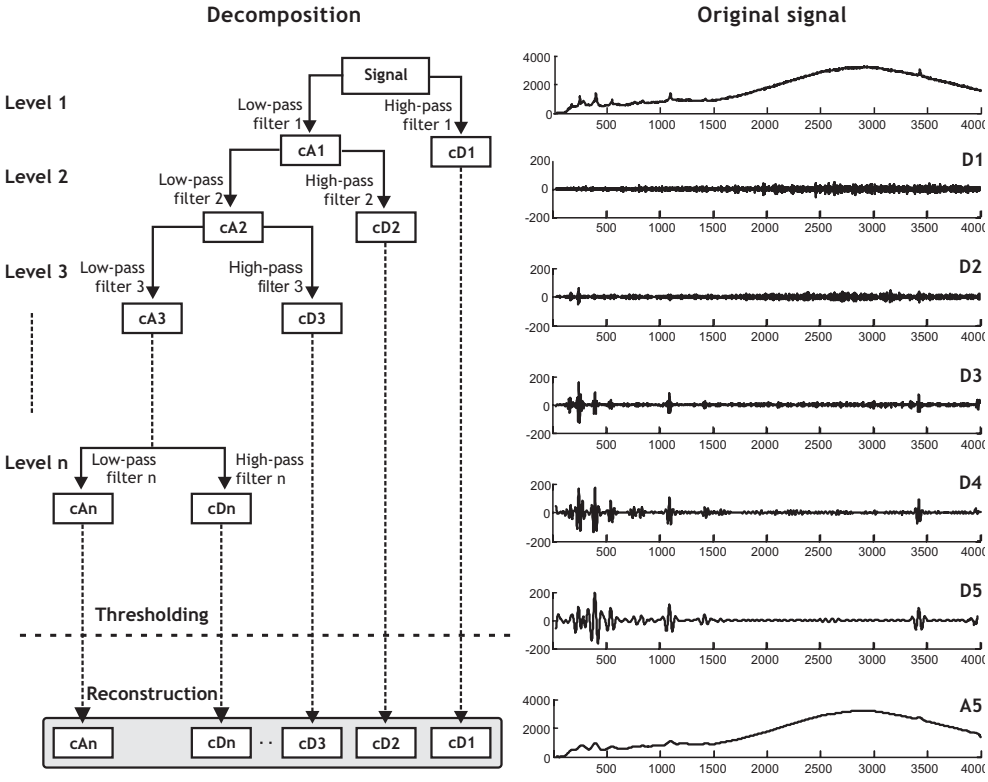

Figure 2. Mallat pyramidal algorithm for the fast decomposition of the DWT. As an example, a signal is decomposed at level 5. D1 to D5 are the detail coefficients while A5 is the approximation coefficients.

Signal processing by WT

Characterization of noise

Proper data filtering requires a good understanding of the nature of noise. In Raman spectroscopy, noise contains contributions from a number of sources, but in dispersive CCD Raman spectrometers noise is usually governed by the sample shot noise limit [4] described in equation 4.

$$noise = \sigma_y = (S + B)^{1/2} \quad (1)$$

Where *S* is the Raman signal and *B* is the background signal.

Different types of noise can be present in a measured spectrum. Depending on the time dependency of its statistics, noise can be classified as stationary (homoscedastic) or non-stationary (heteroscedastic) if any of these statistics is time varying. Raman spectra with minimized instrumental sources of noise and noise controlled by signal and background exhibit non-stationary behaviour. To detect non-stationary noise behaviour, information on the time dependency of the noise is necessary. Since the WT provides information in the time and frequency domain, it is well suited to obtaining this information.

As has been explained in Figure 2, the detail coefficients obtained at the first level of decomposition can be understood as high frequency components and assumed to represent mainly noise. If the amplitude of the detail coefficients is proportional to the signal amplitude, then heteroscedasticity should be suspected [23].

De-noising

Multiscale filtering using wavelets is based on the observation that random noise in a signal is present in all the coefficients while deterministic changes are captured in a small number of relatively large coefficients. Thus, noise is removed by a three-step method:

The noisy signal is transformed into the time-frequency domain by decomposing the signal into a set of orthonormal wavelet basis functions.

The detail coefficients are thresholded by suppressing coefficients below a selected threshold value.

The thresholded coefficients are transformed back into the original domain to obtain the original spectra without the noise.

Threshold selection and thresholding

Selecting the threshold value is a critical step in the filtering process since the accuracy of the reconstructed signal depends on the optimized criterion. Several

methods have been proposed for threshold selection [5]. Standard methods include a level by level time dependent threshold [24] which is the one that is most commonly used in signal denoising. For suppression coefficients there are two main approaches in wavelet transform; hard thresholding and soft thresholding [22]. In addition to these two methods, another recent method also takes into account the information about the neighbouring detail coefficients [25]. The main difference that the authors propose is to threshold the empirical detail coefficients in groups rather than individually [15]. The procedure makes simultaneous decisions to retain or to discard all the coefficients within a block. The thresholding stage that applies this approach is the following; at each resolution level j, the empirical detail coefficients d_{jk} are grouped into disjoint b_i^j of length $L=log\ n$.

Let λ=4.5053 and $S_{ji}^2 = \sum_{(j,k)\in b_i^j} d_{j,k}^2$. Within each block b_i^j, the coefficients are estimated simultaneously via a shrinkage rule (equation 14). The block length L and the thresholding constant λ are chosen on the basis of theoretical considerations [25].

$$d_{j,k} = \left(1 - \lambda L \sigma^2 / S_{ji}^2\right) + d_{j,k} \qquad \text{for all} \qquad (j,k) \in b_i^j \qquad (2)$$

Background removal

Perrin et al. [10] proposed a strategy for removing background and noise simultaneously at the optimal level of decomposition. The approximation coefficients are filtered using a soft thresholding while the detail coefficients are filtered using a hard thresholding. So, to remove background from the spectrum, the approximation coefficients related to the background are set to zero, and those related to the signal are shrunk. This strategy is optimal for signals with a uniform background: however, this is not the case for our Raman signals, which have been proven to have a fluctuating background.

To use this strategy in Raman spectra with fluctuating backgrounds, we propose to use the information obtained during the block thresholding of the detail coefficients. The block thresholding process makes it possible to discriminate the deterministic part of the spectrum in each detail vector. Figure 3 shows five subsets (in grey) of detail coefficients from the vectors D3 to D5 formed with blocks which were not shrunk in the de-noising process and it is easy to see that these subsets correspond to the detail coefficients of the bands of interest. The location of the subsets is then projected onto the approximation coefficients at the last level of decomposition (Figure 3, vector A5). So, those approximation coefficients, which correspond to the deterministic part of the signal, are well localized in the frequency and scale domain. An adapted threshold is defined in order to perform a soft thresholding on the approximation coefficients:

$$a_{j,k} = \begin{cases} sign(a_{j,k})(|a_{j,k}| - T) & |a_{j,k}| > T \\ 0 & |a_{j,k}| \le T \end{cases} \quad (3)$$

$$T = f(k)$$

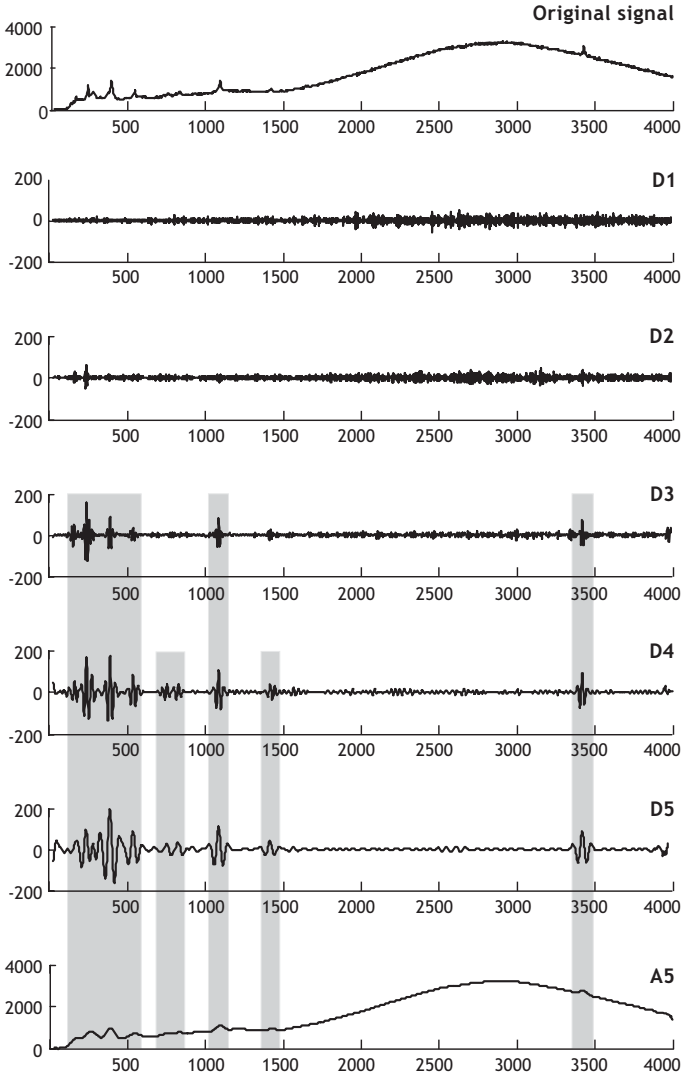

Figure 3. Projection of subsets of blocks obtained from the block thresholding process applied to the Raman spectrum from azurite pigment. Five subsets containing the deterministic part of the signal are shaded in grey in the detail coefficients of D3-D5.

The approximation coefficients at the optimal de-noising level *j* are defined by $a_{j,k}$ where *k=1,2...m* signal points. The threshold level *T* is defined by means of a piecewise cubic *Hermite* interpolation with the approximation coefficients which did not belong to the subsets projected from the detail coefficients. Once both detail and approximation coefficients have been filtered, the signal is reconstructed using the inverse wavelet transform. The novelty of this strategy is that de-noising and background removal in Raman spectra can be performed simultaneously.

Experimental

Two types of Raman spectra have been studied: a simulated noisy Raman spectrum and the Raman spectra of two real and well known ancient pigments (ultramarine blue and azurite).

Simulated spectrum

A simulated spectrum containing four Gaussian peaks of different widths was used to evaluate the performance of the wavelet transform. Background and artificial noise was included depending on the noise characterisation results in the real samples as will be shown later. So a simulated Raman spectrum was produced by adding non-stationary (heteroscedastic) noise (high frequency) and background (low frequency) to an ideal Raman signal emulated by Gaussian functions. Background emulation was performed by means of a polynomial function of degree 7.

Real Raman spectra

Raman spectra from ultramarine blue and azurite ancient pigments, investigated in a cultural heritage study, were collected by a micro-Raman system 1000 from Renishaw. The experimental set-up was kept constant in all the spectra recordings of the reference samples. The excitation radiation, produced by a HeNe laser (632.8nm), was directed by an Olympus metallurgical microscope and it was focused on the sample by a 50x long working distance microscope objective. The laser power on the sample was ~2mW. Rayleigh scattering was appropriately rejected by a couple of Notch filters. A 2D CCD detected the Raman signal while the resolution of the monochromator was about 5cm^{-1}. The continuous scan method (in which the angle of the grating continuously changes as each data point is read from the CCD detector) was used and extended spectra covering the -100 - 1800cm^{-1} spectral range were recorded. The lowest wavenumber limit was selected to confirm the instrument calibration. In addition, the spectral range was kept constant in all

measurements so that the number of data-points per wavenumber was the same in all the recorded spectra.

Programming

All computations and programmed algorithms were performed using Matlab software, version 6.5 for Windows. The wavelet transform applications belong to the wavelet toolbox from Matlab software [24].

Results and discussion

We present the results in two main groups; first the WT de-noising of the spectra and then the simultaneous removal of noise and background from the spectra. Both applications are first applied to the simulated spectrum and then to the two real ones. Before the results are discussed, the methodology followed in each case is presented in detail.

Characterization of noise in real Raman spectra

To determine the characteristics of the noise in the real Raman spectra, the spectra of the two pigments (ultramarine blue and azurite) were decomposed only at the first level. Figure 4 shows the original noisy spectra (4a and 4d, respectively) with the approximation (Figure 4b and 4e) and detail coefficients (Figure 4c and 4f) obtained using the symmlet 8 wavelet. The approximation coefficients are sorted according to their amplitude while the detail coefficients are arranged according to the approximation coefficients to see whether the noise is proportional to the signal. As can be seen proportionality between approximation and detail coefficients can be visually established as the detail coefficients increase along with the increment in the approximation coefficients. Therefore, it can be concluded that noise in our data is heteroscedastic.

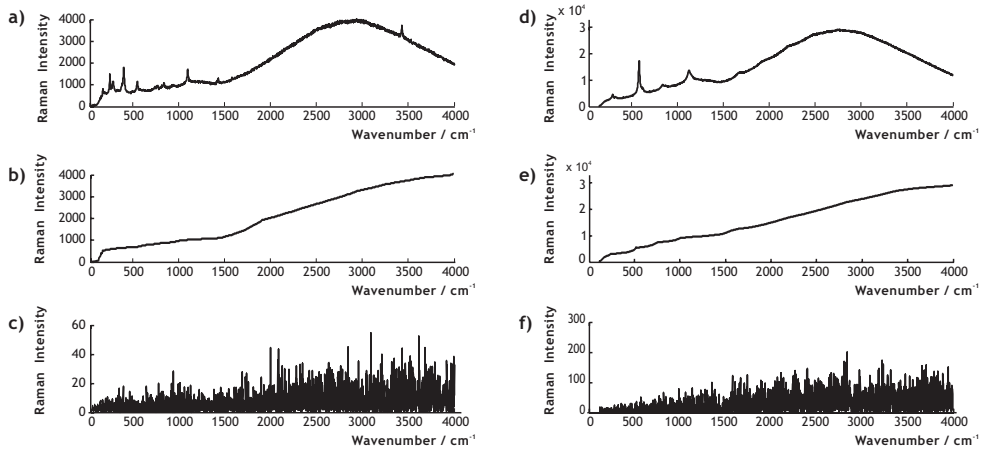

Figure 4. Noise characterization of two Raman spectra from pigments: a) azurite and d) ultramarine blue. b) and e) are the sorted approximation coefficients of azurite and ultramarine, respectively. And finally, c) and f) are the detail coefficients at the first level of decomposition using the symmlet 8 wavelet.

De-noising methodology

Since the noise identified in our Raman spectra is heteroscedastic, we applied two WT de-noising strategies. The first strategy was characterized by a de-noising with an interval dependent threshold. One requirement is that the intervals in which the variance remains constant and the points at which the variance varies, must be known. Then, a level by level time-dependent threshold [24] is defined and, as a consequence, the ability to de-noise non-stationary variance models increases. The second strategy is called block thresholding and uses the information about neighbouring detail coefficients. One requirement is that the noise must follow a normal distribution, so the spectrum must be normalized using the estimated background [25]. The block strategy is summarized in the following three steps.

The total signal is decomposed by the WT using the multiresolution decomposition. The smooth component at the lowest resolution level is the estimated broadband background. An example can be seen in Figure 2 where the smooth component corresponds to *A5*.

The estimated background is subtracted from the signal. Then, the signal is normalised without background, dividing it by the square root of the estimated background spectra. By the end, the noise in the normalized signal is nearly homoscedastic.

The block thresholding procedure is applied to remove noise. The filtered spectrum is renormalised by multiplying it by the square root of the estimated background. In order to evaluate the performance of the de-noising strategies, the estimated background subtracted in step 2 is added.

The performance of the de-noising methodology is evaluated by computing the root mean square (RMS) between the filtered spectrum and the spectrum simulated without noise.

De-noising of simulated data

De-noising the simulated spectrum involves first establishing the proper wavelet level of decomposition and then studying how the type of wavelet influences the process.

The optimal level of decomposition was investigated for the Haar wavelet and the two mentioned de-noising strategies, by calculating the RMS between the filtered and the ideal spectrum at each level of decomposition. Figure 5 shows that with the variance interval strategy the RMS is optimal at level 2 and that at other levels the RMS always increases. These increments indicate that these levels of decomposition have a strong influence on the reconstructed spectrum. So, an excessively deep level of decomposition will result in peak distortion and artifacts. RMS values are better when the block thresholding strategy is applied since the RMS value decreases at each new decomposition level and reaches a stationary minimum at level 7. Local RMS for each of the four simulated bands was also calculated (see Table 1). In general RMS values for each simulated band are very good. A close look shows that the block thresholding strategy provides lower RMS values than the variance change interval (for instance, 0.002 and 0.011 for band 1, respectively).

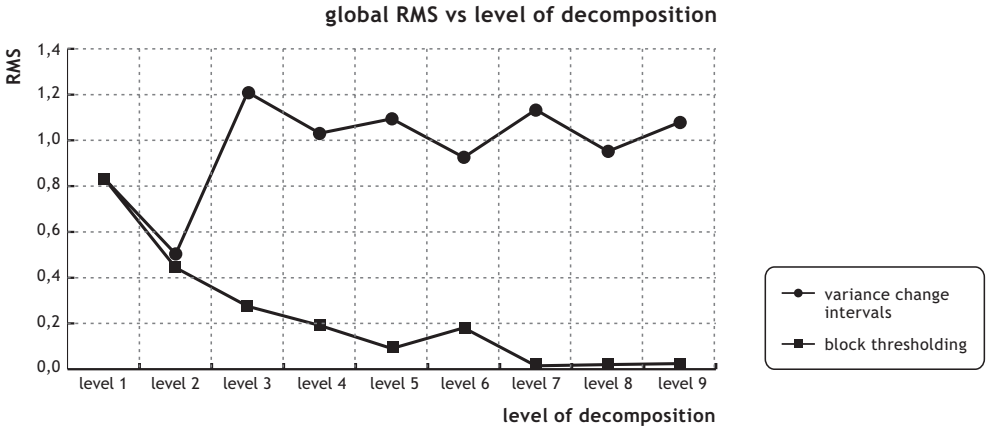

Figure 5. Global RMS study in the two de-noising strategies (the wavelet DB1 is used).

LEVEL	BAND 1		BAND 2		BAND 3		BAND 4	
	VC	BT	VC	BT	VC	BT	VC	BT
1	0.0084	0.0084	0.0115	0.0115	0.0130	0.0130	0.0201	0.0201
2	0.0044	0.0039	0.0076	0.0079	0.0091	0.0085	0.0123	0.0124
3	0.0122	0.0027	0.0163	0.0068	0.0181	0.0071	0.0269	0.0094
4	0.0101	0.0023	0.0134	0.0064	0.0159	0.0063	0.0230	0.0084
5	0.0109	0.0020	0.0148	0.0061	0.0175	0.0054	0.0247	0.0075
6	0.0093	0.0022	0.0126	0.0063	0.0155	0.0062	0.0214	0.0084
7	0.0115	0.0020	0.0153	0.0059	0.0179	0.0047	0.0257	0.0070
8	0.0095	0.0020	0.0133	0.0059	0.0158	0.0048	0.0217	0.0071
9	0.0107	0.0020	0.0147	0.0059	0.0175	0.0048	0.0244	0.0071

Table 1. RMS values for the four Raman bands obtained using the two de-noising strategies: 'VC' variance changes interval de-noising and 'BT' block thresholding. In both, the Haar wavelet was used.

Figure 6 shows the filtered spectra obtained by means of the two de-noising strategies when the levels of decomposition are different. It can be seen that both strategies give good results. However, when the block thresholding is applied at the same level of decomposition, the filtered spectrum is smoother as it gets rid of more noise without changing the width and shape of the Raman bands (Figure 6di, 6dii and 6diii).

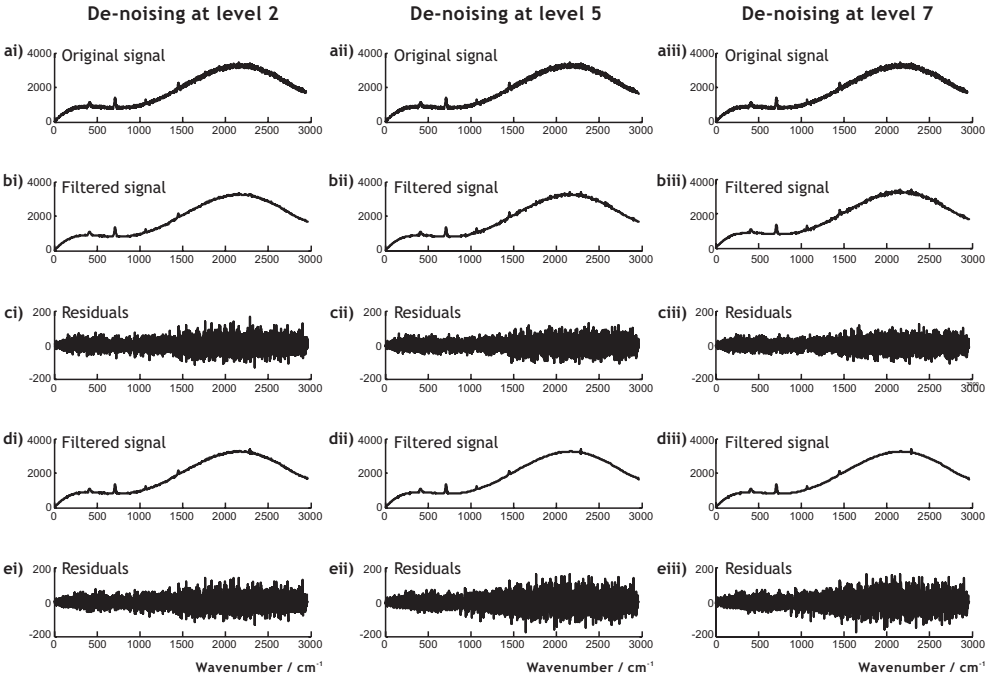

Figure 6. Wavelet de-noising of simulated Raman signals: a) the original signal to be decomposed at levels 2 (ai), 5 (aii) and 7 (aiii); b) the filtered signals at each level using the variance change intervals strategy and c) the corresponding vector of differences between the filtered and the original signal; d), filtered signals at each level using the block thresholding strategy and e) the corresponding vector of differences between the filtered and the original signal.

To determine the most appropriate wavelet for processing the type of signals involved in the study, we studied how each one affected the reconstructed signal at the optimal level of decomposition. A total of 23 different filters from different families (Daubechies, Coiflet, Symmlet) were evaluated by plotting the RMS values (Figure 7). When the variance change intervals were applied at level 2 (Figure 7a), there were no significant differences in any of the four spectroscopic bands. In the block thresholding strategy (Figure 7b and 7c), results significantly improved when the Haar (Db1), Db10 and Db20 wavelets were used.

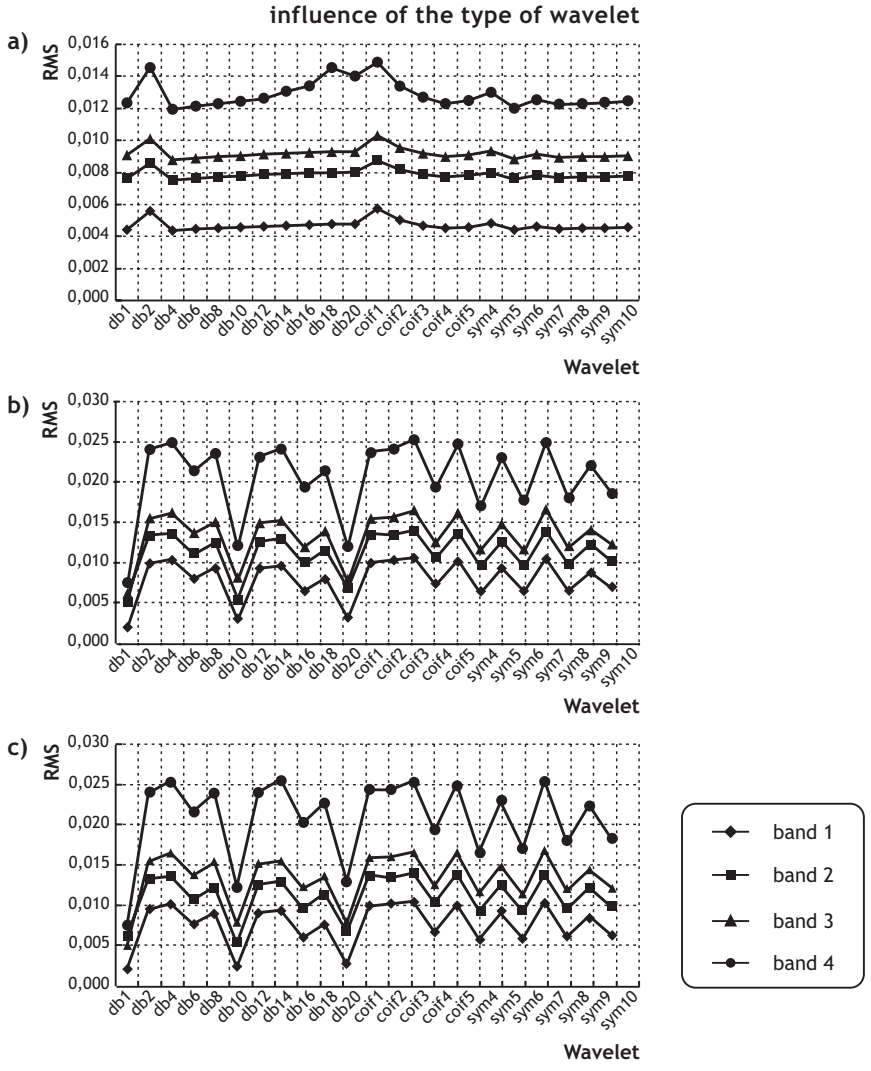

Figure 7. RMS of each individual band obtained using different wavelets. a) Variance change intervals at level 2, b) Block thresholding strategy at levels 5 and c) Block thresholding strategy at level 7.

De-noising of real Raman spectra

Real Raman spectra are de-noised using the two strategies studied with simulated data. The optimal level of decomposition is 5 for the Raman spectrum of azurite and 7 for the Raman spectrum of ultramarine blue (Figure 8). The filtered spectrum provided by both strategies is very satisfactory because noise removal is very good in both cases and the band shapes of the original spectra are preserved. The graphs of residual values (ci, cii and ei, eii) show that the block thresholding strategy de-noises Raman spectra contaminated with heteroscedastic noise most efficiently.

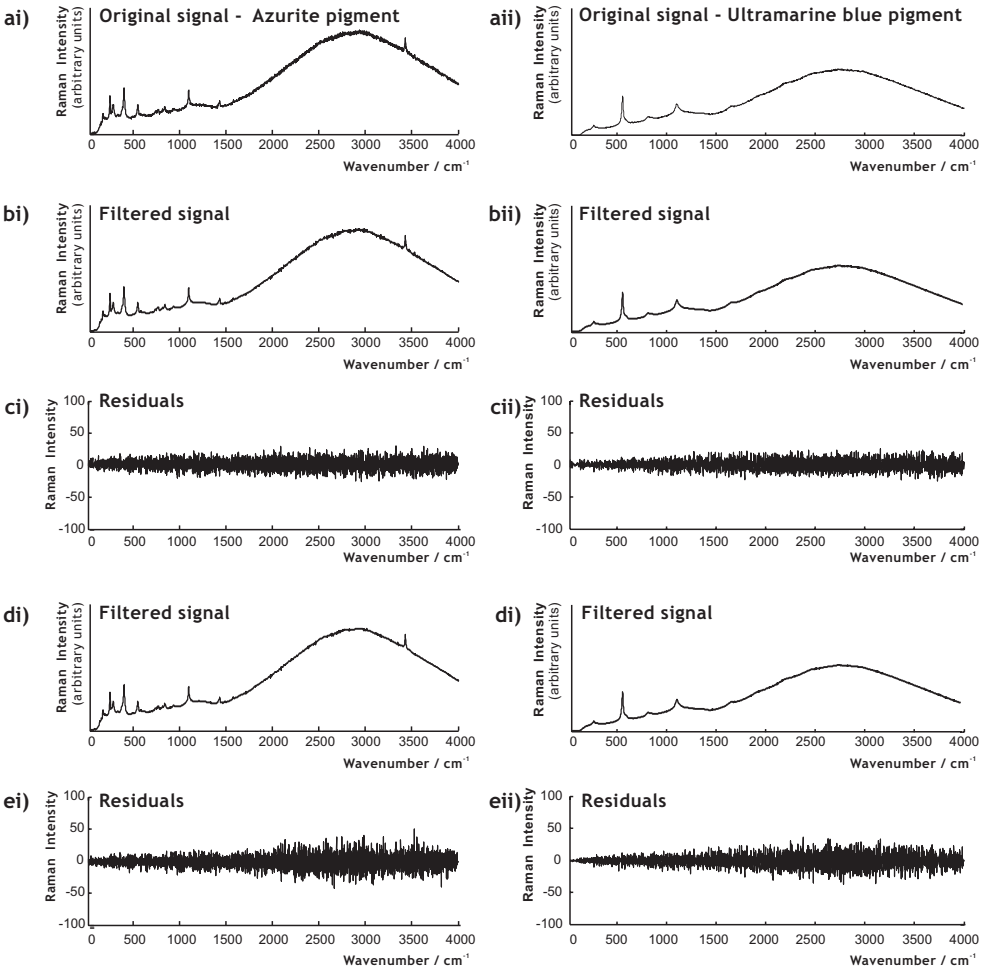

Figure 8. Wavelet de-noising. a) original spectrum from two ancient pigments, azurite (ai) and ultramarine blue (aii); b), reconstructed spectrum and c) vector of differences using the variance change intervals strategy; d) reconstructed signal and e) vector of differences using the block thresholding strategy. For both strategies the Symmlet 8 wavelet was used.

Simultaneous de-noising and background removal

As an example of the results that can be obtained when the background removal strategy discussed above is applied, Figure 9 shows the filtered spectra for the three Raman spectra studied: simulated, ultramarine blue and azurite. The three signals were processed using the Db10 wavelet at decomposition level 7. As it can be seen, each plot shows the original (black) and the filtered (grey) spectra. In all cases, in the simulated and two real spectra, the background is not constant and consists of a few broad bands at the higher wavelengths. The simulated spectrum is the one that has most noise, followed by azurite and ultramarine blue. And in all three cases, in addition to the noise removal, the main background is removed during the de-noising process. As a result, the Raman spectra have no noise or background, and it can be seen that there are no variations in the shape and position of the Raman bands and that such band features as height are well preserved.

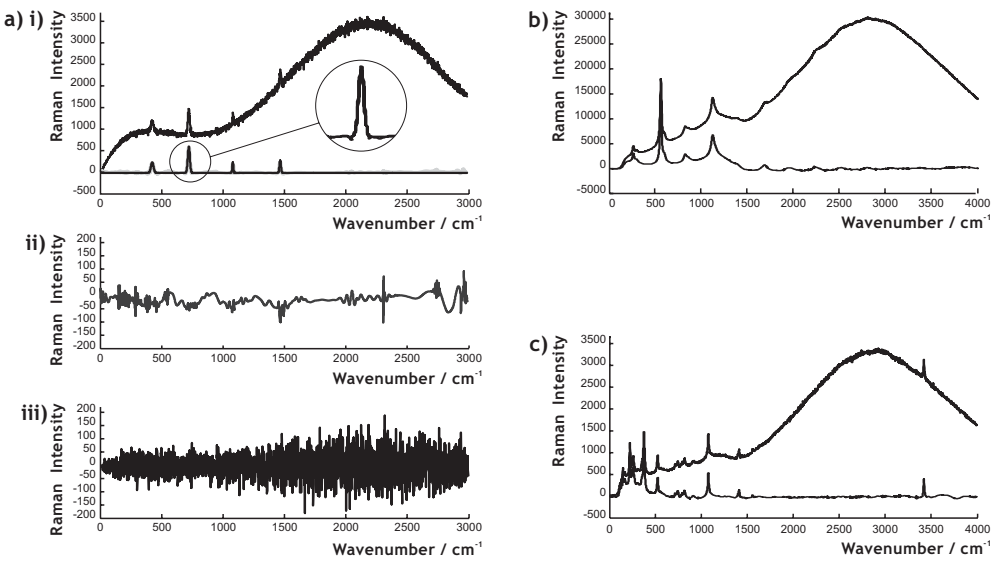

Figure 9. De-noising and simultaneous background removal by means of WT. a) i) simulated spectrum with heteroscedastic noise and background added, the filtered spectrum obtained and the background, noise free simulated signal. ii) Vector of differences between the simulated spectrum (without noise and background) and the filtered spectrum. iii) Original simulated noise. b) Raman spectrum from ultramarine blue pigment, original and filtered and c) Raman spectrum from azurite pigment, original and filtered.

Conclusion

The potential of wavelet transform for de-noising Raman spectra from pigments has been evaluated. The block thresholding strategy has proved to be very efficient at handling the heteroscedastic noise that is usually found in this type of samples inspected by Raman spectroscopy.

The results of de-noising and simultaneous background removal by means of a block thresholding strategy are very satisfactory in both simulated and real signals because noise can be efficiently removed around bands without damaging their shape and area. A combination of de-noising and background removal should improve classification applications and the application of multivariate tools in this type of sample studies.

Acknowledgement

The authors gratefully acknowledge the financial support from the European Community Project, Competitive and Sustainable growth program (G6RD-CT2001-00602). The authors also wish to thank Konstantinos S. Andrikopoulos for providing reference samples and helpful comments.

References

[1] P. Vandenabeele, Journal of Raman Spectroscopy 35, (2004), 607-609.

[2] P. M. Ramos, J. Ferre, I. Ruisanchez and K. S. Andrikopoulos, Applied Spectroscopy 58, (2004), 848-854.

[3] T. L. Weis, Y. N. Jiang and E. R. Grant, Journal of Raman Spectroscopy 35, (2004), 813-818.

[4] R. L. McCreery, Raman Spectroscopy for Chemical Analysis; John Wiley & Sons, Inc: Ohio, United States, (2000).

[5] B. Walczak, Wavelets in Chemistry; Elsevier, (2000).

[6] X. G. Shao, A. K. M. Leung and F. T. Cau, Accounts of Chemical Research 36, (2003), 276-283.

[7] F. Ehrentreich, Analytical and Bioanalytical Chemistry 372, (2002), 115-121.

[8] W. S. Cai, L. Y. Wang, Z. X. Pan, J. Zuo, C. Y. Xu and X. G. Shao, Journal of Raman Spectroscopy 32, (2001), 207-209.

[9] X. N. Li, Y. Z. Liang and F. T. Chau, Chemometrics and Intelligent Laboratory Systems 63, (2002), 139-153.

[10] C. Perrin, B. Walczak and D. L. Massart, Analytical Chemistry 73, (2001), 4903-4917.

[11] V. J. Barclay, R. F. Bonner and I. P. Hamilton, Analytical Chemistry 69, (1997), 78-90.

[12] C. S. Cai and P. D. Harrington, Journal of Chemical Information and Computer Sciences 38, (1998), 1161-1170.

[13] X. G. Shao, L. M. Shao and G. W. Zhao, Analytical Communications 35, (1998), 135-137.

[14] F. Ehrentreich and L. Summchen, Analytical Chemistry 73, (2001), 4364-4373.

[15] T. T. Cai, D. M. Zhang and D. Ben-Amotz, Applied Spectroscopy 55, (2001), 1124-1130.

[16] H. W. Tan and S. D. Brown, Journal of Chemometrics 16, (2002), 228-240.

[17] D. Chen, X. G. Shao, B. Hu and Q. D. Su, Analytica Chimica Acta 511, (2004), 37-45.

[18] C. R. Mittermayr, H. W. Tan and S. D. Brown, Applied Spectroscopy 55, (2001), 827-833.

[19] C. X. Ma and X. G. Shao, Journal of Chemical Information and Computer Sciences 44, (2004), 907-911.

[20] S. G. Mallat, Pattern Analysis and Machine Intelligence, IEEE Transactions on 11, (1989), 674-693.

[21] B. Walczac and D. L. Massart, Chemometrics and Intelligent Laboratory Systems 36, (1997), 81-94.

[22] B. K. Alsberg, A. M. Woodward and D. B. Kell, Chemometrics and Intelligent Laboratory Systems 37, (1997), 215-239.

[23] C. R. Mittermayr, E. Rosenberg and M. Grasserbauer, Analytical Communications 2, (1997), 73-75.

[24] M. Misiti, Y. Misiti, G. Oppenheim and J.-M. Poggi, Wavelet toolbox user's guide; The MathWorks, Inc., (2000).

[25] T. T. Cai, Statistica Sinica 12, (2002), 1241-1273.

3.2.2. Wavelet processing in X-ray fluorescence spectra

Introduction

One of the main advantages of WT is multi-resolution. It provides a concise framework for explaining many aspects of wavelet theory. WT allows us to represent signals at different scales or resolutions. At the coarse level, only the most prominent large features can be seen, whereas at higher levels finer details are captured. Raman and XRF data are multiscale in nature due to deterministic features occurring at different resolutions and stochastic measurements with varying contributions over time and frequency.

A proper analysis of that kind of data requires their representation at multiple resolutions. Such representation can be achieved by expressing the signal as a weighted sum of orthonormal basis functions defined in the time-frequency space such as wavelets. Raman and XRF signal may be represented at multiple scales by decomposition on a family of wavelets and scaling functions. In Figure 3.1 the XRF spectrum of pigment cinnabar (HgS) is shown along the corresponding wavelet tree or wavelet prism. The original spectrum (S) can be represented as the sum of all detail spectra (D_i) and the last scaled spectrum (A8).

$$S = A8 + D8 + D7 + D6 + D5 + D4 + D3 + D2 + D1 \qquad (1)$$

This decomposition results in a complete binary tree of basis functions that covers a wide variety of time-frequency localizations and shapes.

Classification can be performed at different levels of resolution in order to avoid low frequency components present in the signals, and also to detect when certain patterns change significantly in a particular scale. These benefits are investigated and discussed in chapter 6 of this thesis.

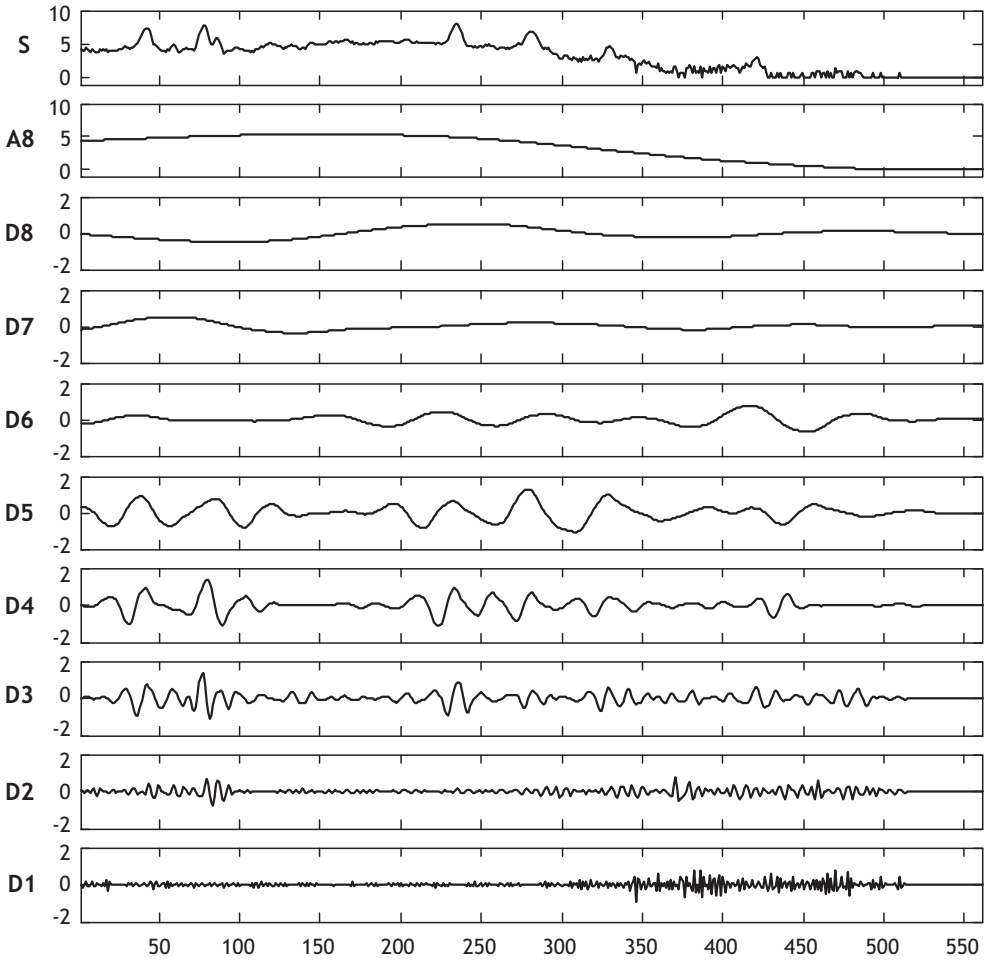

Figure 3.1. Multi-resolution decomposition: the original signal *S* is the XRF spectrum of cinnabar pigment and decomposition is performed until level 8 with wavelet Db7.

Signal de-noising

Real XRF spectra are de-noised using the algorithms described in the previous section for Raman data. The dataset consists of four XRF spectra of caput mortum violet pigment samples. The level of decomposition used is 4 and the wavelet basis used is the Db 4. Preliminary results of filtered spectra were very satisfactory: noise was totally removed while the band shapes of the original spectra were preserved (See Figure 3.2).

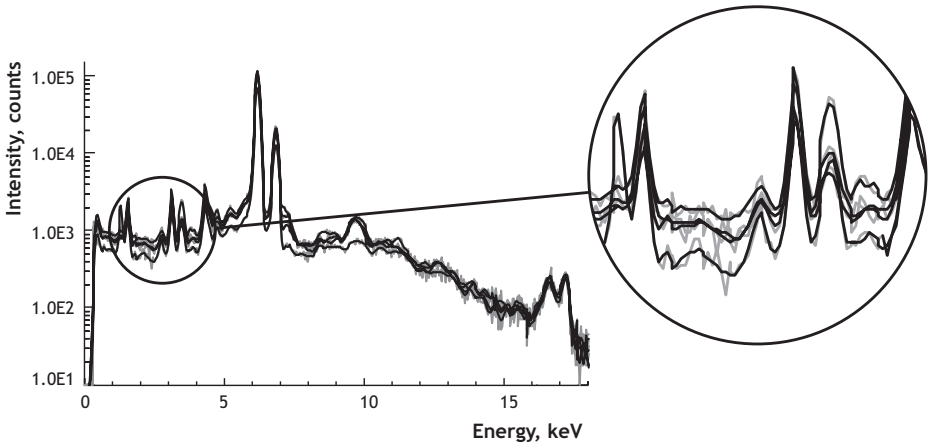

Figure 3.2. Wavelet de-noising performed on four XRF spectra of caput mortum violet pigment. The WT decomposition was performed up to level 4 using wavelet Db5.

Background estimation

The capabilities of WT to remove background components in XRF spectra will be given by statistical evaluation of prediction results obtained for the composition of reference standard samples. In this thesis, XRF spectra are used to improve qualitative analysis of pigment samples. Although the main purpose of XRF analysis is to achieve an elementary composition of a sample, in our particular case XRF spectra are used in a fingerprint model and therefore the elementary composition is not extracted.

The XRF dataset of ochre pigments was used to evaluate background correction by means of WT. The main background is removed during the de-noising process. In Figure 3.3 it can be seen that there are no variations in the shape and position of the XRF bands and that such minor peak features are well preserved.

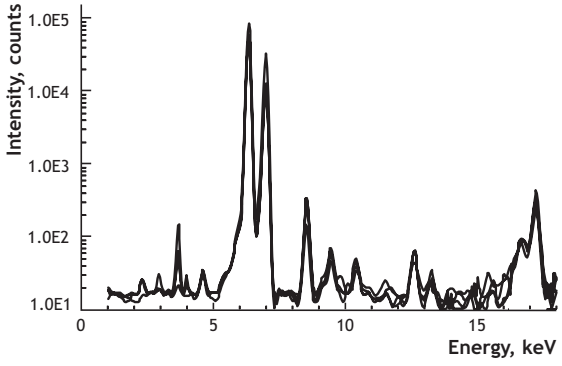

Figure 3.3. De-noising and suppression of background signal components, by means of WT, onto a set of 4 XRF spectra of caput mortum violet pigment. The WT decomposition is performed at level 7 with wavelet Db9.

Preliminary results indicate that WT could be a good complement for background estimation in XRF data. As we discussed in the previous section, XRF spectra are the result of many processes which can produce a very complex shape modelled by using linear or exponential power series, or a linear combination of mutually orthogonal polynomials.

3.3. REFERENCES

[1] P. M. Ramos and I. Ruisánchez, Journal of Raman Spectroscopy 36, (2005), 848-856.

[2] D. L. Massart, B. G. M. Vandeginste, L. M. C. Buydens, S. D. Jong, P. J. Lewi and J. Smeyers-Verbeke, Handbook of Chemometrics and Qualimetrics: Part B; Elsevier, 1998

[3] K. H. A. Janssens, F. C. V. Adams and A. Rindby, Microscopic X-ray Fluorescence Analysis; John Wiley & Sons, LTD, (2000).

[4] Shengxiang Bao, X-Ray Spectrometry 28, (1999), 141-144.

[5] B. Vekemans, K. Janssens, L. Vincze, F. Adams and P. VanEspen, Spectrochimica Acta Part B Atomic Spectroscopy 50, (1995), 149-169.

[6] B. K. Alsberg, A. M. Woodward, M. K. Winson, J. Rowland and D. B. Kell, Analyst 122, (1997), 645-652.

[7] V. J. Barclay, R. F. Bonner and I. P. Hamilton, Analytical Chemistry 69, (1997), 78-90.

[8] C. S. Cai and P. D. Harrington, Journal of Chemical Information and Computer Sciences 38, (1998), 1161-1170.

[9] W. D. Cao, X. Y. Chen, X. R. Yang and E. K. Wang, Electrophoresis 24, (2003), 3124-3130.

[10] F. T. Chau, T. M. Shih, J. B. Gao and C. K. Chan, Applied Spectroscopy 50, (1996), 339-348.

[11] F. T. Chau, J. B. Gao, T. M. Shih and J. Wang, Applied Spectroscopy 51, (1997), 649-659.

[12] F. Ehrentreich and L. Summchen, Analytical Chemistry 73, (2001), 4364-4373.

[13] F. Ehrentreich, Analytical and Bioanalytical Chemistry 372, (2002), 115-121.

[14] X. N. Li, Y. Z. Liang and F. T. Chau, Chemometrics and Intelligent Laboratory Systems 63, (2002), 139-153.

[15] B. F. Liu, Y. Sera, N. Matsubara, K. Otsuka and S. Terabe, Electrophoresis 24, (2003), 3260-3265.

[16] C. R. Mittermayr, S. G. Nikolov, H. Hutter and M. Grasserbauer, Chemometrics and Intelligent Laboratory Systems 34, (1996), 187-202.

[17] B. K. Alsberg, Journal of Chemometrics 14, (2000), 529-539.

[18] B. R. Bakshi, Journal of Chemometrics 13, (1999), 415-434.

[19] W. S. Cai, L. Y. Wang, Z. X. Pan, J. Zuo, C. Y. Xu and X. G. Shao, Journal of Raman Spectroscopy 32, (2001), 207-209.

[20] X. G. Shao, L. M. Shao and G. W. Zhao, Analytical Communications 35, (1998), 135-137.

[21] X. G. Shao, W. S. Cai, P. Y. Sun, M. S. Zhang and G. W. Zhao, Analytical Chemistry 69, (1997), 1722-1725.

[22] C. L. Stork, D. J. Veltkamp and B. R. Kowalski, Applied Spectroscopy 52, (1998), 1348-1352.

[23] B. Walczac and D. L. Massart, Chemometrics and Intelligent Laboratory Systems 36, (1997), 81-94.

[24] B. Walczak, B. vandenBogaert and D. L. Massart, Analytical Chemistry 68, (1996), 1742-1747.

[25] D. Chen, X. G. Shao, B. Hu and Q. D. Su, Analytica Chimica Acta 511, (2004), 37-45.

[26] X. G. Shao and C. X. Ma, Chemometrics and Intelligent Laboratory Systems 69, (2003), 157-165.

4

Chapter 4: Soft computing processing

This chapter describes two fuzzy logic models for pigment identification. The first one is intended for discrimination of pigments studied by Raman spectroscopy. The performance of this methodology as a new tool to process Raman data automatically is presented in the paper: *Fuzzy Logic for Identifying Pigments Studied by Raman Spectroscopy*. The second one incorporates the XRF information to improve the first Raman model; therefore, a Raman-XRF fuzzy logic model is developed. Fuzzy logic models are fully described and the results obtained are discussed. Finally, benefits and drawbacks of these methodologies are presented.

4.1. INTRODUCTION

Interpretation of Raman spectra of pigments may be managed in many cases without relying on reference substances. The qualitative interpretation of Raman spectra on the basis of the recognised relations between molecular structure and spectroscopic features is the domain of the expert spectroscopist.

Additional information regarding the structure and spectral properties of the compounds can be added to the model. This information usually exists as knowledge or experience of spectroscopists and is not available in reference books. One of the key features of fuzzy logic is its ability to deal with these types of knowledge as well as with its typical uncertainty. For that reason, fuzzy techniques have a better chance than traditional approaches to become a fundamental component of any intelligent instrumentation system [1-4].

The subject of this section is the design of a fuzzy model for data fusion and classification. This approach attempts to provide a more complete representation of the information with regard to the relations between structure and information extracted from Raman and XRF spectra [5-12].

4.2. Fuzzy logic for identifying pigments studied by Raman spectroscopy.

Pablo M Ramos[1], Joan Ferré[1], Itziar Ruisánchez[1] and Konstantinos S. Andrikopoulos[2].

1. *Department of Analytical Chemistry and Organic Chemistry. Rovira i Virgili University. Campus Sescelades, C/. Marcel·lí Domingo, s/n 43007 Tarragona, Spain*
2. *"Ormylia" Art Diagnosis Center, Sacred Convent of the Annunciation IMSP Ormylia-Chalkidiki, EL-63071 Ormylia, Greece*

Applied Spectrocopy 58, 2004, 848-854.

Applied Spectroscopy 58 (2004), 848-854

FUZZY LOGIC FOR IDENTIFYING PIGMENTS STUDIED BY RAMAN SPECTROSCOPY

Pablo Manuel Ramos, Joan Ferré and Itziar Ruisánchez

Department of Analytical Chemistry and Organic Chemistry. Universitat Rovira i Virgili, Pl. Imperial 1, 43005, Tarragona (Spain).

Konstantinos S. Andrikopoulos

"Ormylia" Art Diagnosis Centre, Sacred Convent of the Annunciation IMSP Ormylia-Chalkidiki EL-63071 Ormylia (Greece).

Abstract

Fuzzy logic and linguistic variables are used for the automatic interpretation of Raman spectra obtained from pigments found in cultural heritage art objects. Featured bands are extracted from a Raman spectrum of a reference pigment and the methodology for constructing the library is illustrated. An unknown spectrum is then interpreted automatically and a process for identifying the corresponding pigment is described. A reference library consisting of 32 pigments was built and the effectiveness of the algorithm was tested by the Raman spectroscopic analysis of 10 pigments that are known to have been extensively used in Byzantine hagiography. Binary mixtures of these pigments were also tested. The algorithm's level of identification was good even though extra peaks, noise and background signals were encountered in the spectra.

Index headings: Micro-Raman spectroscopy; Fuzzy logic; Identification algorithm; Ancient pigments; Spectral identification.

Introduction

In recent decades the applications of micro-Raman spectroscopy to the study of pictorial materials have increased considerably [1-9]. It is particularly well suited to identifying ancient pigments in cultural heritage studies since it provides a fingerprint of the material being analysed [10]. The ever increasing contribution of Raman spectroscopy to the study of works of art can be partially ascribed to the major improvements that have been, or are being, made to the configuration of Raman instrumentation. The development of portable instruments [11] for the *in situ* measurements and the collection of appropriate information in a non-destructive way [1] have a particularly important role in these improvements.

The Raman spectra of pigments obtained *in situ* from paintings often interfere

quite strongly with fluorescence backgrounds, signals from possible varnish [12] and extra peaks from impurities. So, a direct comparison between reference spectra of pure powdered pigments and spectra obtained directly from the painting is not enough for automatic identification. Moreover, generally speaking, band wavelengths can shift and band heights can change because they depend on instrumental parameters such as laser intensity, light polarisation, excitation wavelength etc. as well as the physicochemical parameters of the materials studied such as grain size, crystal quality, impurities, etc,. Therefore, the identification of a pigment is a process in which data are usually vague and uncertain. Indeed, Raman spectra are subjectively interpreted by experienced analysts on the basis of the recognized relations between molecular structures and spectroscopic features. The human expert strategy for identifying pigments generally starts by selecting a group of possible pigment(s) candidates based on the most intense or main band appearing in the collected spectrum. The final decision is then made by inspecting the remaining bands and taking into account the differences between the band intensities and wavenumbers with respect to the reference spectrum.

Clearly fuzzy logic can handle this task. Fuzzy logic is a soft computing technique, which provides flexible information processing capabilities for handling ambiguous situations in real life. Its aim is to exploit the tolerance of imprecision, uncertainty, approximate reasoning and partial truth in order to achieve tractability, robustness, low cost solutions and close resemblance to the making of human-like decision.

In this article, we describe the development of a fuzzy logic system for automatically identifying pigments from Raman spectra. The algorithm will improve the benefits of a portable instrument. The system is designed as a software complement in a portable micro-Raman instrument for studying cultural heritage. First, we discuss how featured bands are extracted from a Raman spectrum obtained from a reference pigment and illustrate the methodology for constructing the reference library. Second, we describe the automatic interpretation of an unknown spectrum and the corresponding pigment identification process. An important issue in this step is to use the fuzzy system to take into account the uncertainty associated to the band wavenumber and intensity. In the final section, we discuss the limitations and improvements found in the system.

Fuzzy logic elements

Fuzzy theory, introduced by Zadeh [13], is a powerful and general technology for processing information. It has a considerable number of applications in areas such as control systems [14], pattern recognition [15], signal processing [16] and data classifications [17]. Among others, Otto has made an excellent survey of

fuzzy theory and applications in analytical chemistry [18]. One of the reasons for the success of fuzzy expert systems in instrumentation and control is their flexible representation of human decision making. Fuzzy theory allows the user to specify concepts and rules by use of linguistic variables which address the intrinsic imprecision of a physical system.

A fuzzy set can be considered as an extension of a classical "crisp" set. Crisp sets permit only full or no membership, while fuzzy logic permits partial membership. A fuzzy set, say A, defined in the domain U, is described by a membership function m_A which maps to the real interval [0,1]. For each $u \in U$, $m_A(u)$ gives the degree of membership of u to the set A, where 1 denotes full membership and 0 denotes no membership. A membership function $m_A(u)$, which characterises a spectrum feature, may be described by a vector $m_A(u)=[m_A(u_1),m_A(u_2),\ldots,m_A(u_n)]$ or by a graph of $m_A(u)$. In Figure 1a, the membership function $m_A(u_i)$, is used to describe imprecision at each peak wavenumber of the spectra [18].

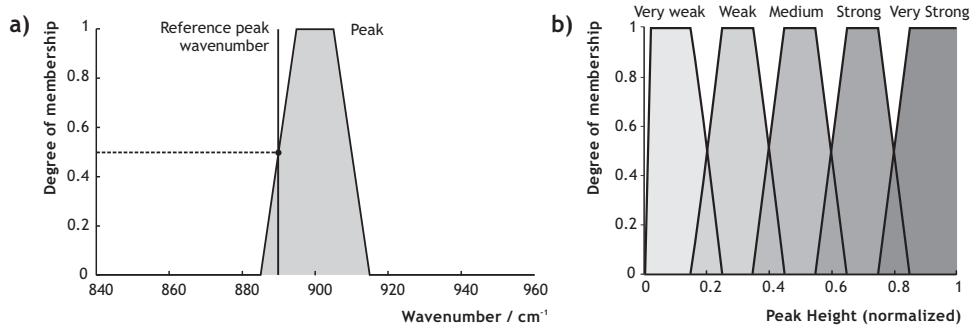

Figure 1. Fuzzy membership functions for feature data extraction. **(a)** Trapezoidal membership functions for peak wavenumber evaluation and **(b)** linguistic variables used to categorize the band intensity.

Fuzzy sets are often identified by linguistic labels, which enable computer programs to store and process vague and verbally described knowledge [19]. A linguistic variable, as its name suggests, is a variable whose values are words or sentences in a natural or synthetic language. For example *"intensity"* is a linguistic variable often used by analysts. In general, the values of a linguistic variable can be generated by a context-free grammar from a primary term (for example *"weak"*), its antonym (*"strong"*), a collection of modifiers (*"very"*, *"not"*, *"quite"*, etc.) and the connectives "and" and "or". In Figure 1b, Raman intensity has been represented by five linguistic variables, "weak", "very weak" and "medium", "strong" and "very strong". The intensity is given in absolute Raman intensity units and normalised to the range [0, 1]. A fuzzy system is a non-linear mapping of a set of input variables to an output variable, defined by the set of fuzzy rules. The inference mechanism is the process which numerically evaluates the information embedded in the fuzzy rulebase system in order to yield the final result.

Algorithm pigment identification

The first step in the identification algorithm is the extraction of the input data: that is to say, the Raman bands that will be used in the fuzzy system to perform the automatic identification. The crisp set consisting of the input data from the unknown pigment is then fuzzified, which means that membership functions are used to evaluate the wavenumber and height of the Raman bands, as described in Figure 1. The fuzzy identification rules of the algorithm are based on the reference library and knowledge from human experts. Finally, the fuzzy system gives an output by means of the de-fuzzification process. The output result is discrete and indicates whether the unknown pigment is in the reference library or not. Figure 2a shows a scheme of the whole procedure and Figure 2b shows the basic configuration of the system with the fuzzy terms associated to each step.

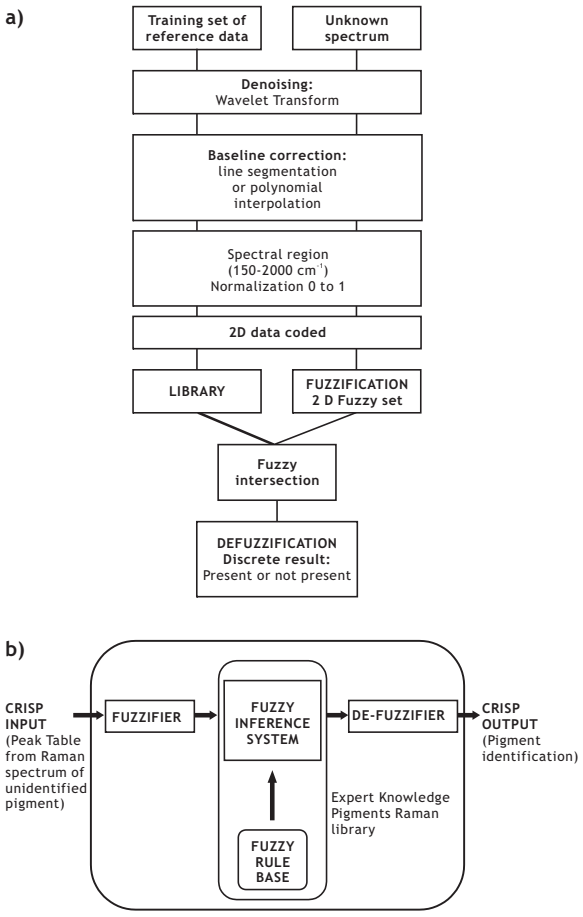

Figure 2. (a) Steps of the identification algorithm for both the reference library and unknown pigment identification. (**b)** Basic configuration and terminology of the fuzzy system.

Pre-processing

Before the fuzzy procedure is applied, a previous denoising process is necessary along with a baseline correction to remove background signals usually caused by fluorescence. Noise was suppressed using the wavelet transform [20, 21] which is a method that is well suited to eliminate noise signal while maintaining the shape of the band of interest. The wavelet transform first decomposes the signal into groups of frequencies. The signal is then reconstructed and the high frequencies associated to noise removed. The advantage of the wavelet transform is that it is easy to implement for an automated pre-treatment. In this study, we used the "Coiflet 5" wavelet, although the user is able to select the level of decomposition depending on the level of noise.

Baseline correction can be performed by polynomial interpolation or line segmentation. The algorithm gives an initial estimate of the points for the baseline correction but also makes manual correction by the user possible.

Data coding

Peak picking is performed manually. The user selects the Raman bands that are considered to be characteristic of the compound. The wavenumber and intensity of each band are thus extracted. The intensity is then stored in linguistic variables by a fuzzy system, which categorizes them in such terms as *"very weak"*, *"weak"*, *"medium"*, *"strong"* and *"very strong"*. Now the peak wavenumber and the verbal term of intensity are the co-ordinates of a two-dimensional crisp set where the membership function $m(x,y)$ has a value of 1 when x is equal to peak wavenumber and y is equal to peak intensity. Otherwise $m(x,y)$ is 0. Figure 3 illustrates the complete process for a reference pigment that belongs to the library.

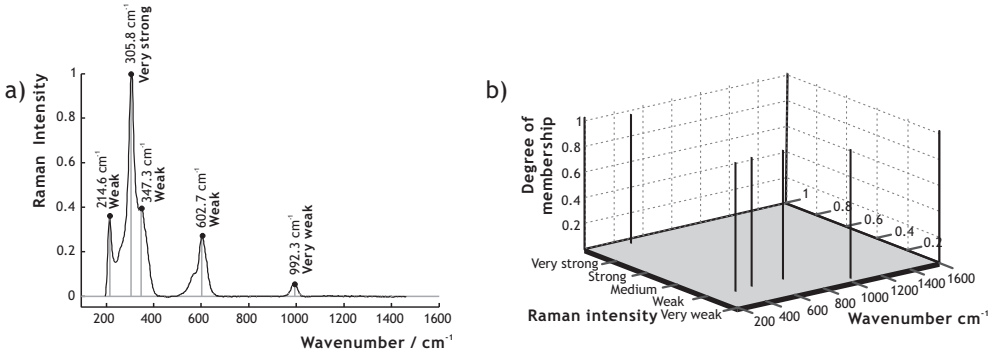

Figure 3. a) Peak wavenumber and intensity (in linguistic terms) extracted from the original spectra, **b)** 2-dimensional data coding (crisp set) depending on wavenumber and intensity.

Library building and upgrading

The library consists of the two-dimensional data (crisp set) coded from the spectrum of each reference pigment. It can be easily upgraded whenever a new reference pigment is analysed just by adding the spectra once it is codified according to the procedure described in the Data Coding subsection above.

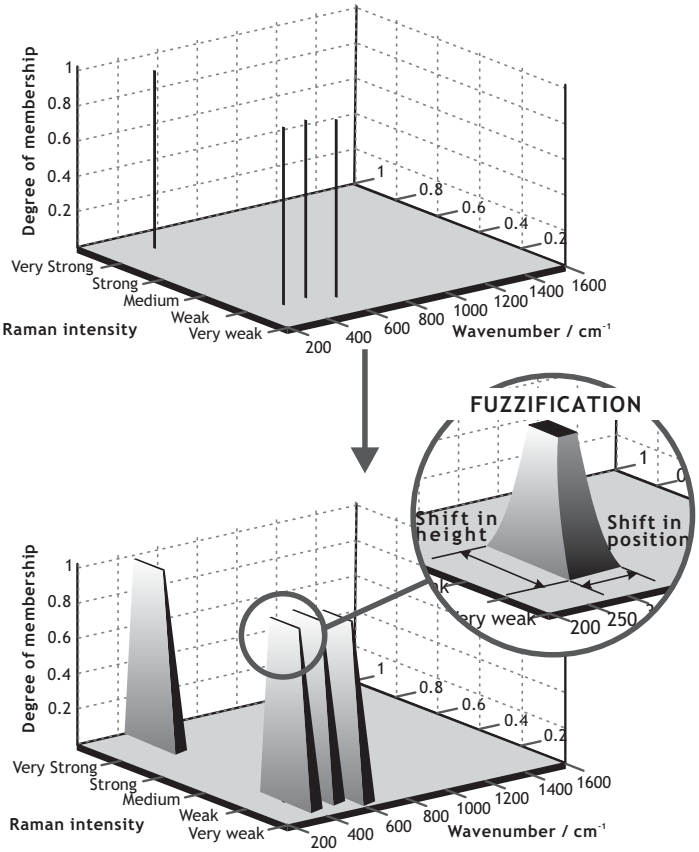

Figure 4. Fuzzification of unknown coded data with uncertainty added to both the band intensity and wavenumber.

Pigment identification

The pigment is automatically identified from its Raman spectrum by the fuzzy system as follows. Using the same procedure as the one explained above in the Data coding subsection, the coded data from the unknown Raman spectrum are fuzzified to make a two-dimensional fuzzy system. But, unlike the reference spectra, uncertainty is added to the peak wavenumber and intensity by means

of a trapezoidal membership function (Figure 4). A width in 20 cm^{-1} in the lower base and 10 cm^{-1} for the upper base of the trapezoid was encountered optimal to be applied in the system. The uncertainty takes into account the variations in the spectrum features caused by changes in environmental conditions during the measurement or band shifts due to changes in laser intensity, etc. Most of the analysts' knowledge can be used to model the optimal membership function, which represents the uncertainty, imprecision and vagueness in the data.

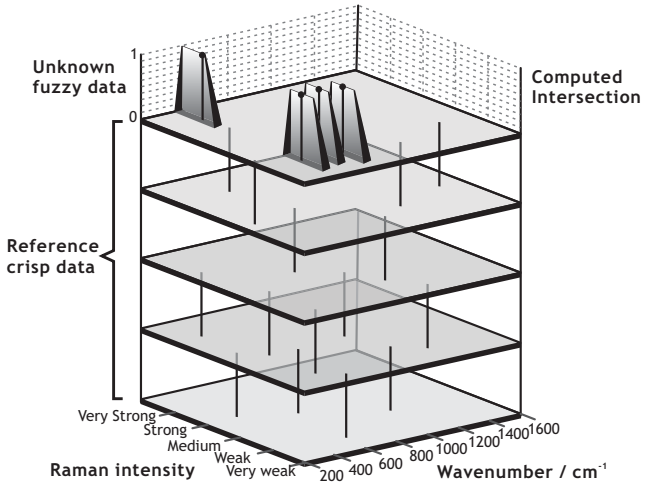

Figure 5. Computed intersection between the fuzzy set (unknown pigment) and each crisp set stored in the library (reference pigments).

The two-dimensional membership function [18] for the unknown spectra is obtained by the outer product of the vectors forming the trapezoidal membership functions for wavenumber and intensity. The identification process involves computing the intersection between the 2D fuzzy set of the unknown spectrum with each of the 2D crisp sets stored in the reference library (Figure 5). First, the minimum between those two sets (Eq. 1) is computed for each band.

$$m_A(band_i)=min(reference\ crisp,\ unknown\ fuzzy\ (band_i)) \quad (1)$$

As a result, a score is obtained for each band in the computed intersection. These scores are then weighted using a factor, called P, that represents the probability of occurrence [22] of the Raman band. Here we use the band intensity as a value of P. So the largest bands have the highest scores and each band in the unknown pigment spectrum has a membership degree in the reference pigment with a value between 0 and 1. So, the algorithm strategy reflects the human approach: it gives most importance to the largest bands first and then to the secondary ones. Finally, the final score for a spectrum candidate is obtained by the sum of each band score intersection value ($m_A(band_i)$); the final result is weighted with a factor, called F,

that is the number of reference bands encountered in the unknown pigment spectra divided by the total number of bands in the reference pigment spectrum (Eq. 2). So when an unknown pigment spectrum contains a high number of reference pigment bands the score will be high. (Eq. 3).

$$F_{candidate} = \left(number\ of\ identified\ reference\ bands \Big/ total\ reference\ bands \right) \quad (2)$$

$$M_{spectrum\ candidate} = \frac{\left(\sum_{i=1}^{n} \left(m_A(band_i) \times P_i \right) \right)}{\sum_{i=1}^{n} P_i} \times F_{candidate} \quad (3)$$

where n is the number of bands in the spectrum of the unknown pigment, *P* is the probability of occurrence and $F_{candidate}$ is the index of bands encountered in the spectrum of candidate pigments.

The value $M_{spectrum\ candidate}$ is between [0, 1] and indicates the membership value obtained from the unknown fuzzified spectrum within the reference spectrum of the library. A value equal or close to 1 indicates full membership, which means absolute relation to the reference spectrum. On the other hand, a value equal or close to 0 indicates no membership, which means no relation to the reference spectrum. Following the same philosophy, this result is better expressed by textual not numerical phrases. So the results from the intersections are defuzzified [22, 23] using three categories, *"present"*, *"possibly present"* or *"not present"*. The first two categories indicate that the pigment is present and the third one indicates that it is clearly not present.

In addition to this pigment identification information, more detailed information about the bands identified and the probability factors applied to peak's certainty can be obtained. The membership value and the quality of the match of each reference band with the corresponding identified band can be also displayed.

Experimental

Raman spectra were collected by a micro-Raman system 1000 from Renishaw. The experimental set-up was kept constant in all spectra recordings of the reference samples. The excitation radiation, produced by a HeNe laser (632.8 nm), was directed into an Olympus metallurgical microscope and focused on the sample by a 50x long working distance microscope objective. The laser power on the sample was ~2 mW. Rayleigh scattering was appropriately rejected by a

couple of notch filters. A 2D CCD detected the Raman signal while the resolution of the monochromator was about 5 cm^{-1}. The continuous scan method (in which the angle of the grating continuously changes as each data point is read from the CCD detector) was used, and extended spectra covering the -100 – 1800 cm^{-1} spectral range were recorded. The lower wavenumber limit was selected to confirm the calibration of the instrument. In addition, the spectral range was kept constant in all measurements so that the number of data-points per wavenumber was the same in all the recorded spectra.

Reference spectra are pigments obtained from one of the most well known collections of artists' pigments, that is Kremer's collection. The spectra referring to unknown pigments are obtained from minute samples of Byzantine icons. These samples have an unknown composition that may have compositional differentiation and/or contribution of other materials (e.g. binding media etc.) in the corresponding spectra. The most important differentiation between the reference spectrum and the spectrum of the unknown pigment is the background that may be caused by fluorescence of the aged sample and/or internal fluorescence of the pigment.

The fuzzy algorithms were programmed with Matlab software version 6.5. The wavelet transform applications belong to the wavelet toolbox from Matlab software.

Results

A reference library was constructed consisting of 32 pigments, most of which were powders from Kremer's collection and are known to have been used in antiquity. The algorithm's performance was evaluated with spectra from ten of the 32 pigments, with shifts in peak wavenumber and different background profiles due to different instrumental measurement conditions. The fuzzy algorithm has a satisfactory influence on the certainty levels of the pigments identified, as the results show. For example, Table 1 shows the identification scores for five of the ten pigments. Red lead (Pb_3O_4), cinnabar (HgS), ultramarine blue ($Na_{6-10}Al_6Si_6O_{24}S_{2-4}$), yellow ochre ($Fe_2O_3$, H_2O, clay) and hematite (Fe_2O_3) are clearly identified and their final algorithm score is close to 1.

To illustrate the procedure for identifying pigments and the final result given by the fuzzy algorithm, we present three examples. First we discuss in detail the spectra obtained from the ultramarine blue pigment; then we deal with iron (III) oxide pigments; and finally we identify a spectrum obtained from a mixture of two pigments: red lead and cinnabar. In the first case, after applying the fuzzy algorithm to an unknown spectrum (Figure 6a), three possible candidates (reference pigments from the library) are selected (Figure 6b). Of these, only one has a score close to

1 and this is converted by means of the de-fuzzified step to "almost present" and corresponds to the reference ultramarine blue, (Figure 6c). The scores of the other two reference pigments, on the other hand, are close to zero and are converted by means of the de-fuzzyfied step to "not present". It is clear that the background and impurity interferences of the unknown spectrum are different from those of the reference spectrum (Figure 6c). Figure 6c also shows that the vagueness in the intensity and the shifts in the Raman bands can be well handled by the algorithm and that identification can be correct despite these obstacles because the final algorithm score is close to 1 (0.83). The situation is similar for the other pigments shown in Table 1: red lead, cinnabar and yellow ochre are properly identified as they all have a final score close to 1.

Special attention should be paid to those cases in which the algorithm identifies a group of pigments as candidates, for example with pigments from iron (III) oxide like hematite and caput mortum pigments. In this case, after applying the fuzzy algorithm to an unknown spectrum, it was identified as hematite (score 0.99), caput mortum (score 0.99) and caput mortum violet (score 0.71) (see Table 1). But it corresponds to hematite. As these pigments have the same Raman spectrum [24], we consider that this is not a limitation of the algorithm but that pigments with similar or very close chemical composition give the same bands in a Raman spectrum. Indeed, all three pigments have the same structure (except from trace minerals), being the main component iron (III) oxide (Fe_2O_3). So, a complementary technique and the experience of an analyst would be necessary before the pigment could be definitively identified. An interesting technique is X-ray fluorescence, which enables element identification. This information is complementary to the one provided by Raman spectroscopy.

Similar situation happens with some ochre pigments all of which have approximately the same Raman spectra [25] but there are some differences can be found due to the presence of Al, Si, or Mn. The ochre spectra correspond to the main component that is, iron oxide, but there may also be some weak or very weak bands due to the fact that alumino-silicate materials and manganese oxide have low Raman signal. As is the previous case of the iron oxide pigments, in some ochre cases several pigments are identified as possible candidates and a complementary technique and the experience of an analyst would be necessary to definitively identify the pigment. The fuzzy algorithm may also contain other routines able to handle extra parameters provided by other techniques apart from Raman spectroscopy.

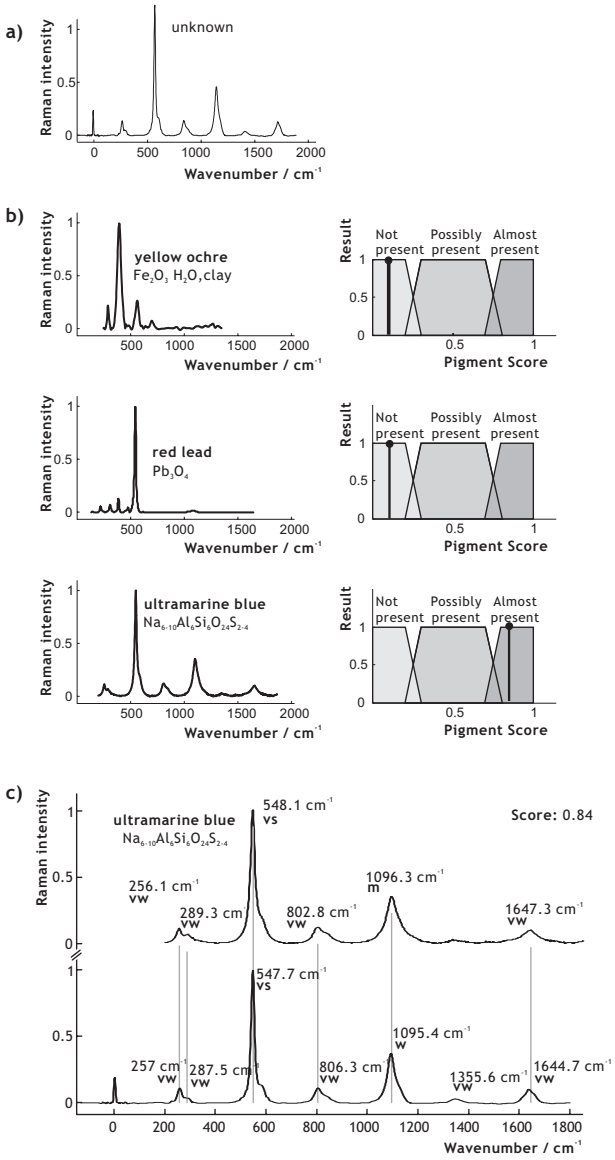

Figure 6. Identification process for an unknown pigment. a) Spectrum of the unknown pigment. b) Three possible pigment candidates with the final de-fuzzified identification. c) Spectrum of the unknown pigment identified by the algorithm as ultramarine blue. The shifts and the intensity of the bands are shown. Intensity is abbreviated in the following way; vw: very weak, w: weak, m: medium, s: strong and vs: very strong.

The Raman spectra from a set of mixtures of cinnabar and red lead were used to see how the algorithm dealt with mixtures. In Figure 7 we show the algorithm identification of a Raman spectrum from a mixture of red lead (67.1%) and cinnabar (32.9%). When the spectrum from the unknown sample (Figure 7a) goes through

the reference library, the algorithm selects two candidates with a score close to 1 (Figure 7b). Cinnabar, with a score of 1, and red lead, with a score of 0.8, are identified as being present in the unknown sample. Figure 7c shows an overlay of the three spectra (unknown, cinnabar reference and red lead reference). The Raman bands considered are specified, with their wavenumbers and respective intensities.

	KREMER CODE	RED LEAD	CINNABAR	ULTRA-MARINE	YELLOW OCHRE	HEMATITE	RED LEAD 67,1% CINNABAR 32,9%
alabaster	58340	0.00	0.00	0.00	0.01	0.01	0.00
burnt sienna	40430	0.00	0.00	0.00	0.00	0.11	0.00
cadmium red	2111	0.00	0.00	0.00	0.00	0.00	0.00
cadmium yellow	2103	0.00	0.01	0.00	0.00	0.00	0.01
caput mortum	4870	0.00	0.00	0.00	0.00	**0.99**	0.00
caput mortum violet	4875	0.00	0.00	0.00	0.00	**0.71**	0.00
chalk bolognia	58150	0.00	0.00	0.00	0.00	0.01	0.00
chalk kabania	58000	0.00	0.00	0.00	0.00	0.01	0.00
chromium (III) oxide	-	0.17	0.00	0.09	0.03	0.00	0.09
cinnabar	10620	0.00	**1.00**	0.13	0.00	0.00	**1.00**
cobalt blue	4570	0.01	0.00	0.00	0.00	0.00	0.00
green earth cyprus	-	0.01	0.00	0.00	0.01	0.00	0.01
gypsum anhydrite	58320	0.00	0.00	0.00	0.01	0.01	0.00
gypsum bologna	58150	0.00	0.00	0.00	0.00	0.01	0.00
hematite	-	0.00	0.00	0.00	0.00	**0.99**	0.00
lead white	46000	0.01	0.00	0.00	0.00	0.00	0.00
lithopone	-	0.00	0.00	0.00	0.00	0.00	0.00
malachite	1031	0.00	0.00	0.00	0.00	0.00	0.00
massicot	-	0.04	0.00	0.00	0.00	0.01	0.02
naples yellow	43130	0.00	0.00	0.00	0.00	0.22	0.00
natural gypsum	58300	0.01	0.02	0.00	0.00	0.00	0.01
prussian blue	4521	0.08	0.00	0.00	0.00	0.00	0.17
pyrolusite	-	0.02	0.01	0.00	0.00	0.00	0.03
quartz	-	0.00	0.00	0.00	0.00	0.00	0.00
red lead	4250	**1.00**	0.00	0.00	0.01	0.00	**0.80**
red ochre	4002	0.00	0.00	0.01	0.00	0.00	0.00
titanium dioxide	-	0.00	0.00	0.00	0.00	0.02	0.00
titanium orange	43300	0.00	0.00	0.00	0.00	0.00	0.00
ultramarine blue	4502	0.00	0.00	**0.83**	0.01	0.00	0.00
verdigris	4445	0.00	0.00	0.00	0.00	0.00	0.00
viridian	4425	0.00	0.00	0.00	0.00	0.01	0.00
yellow ochre	40010	0.18	0.00	0.00	**0.94**	0.00	0.09

Table 1. Interpretation result from the fuzzy logic algorithm. The results showed are for the pigments red lead, cinnabar, ultramarine blue, yellow ochre, hematite and a mixture of red lead and cinnabar.

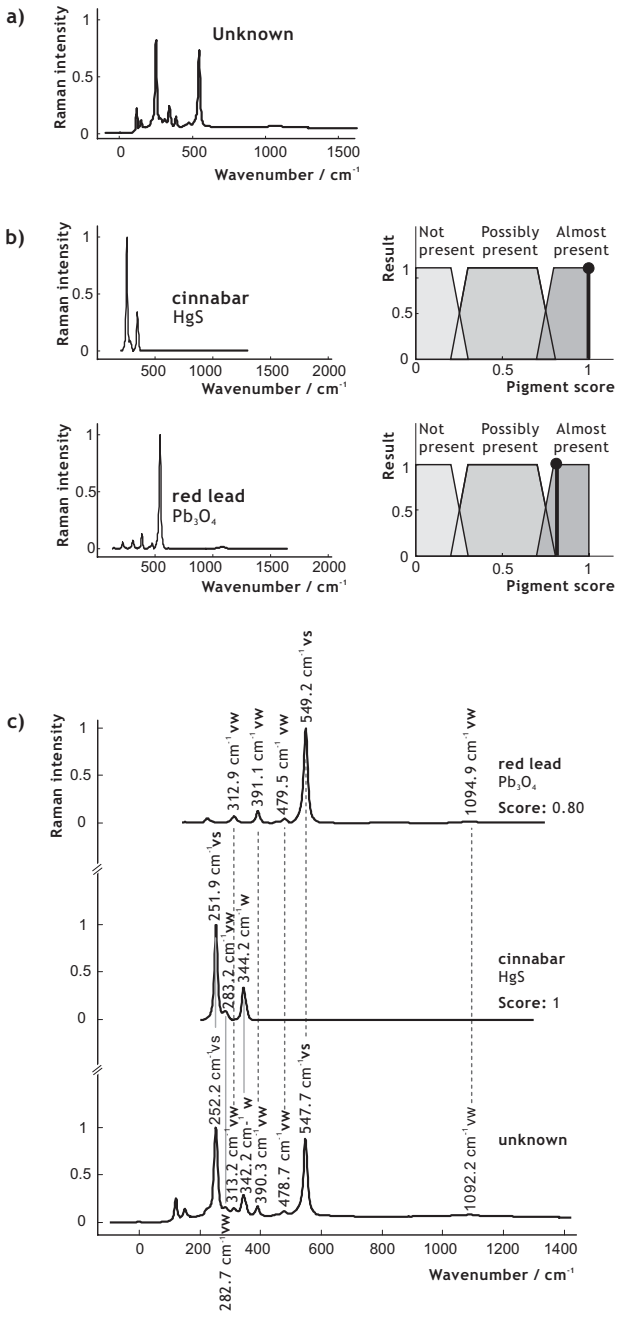

Figure 7. Identification of the components of a mixture of pigments. a) Spectrum of a mixture of pigments to be identified by the algorithm, formed by red lead (67.1%) and cinnabar (32.9%). b) Two possible pigments candidates with the final de-fuzzified identification. c) Spectrum of the mixture identified by the algorithm as red lead and cinnabar. The wavenumber and the intensity of the bands in each reference spectrum are shown. Intensity is abbreviated in the following way; vw: very weak, w: weak, m: medium, s: strong and vs: very strong.

Some limitations arise regarding the reference samples. The fact that there are no certified standards for ancient pigments makes it difficult to fully validate the algorithm, which would be possible with other types of sample such as modern pigments or inks.

Conclusions

We have shown how the algorithm can use fuzzy logic to identify automatically pigments from cultural heritage art objects. The results show how the system performs in comparison with experienced analysts. Pattern matching algorithms and fuzzy logic operations make it possible to follow the human strategy for interpreting spectra. They also allow the algorithm to learn from previous analyses and to handle uncertainty and vagueness in the data. This algorithm is a novel approach to a fully automated system for the interpretation of Raman spectra. The algorithm has been checked with 10 Byzantine pigments and a mixture of two of them. Due to the inherent limitations of the Raman technique, in some cases such as the one with iron (III) oxide and with some ochre pigments, when a family of possible candidates is selected, a complementary technique that gives elemental information may be required. Finally, although the algorithm has been checked with ancient pigments, in principle the same methodology can be applied to other types of sample such as modern pigments or dyes.

Acknowledgments

The authors acknowledge financial support from the European Community Project, Competitive and Sustainable growth program (G6RD-CT2001-00602).

References

[1] A. Perardi, L. Appolonia and P. Mirti, Analytica Chimica Acta 480, 317 (2003).

[2] S. Daniilia, D. Bikiaris, L. Burgio, P. Gavala, R. J. H. Clark and Y. Chryssoulakis, Journal of Raman Spectroscopy 33, 807 (2002).

[3] R. J. H. Clark, Comptes Rendus Chimie 5, 7 (2002).

[4] L. Burgio and R. J. H. Clark, Journal of Raman Spectroscopy 31, 395 (2000).

[5] P. Vandenabeele, A. v. Bohlen, L.Moens, R. Klockenkamper, F. Joukes and G.

Dewispelaere, Analytical letters 33, 3315 (2000).

[6] P. Vandenabeele, B. Wehling, L. Moens, B. Dekeyzer, B. Cardon, A. v. Bohlen and R. Klockenkamper, Analyst (Cambridge, U.K.) 124, 169 (1999).

[7] H. G. M. Edwards, L. F. C. d. Oliveira, P. Middleton and R. L. Frost, Analyst (Cambridge, U.K.) 127, 277 (2002).

[8] H. G. M. Edwards, P. S. Middleton, S. E. J. Villar and D. L. A. de Faria, Analytica Chimica Acta 484, 211 (2003).

[9] K. Castro, M. D. Rodriguez Laso, L. A. Fernandez and J. M. Madariaga, Journal of Raman Spectroscopy 33, 17 (2002).

[10] L. Burgio, D. A. Ciomartan and R. J. H. Clark, Journal of Raman Spectroscopy 28, 79 (1997).

[11] B. M. Cullum, J. Mobley, Z. H. Chi, D. L. Stokes, G. H. Miller and T. Vo-Dinh, Review of Scientific Instruments 71, 1602 (2000).

[12] P. Vandenabeele, B. Wehling, L. Moens, H. Edwards, M. De Reu and G. Van Hooydonk, Analytica Chimica Acta 407, 261 (2000).

[13] L. A. Zadeh, Information and Control 12, 94 (1968).

[14] L. A. Zadeh, Computer 21, 83 (1998).

[15] N. W. Daniel, I. R. Lewis and P. R. Griffiths, Applied Spectroscopy 51, 1868 (1997).

[16] F. Russo, IEEE Transactions on Instrumentation and Measurement, 45, 683 (1996).

[17] L. A. Zadeh, IEEE Computer 1, 83 (1988).

[18] M. Otto, Chemometrics and Intelligent Laboratory Systems 4, 101 (1988).

[19] F. Ehrentreich, Fresenius' J. Anal. Chem. 357, 527 (1997).

[20] V. J. Barclay, R. F. Bonner, and I. P. Hamilton, Analytical Chemistry 69, 78 (1997).

[21] F. Ehrentreich and L. Summchen, Analytical Chemistry 73, 4364 (2001).

[22] P. H. Abbott and M. J. Adams, X Ray Spectrometry 26, 125 (1997).

[23] F. Ehrentreich, Fresenius' J. Anal. Chem. 359, 56 (1997).

[24] L. F. C. de Oliveira, H. G. M. Edwards, R. L. Frost, J. T. Kloprogge and P. S. Middleton, Analyst (Cambridge, U.K.) 127, 536 (2002).

[25] D. Bikiaris, S. X. Daniilia, S. Sotiropoulou, O. Katsimbiri, E. Pavlidou, A. P. Moutsatsou and Y. Chryssoulakis, Spectrochimica Acta Part A 56, 3 (2000).

4.3. A FUZZY LOGIC MODEL TO JOINTLY PROCESS RAMAN AND XRF DATA

4.3.1. Introduction

In order to improve the identification of pigment samples by means of the fuzzy identification system based on the Raman spectra, we introduce information extracted from XRF analysis. This information can improve the identification system in two ways.

First, it allows performing pre-classification of pigments grouping them by the main elements present. In that sense, Raman classification is then focused in the study of a few groups of candidates. For example, the identification of those pigments which have lead as one of the main components as is the case of the minium pigments (Pb_3O_4).

Secondly, ambiguous Raman identification results are improved by adding the information about the abundance of minor elements present in the sample obtained by XRF analysis, as is the case of the identification of ochre pigments (Fe_2O_3).

4.3.2. Modifications to the previous fuzzy algorithm and calibration

According to the methodology described in the previous paper, the information obtained from the Raman analysis -peak intensities and peak positions- is represented in a 2D fuzzy map. This new model incorporates also the information given by the XRF analysis. In that way, the information extracted from both, Raman and XRF analysis, is coded in a matrix.

Library building and upgrading are done in the same way and now the two dimensional data coded contains all the information extracted from both XRF analysis. This process is represented in Figure 4.1. [13, 14].

Identification

The pigment is automatically identified from its coded Raman-XRF data using the same procedure as the one explained for the Raman model. The coded data, extracted from the Raman and XRF spectra of an unknown sample, are fuzzified to make a two-dimensional fuzzy system. The corresponding uncertainty is added to the peak positions and peak intensities by means of a trapezoidal membership function (Figure 4.2). This membership function is dependent on the uncertainty associated to the instrument and the empirical shifts observed. The shape of the membership function also depends on the existence of other peaks from other pigments. Hence, in order to discriminate pigments with close spectra, the membership function is adapted when a new pigment is incorporated to the library.

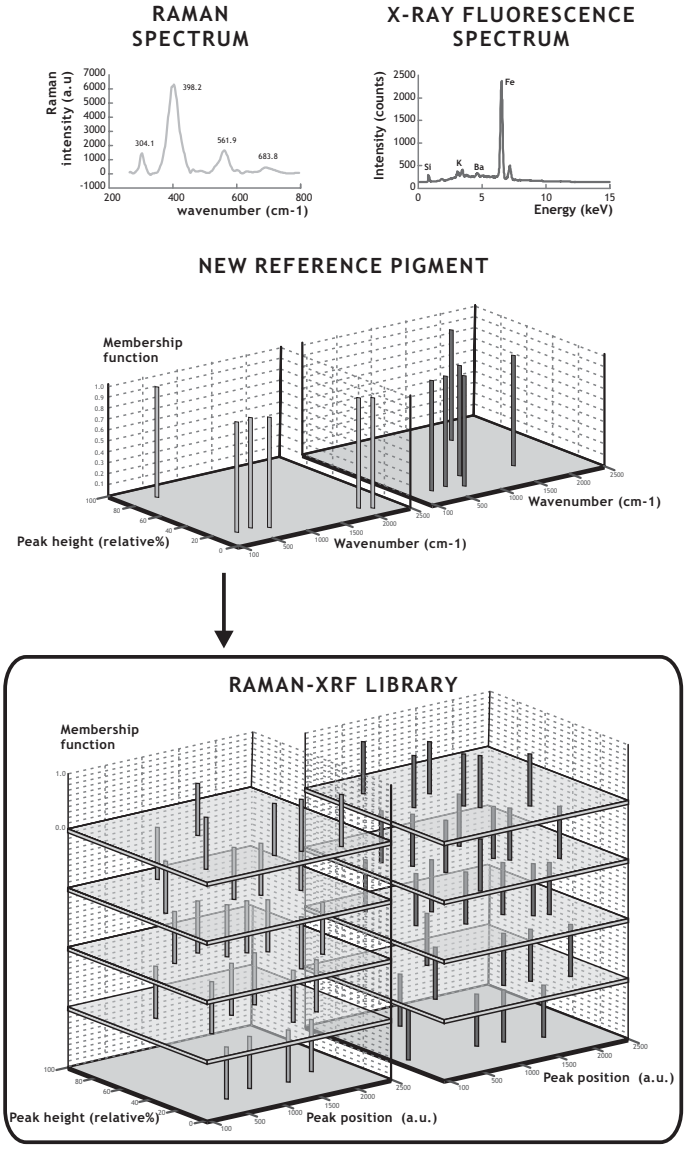

Figure 4.1. Peak position and intensity extracted from the original Raman and XRF spectra, and displayed in a 2-dimensional data coding (crisp set).

Raman and XRF data reduction is evaluated in the reference library by computing the fuzzy intersection (Figure 4.2). This process uses the advantage obtained from related data and the result obtained by XRF technique guides the computing of the fuzzy intersection of Raman data. The qualitative correlations among related data are used as confirmatory or non-confirmatory evidence for pigment identification.

The result obtained from the fuzzy intersection reflects the grade of containment between the unknown pigment and the reference candidates. The grade of containment represents the score obtained. To represent this number in a textual result as "present" or "not present" a defuzzification process is undertaken.

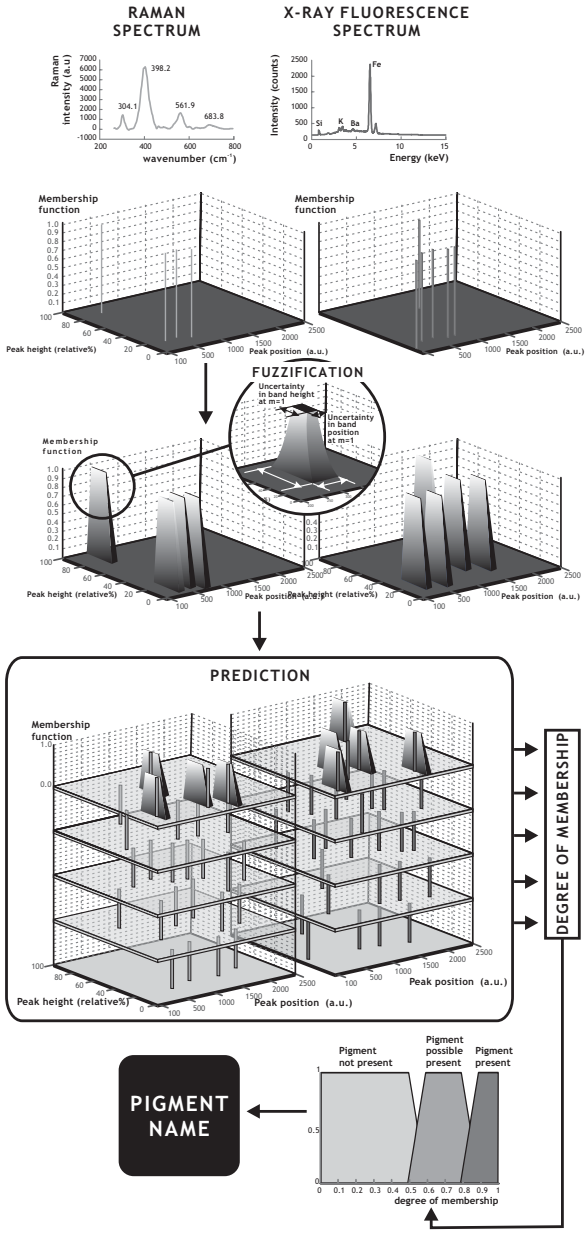

Figure 4.2. Computed intersection between the fuzzy set (unknown pigment) and each crisp set stored in the library (reference pigments).

4.3.3. Results

A reference library was constructed using the spectral information of a set of 28 pigments, mainly described in chapter 2 of this thesis. The fuzzy algorithm has a satisfactory influence on the certainty levels of the pigments identified, as the results shown in Table 4-1. Preliminary discrimination is performed by means of major elements present in the pigments. Final classification is done in each group by means of Raman analysis and it is improved with the information of the minor elements given by the XRF analysis.

Discrimination is improved for all samples, and those composed by iron (III) oxide pigments could be better identified with respect to those results obtained using only Raman information. As an example, this system allows the discrimination of ochre pigment samples, but discrimination between hematite and caput mortum pigments is still a dificult task due to the intrinsic characteristics of both.

Most of the samples are discriminated with the highest score values, and no misclassifications among samples are found. The additional information extracted from XRF analysis could be successfully handled by this fuzzy logic model in order to perform a better discrimination of the pigment samples. The quantification XRF analysis can be added to this model in order to refine the discrimination process.

		KREMER CODE	NAPLES YELLOW	MINIUM	LEAD WHITE	CINNABAR	RED OCHRE	HEMATITE	CAPUT MORTUM	CAPUT MORTUM VIOLET	BURNT SIENNA	YELLOW OCHRE
	NAPLES YELLOW	43230	**1.00**	0.05	0.06	0.00	0.00	0.00	0.00	0.00	0.00	0.00
Pb	MINIUM	42500	0.02	**1.00**	0.11	0.00	0.00	0.00	0.00	0.00	0.00	0.00
	LEAD WHITE	46000	0.14	0.14	**1.00**	0.00	0.00	0.00	0.00	0.00	0.00	0.00
Hg	CINNABAR	10620	0.00	0.00	0.00	**1.00**	0.00	0.00	0.00	0.00	0.00	0.00
	RED OCHRE	40020	0.00	0.00	0.00	0.00	**1.00**	0.05	0.10	0.08	0.10	0.10
	HEMATITE	-	0.00	0.00	0.00	0.00	0.10	**0.95**	0.60	0.33	0.13	0.15
Fe	CAPUT MORTUM	48700	0.00	0.00	0.00	0.00	0.06	0.88	**0.97**	0.33	0.10	0.12
	CAPUT MORTUM VIOLET	48750	0.00	0.00	0.00	0.00	0.05	0.33	0.22	**1.00**	0.10	0.12
	BURNT SIENNA	40430	0.00	0.00	0.00	0.00	0.02	0.14	0.08	0.10	**1.00**	0.09
	YELLOW OCHRE	40010	0.00	0.00	0.00	0.00	0.02	0.13	0.10	0.11	0.19	**1.00**

Tabla 4.1. Classification by means of a Raman - XRF fuzzy logic system.

4.4. FUZZY LOGIC CAPABILITIES

Fuzzy logic models enable a more thorough use of the available knowledge in computer-based spectrum interpretation by means of an extended knowledge representation [14, 15]. Classical logic behaves according to a yes-or-no type rather than a more-or-less type. A band is strong or not strong, medium or not medium, weak or not weak, there is no transition. In the framework of classical logic it is impossible to translate human projection of gradations into a formal and mathematically treatable description. In that sense, classical binary logic can not deal with the extended information, such as exception from rules and reduction of the validity of the rules.

Fuzzy logic deals with a very different aspect of the incompleteness of information [2, 7, 11, 12]. The key advantage of fuzzy methods is how they reflect the human mind in its remarkable ability to store and process information that is consistently imprecise and uncertain. Self-learning fuzzy systems can be developed for classification purposes. In particular, we have presented a system for pigment identification which is based in a simple and efficient learning method. The proposed model allows the incorporation of data from other techniques in order to jointly process different analysis performed on the same sample. Considering the rapidly growing advances of fuzzy logic applications, it is expected that fuzzy techniques will render an increasingly valuable contribution to the design of any advanced instrumentation system [16-18].

4.5. REFERENCES

[1] G. Wirth, D. F. Bale and D. A. Mlynski, (1996).

[2] L. A. Zadeh, Computer 21, (1998), 83-93.

[3] S. Smith and A. Kandel, Verification and validation in fuzzy expert systems, IEEE International Conference on Systems, Man and Cybernetics, 1995. 'Intelligent Systems for the 21st Century'.,, 1995.

[4] P. H. Abbott and M. J. Adams, X Ray Spectrometry 26, (1997), 125-131.

[5] L. A. Zadeh, Psicothema 8, (1996), 421-429.

[6] L. A. Zadeh, Discovering the World with Fuzzy Logic VOL 57, (2000), 3.

[7] L. A. Zadeh, Quo Vadis Computational Intelligence VOL 54, (2000), 123-143.

[8] L. A. Zadeh, Discovering the World with Fuzzy Logic VOL 57, (2000), 4-28.

[9] L. A. Zadeh, IEEE Transactions on Fuzzy Systems 9, (2001), 3-4.

[10] F. Russo, IEEE Transactions on Instrumentation and Measurement 45, (1996), 683-689.

[11] L. A. Zadeh, IEEE Computer 1, (1988), 83-93.

[12] L. A. Zadeh, Information and Control 12, (1968), 94-102.

[13] M. Otto, Chemometrics and Intelligent Laboratory Systems 4, (1988), 101-120.

[14] F. Ehrentreich, Fresenius Journal of Analytical Chemistry 359, (1997), 56-60.

[15] F. Ehrentreich, Fresenius Journal of Analytical Chemistry 357, (1997), 527-533.

[16] M. J. Soneira, R. Perez-Pueyo and S. Ruiz-Moreno, Journal of Raman Spectroscopy 33, (2002), 599-603.

[17] R. Perez-Pueyo, M. J. Soneira and S. Ruiz-Moreno, Journal of Raman Spectroscopy 35, (2004), 808-812.

[18] P. M. Ramos, J. Ferre, I. Ruisanchez and K. S. Andrikopoulos, Applied Spectroscopy 58, (2004), 848-854.

5

Chapter 5: Data-fusion and hard computing processing

This chapter describes three data-fusion strategies used to combine the outputs of Raman and XRF techniques. Their performances are evaluated with the classification of ochre pigments. Classification tools used are Principal Components Analysis (PCA) and Partial Least Squares – Discriminant Analysis (PLS-DA). Classification results obtained performing different data-fusion strategies are compared with those results obtained performing a single classification model for each technique. Discussed results, benefits and drawbacks of each strategy are presented in the paper: *Micro Raman and X-ray fluorescence spectroscopy data fusion for the classification of ochre pigments.*

5.1. Micro Raman and X-ray fluorescence spectroscopy data fusion for the classification of ochre pigments.

Pablo. M. Ramos[1], Itziar Ruisánchez[1], Konstantinos S. Andrikopoulos[2], and Koen Janssens[3]

1. *Department of Analytical Chemistry and Organic Chemistry. Rovira i Virgili University. Campus Sescelades, C/. Marcel·lí Domingo, s/n 43007 Tarragona, Spain*
2. *"Ormylia" Art Diagnosis Center, Sacred Convent of the Annunciation IMSP Ormylia-Chalkidiki, EL-63071 Ormylia, Greece*
3. *Micro and Trace Analysis Center, University of Antwerp, Belgium*

Applied Spectroscopy, submitted.

Applied Spectroscopy, submitted.

MICRO RAMAN AND X-RAY FLUORESCENCE SPECTROSCOPY DATA FUSION FOR THE CLASSIFICATION OF OCHRE PIGMENTS

Pablo Manuel Ramos[1], Itziar Ruisánchez[1], Konstantinos S. Andrikopoulos[2], and Koen Janssens[3]

1. *Department of Analytical Chemistry and Organic Chemistry. Rovira i Virgili University. Campus Sescelades, C/. Marcel·lí Domingo, s/n 43007 Tarragona, Spain*
2. *"Ormylia" Art Diagnosis Center, Sacred Convent of the Annunciation IMSP Ormylia-Chalkidiki, EL-63071 Ormylia, Greece*
3. *Micro and Trace Analysis Center, University of Antwerp, Belgium*

Abstract

Three different data-fusion architectures are evaluated for the combination of the outputs of a Raman and XRF combined instrument. The studied application deals with the classification of ochre pigments investigated in the field of cultural heritage. The fusion architectures are based on different strategies defined in three levels. The first level is performed by the direct combination of the signals, the second level combines extracted features and the third level combines class assignments provided individually by each technique. Those assignments are combined using fuzzy aggregation connective operators and the majority vote rule. The classification tools used are Principal Components Analysis (PCA) and Partial Least Squares – Discriminant Analysis (PLS-DA). Classification results obtained performing different data-fusion strategies are compared with those results obtained performing a single classification model for each data source. Our results show that the combination of signal features is the most suitable for a rapid and unique processing of both types of spectra. Benefits and drawbacks of each strategy are also discussed.

Keywords: Data fusion; Fuzzy aggregation connectives; micro Raman spectroscopy; micro X-ray spectrometry; Ancient pigments.

Introduction

It is well known that micro Raman (Raman) and micro X-ray fluorescence (XRF) spectroscopy are extensible used in the field of cultural heritage. Raman

provides a "fingerprint" of the material analysed while XRF provides a qualitative and quantitative elementary composition [1-3]. Their ever increasing contribution to the study of works of art is partly due to recent major improvements in the configuration of new instrumentation [2, 4], where the development of portable instruments for taking in situ measurements and collecting suitable information in a non-destructive way has played a significant role.

Since the turn of the century, a new generation of analytical instruments has been developed. The first prototype of an instrument combining Raman and XRF techniques, with all the attributes of both, is currently being tested in art and archaeological studies [5].

Thanks to this improvement in analytical instrumentation we can now obtain micro Raman and XRF spectra from the same spot on the sample. A new perspective on data processing is therefore needed in order to find tools for processing large amounts of data from several sources (complementary techniques) quickly and easily and, by means of data fusion, obtain a single result. Data fusion is a formal framework in which the means and tools for combining data from several sources are expressed. It has been widely applied to robotics, remote sensing, image analysis and analytical chemistry [6-9]. In most data fusion systems, the information extracted from each technique is represented as a degree of belief in an event with real values. This takes into account the imprecise, uncertain and incomplete nature of information. These degrees of belief are combined through numerical fusion operators. Fuzzy set theory has predominantly been used at the combination stage [10]. Aggregation operations can be applied by simple fuzzy aggregation connective operators. The aim of this paper is to perform an improved classification of the pigments studied in the field of cultural heritage, by means of different strategies of data fusion.

Theory

Data fusion

Data fusion combines information from several sources to produce a single model or decision. Hall and Llinas [11] propose different techniques for multisensor data fusion and define three types of architectures which can be used: 1) data level fusion or low level fusion, 2) feature level fusion or mid level fusion, and 3) decision level or high level fusion. The three architectures are described in Figure 1.

In low level fusion, each sensor observes an object and the raw sensor data are combined. Afterwards, an identity declaration process is performed. This can be achieved, by extracting a feature vector from the fused data, and perform a

transformation between the feature vector and a declaration identity. There are several methods that could be applied for this feature based identity declaration, for example multivariate classification methods. In order to fuse raw data, these data must be commensurate and must be properly associated. Thus, for example, if two sensors from the same spectroscopic techniques are used, the spectra must be able to be co-aligned on a same scale. If different spectroscopic techniques are used, the spectra need to be balanced in order to perform a correct data sensor association.

Mid level fusion is a feature level where features are extracted from each sensor observation. In this work, variable selection is performed using the method proposed by Indahl and Naes. This method identifies the local positive maxima and negative minima of the loading weights which define the directions in the variable space with good classification power [12, 13]. In our application, we use the loading weights obtained from the standard PLS-DA algorithm and select a small set of wavelengths around each selected point to provide more stable models. These features are concatenated together into a single feature vector which is the input to an identity declaration technique such as the principal components analysis or the cluster algorithm. The output then becomes a fused declaration of target identity based on the combined feature vectors from all the sensors. Data alignment and association/correlation must still be performed prior to linking the feature vectors from individual sensors into a single large feature vector.

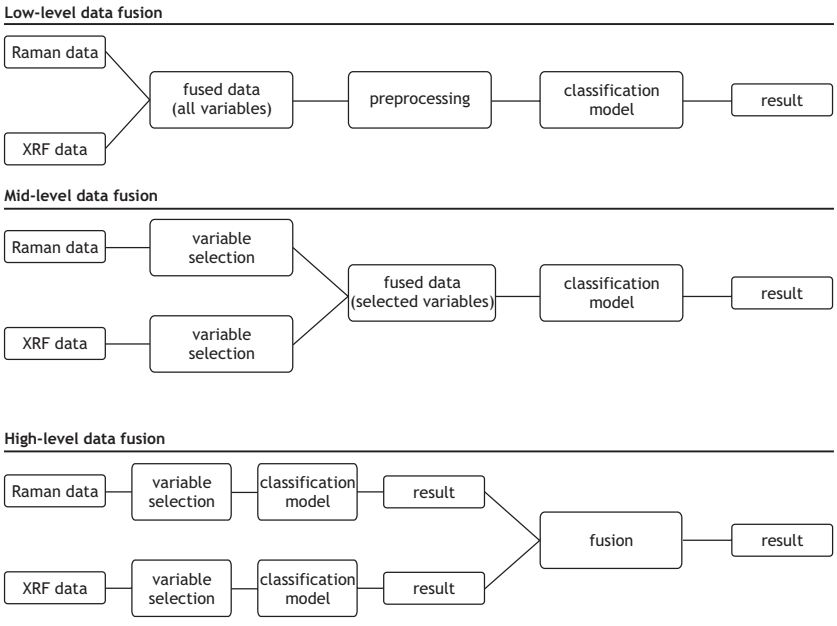

Figure 1. Data-fusion architectures.

High level is a decision level fusion. In this architecture, each sensor performs an identity declaration process based only on its own single-source data. That is, each sensor converts observed target attributes into a preliminary declaration of target identity. The identity declarations provided by the individual sensors are combined using decision level fusion techniques such as heuristic techniques, Bayesian techniques, or the Defter-Shafer method [14]. In this paper we used soft computing solutions: from fuzzy set theory, we applied simple-to-sophisticated fuzzy aggregation connective operators to combine the classifiers.

PLS-DA

As its name implies, in PLS-DA (Partial least squares – Discriminant analysis) a PLS model is developed to predict the class assignment of each sample. We will not go into details on the theory of PLS and PLS-DA here since it has largely been described elsewhere [15, 16]. PLS-DA is carried out using an exclusive binary coding scheme with one bit per class. For example, if we want to discriminate between four classes, a response encoded {0, 0, 1, 0} means that the sample belongs to class 3. During the calibration process the PLS-DA method is trained to compute the four membership values one for each class. The sample is then assigned to the class that shows the highest membership value. The resulting class assignment is expressed in terms of a value form 0 to 1, but these values are the projected results in the multidimensional space defined by the factors selected. The fact is that these values are normally distributed around 0 when the prediction is "not being in a class" and around 1 when the prediction is "to be in a class". For that reason it is possible to obtain prediction values below 0 (negative values) and also above 1.

Fuzzy aggregation connectives

Fuzzy theory, introduced by Zadeh [17], is a powerful theory for processing information. It has a considerable number of applications in areas such as control systems, pattern recognition, and signal processing [18, 19]. One reason for the success of the fuzzy set theory in instrumentation and control is its flexible representation of human decision making.

A fuzzy set, e.g. *A*, defined in the domain *U*, is described by a membership function m_A which maps to the real interval [0,1]. For each $u \in U$, $m_A(u)$ gives the degree of membership of *u* to the set *A*, where 1 denotes full membership, 0 denotes no membership and any other value means partial membership.

We chose simple rescaling to devise the membership functions from PLS-DA

predicted values. Let $x_{i,k}(c_j)$ be the predicted value obtained from sample *i(th)* for the *kth* class when the block c_j from the multiscale representation is processed. Then:

$$m_{A_{i,k}}(c_j) = \frac{x_{i,k}(c_j) - \min(x_{i,k}(c_j))}{\max(x_{i,k}(c_j)) - \min(x_{i,k}(c_j))} \quad (1)$$

Hence, the prediction given by PLS discriminant analysis is represented as measures or degrees of belief in the fact that respective samples either belong to a class or not. Its representation as numerical degrees leads to a quantification of its characteristics (uncertain, imprecise, and incomplete) which have to be taken into account in a fusion process. Fuzzy aggregation connectives will be used to combine them.

There is a wide variety of fuzzy connective and aggregation operators [20, 21]. The most common and used ones belong to the class of context independent constant behaviour (CICB) operators [10]. This class is composed of operators which have the same behaviour whatever the values of the information to combine, and which are computed without any contextual or external information.

Let a_1 and a_2 denote two real variables representing the degrees of belief to be combined and take the values into the interval *I*, which is [0,1]. The extreme values of *I* play particular roles. Value 0 means that, for a prediction, the processed block provides a null measure because it considers that this sample does not belong to the class under study. On the contrary, value 1 means that the processed block considers that the sample belongs to the class under study and this value represents a total certainty. Values between 0 and 1 represent degrees of uncertainty or partial knowledge on the information. They can also be interpreted as imprecision, or as a quantity of information available about the event. An aggregation connective is consider a function *F* acting on a_1 and a_2, defining the combination or fusion operator, and under the closure property assumption, $F(a_1,a_2)$ also has values in *I* [10].

Simple aggregation operators

1. Pessimistic-type aggregation:

   Product: $F_1(a_1,a_2,\ldots,a_n) = a_1 x\ a_2 x\ \ldots\ x\ a_n$

   Minimum: $F_2(a_1,a_2,\ldots,a_n) = min\ \{a_1,a_2,\ldots,a_n\}$

2. Indifferent-type aggregation:

   Arithmetic average, (AA): $F_3(a_1,a_2,\ldots,a_n) = \frac{1}{n}\ (a_1 + a_2 + \ldots + a_n)$

3. Optimistic-type aggregation:

   Maximum: $F_2(a_1,a_2,\ldots,a_n) = max\ \{a_1,a_2,\ldots,a_n\}$

Pessimistic aggregation reduces the less certain information and has the major confidence in the sensor which gives the smallest measure. It searches for a simultaneous satisfaction of criteria or objectives. On the contrary, optimistic aggregation increases the certainty we have about information and has major confidence in the block which gives the greatest or the most certain prediction. It expresses redundancy between criteria. An indifferent type of aggregation provides a global prediction, intermediate between the partial predictions provided by the technique.

Majority vote rule is implemented as a decision rule to obtain the ensemble decision. This method is simple to implement, it does not assume prior knowledge of the behavior of the individual classifiers. The majority vote rule assigns the pigment sample *x* to the class label most represented among the classifiers and connective outputs [22].

Experimental

Samples and instruments

The pigments studied belong to one of the best-known collections of artists' pigments, the "Kremer's collection" and they consist of a set of ochre pigments, with iron oxide (III) (Fe_2O_3) as the main component. The pigments included in this set were: hematite, caput mortum, caput mortum violet, yellow ochre, red ochre and burnt sienna. The study of iron (III) oxide pigments and ochre differentiation is an important task in the study of ancient pigments, where complementary techniques need to be used [23-25].

For each pigment, simultaneous Raman and XRF spectra were obtained at different spots on the pigment. In both cases, three measurements were used to build the PLS-DA model and one measurement, not included in the models, was used for prediction. The spectra designated to be references or samples were selected at random. In Figure 2 the Raman and XRF spectra of the studied pigments are presented.

The instrument used was a prototype of a micro Raman and micro XRF instrument which combines the excitation radiation, from both techniques applied to a small sample area that allows a position sensitive analysis with a spatial resolution of 5-50 microns. It consists of an energy dispersive micro-beam X-ray fluorescence spectrometer with a fine focus X-ray tube (max. 50 kV, 30 W), a polycapillary optic with a spot size of approximately 30 µm (MoK) and a drift chamber detector with a sensitive area of 5 mm^2 and energy resolution of < 140 eV (MnK). The Raman

spectrometer component (Jobin Yvon) has two wavelengths laser excitation (633 nm and 785 nm), a fiber optic connection of the measuring head to the spectrometer and a compact axial optical spectrometer for these two wavelengths. The spectral range is 130 cm^{-1} – 3270 cm^{-1} for 633 nm, 130 cm^{-1} – 2240 cm^{-1} for 785 nm and the resolution 3 cm^{-1}/pixel for 633 nm and 2 cm^{-1}/pixel for 785 nm.

The Raman-XRF microprobe has a camera to select different grains and perform measurements on each one of them. So, with this instrument we measure on a single grain, and then is possible to manage the problem of a mixture of pigments.

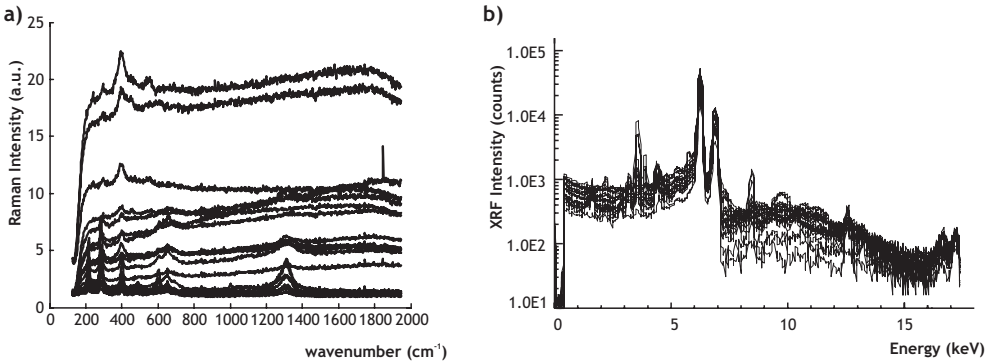

Figure 2. a) Raman spectra and b) XRF spectra from ochre pigments.

Software

The algorithms were programmed with the Matlab software version 6.5. The wavelet transform applications belonged to the wavelet toolbox 2.0 from Matlab software, PLS applications belonged to the PLS toolbox 3.5 from Eigenvector Research Incorporated.

Results and discussion

First of all, classification of ochre pigments is discussed by means of each individual technique (first Raman spectroscopy and then X-ray fluorescence). In both studies principal component analysis is performed for a pre-visualization of the patterns present in each data set. After that, partial least squares – discriminant analysis is used for the classification and prediction of different groups of ochre pigments. Secondly, the three described data fusion strategies are implemented in order to improve the classification results of the ochre samples. Finally, results obtained with the different strategies are compared and the benefits and drawbacks of these methodologies applied to these types of data are discussed.

Raman classification

Principal components analysis (PCA) was performed to view group distribution of Raman data (Figure 3). Samples from known classes are denoted with labels beginning with HM (hematite), CM (caput mortum), CMv (caput mortum violet), YO (yellow ochre), RO (red ochre) and BS (burnt sienna). Unknown samples are labeled with the term "sample 1-6" and are shown as filled dark grey circles.

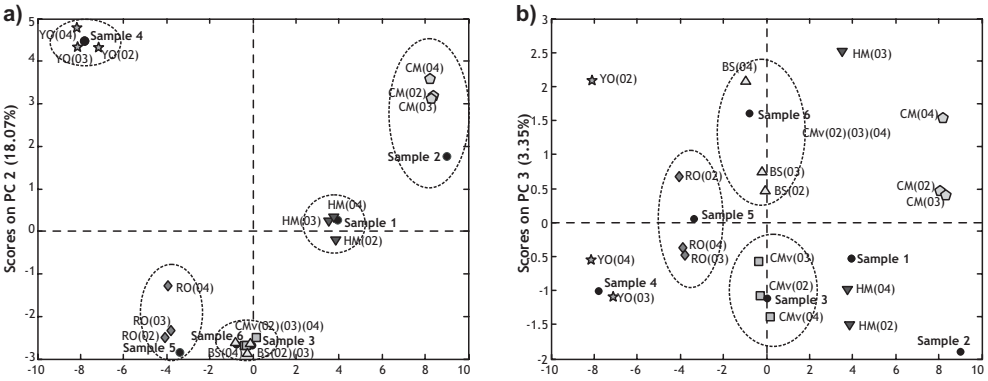

Figure 3. PCA on Raman spectra. a) PC1 – PC2 score plot; and b) PC1 – PC3 score plot.

Although a satisfactory separation of classes is achieved, the plot of PC1 vs. PC2 is not enough for grouping all samples in their corresponding classes. Classes CMv and BS cannot be differentiated but their separation can be achieved by projecting the data in the PC1 vs. PC3 plot.

Classification and prediction of new samples was performed by means of PLS-DA. The model was performed using five latent variables which were determined by the leave-one-out cross-validation method. Classes can be visually discriminated plotting the score values of LV1 - LV2 and LV1 – LV3 (Figure 4a-b). The score plots represent a similar separation of data obtained by PCA. The loading weights of the PLS-DA model were inspected in order to determine the variables responsible for the discrimination between classes (Figure 4c). The highest (positive and negative) values are marked and associated with their corresponding variable in the original Raman spectra. It can be seen that the PLS-DA model discriminates the pigment samples using the information about differences in relative intensities and shapes of the Raman bands.

Table 1 shows the predictions of unknown samples. The model cannot predict the hematite and caput mortum samples correctly, and both classes are misclassified. This limitation of the model is also denoted by the predicted probability results obtained in the analysis of caput mortum samples, where hematite (P1) and caput mortum (P2) classes have predicted probability values equal to 1. Also, future

samples of red ochre pigments might be misclassified by the model. Since red and yellow ochre (P4 and P5) classes have predicted probability values close to 1 when a sample of red ochre is evaluated. In this case, a red ochre sample has a probability value of 1 to be predicted as red ochre and a value of 0.90 to be predicted as yellow ochre. The reduced values of Q_{red} and T^2_{red} show that not all the samples are within the 95% limits of the classes (Table 1). The values corresponding to red ochre (1.47) and burnt sienna (1.20) are higher than 1 and therefore they are out of the interval confidence given for the PLS-DA model.

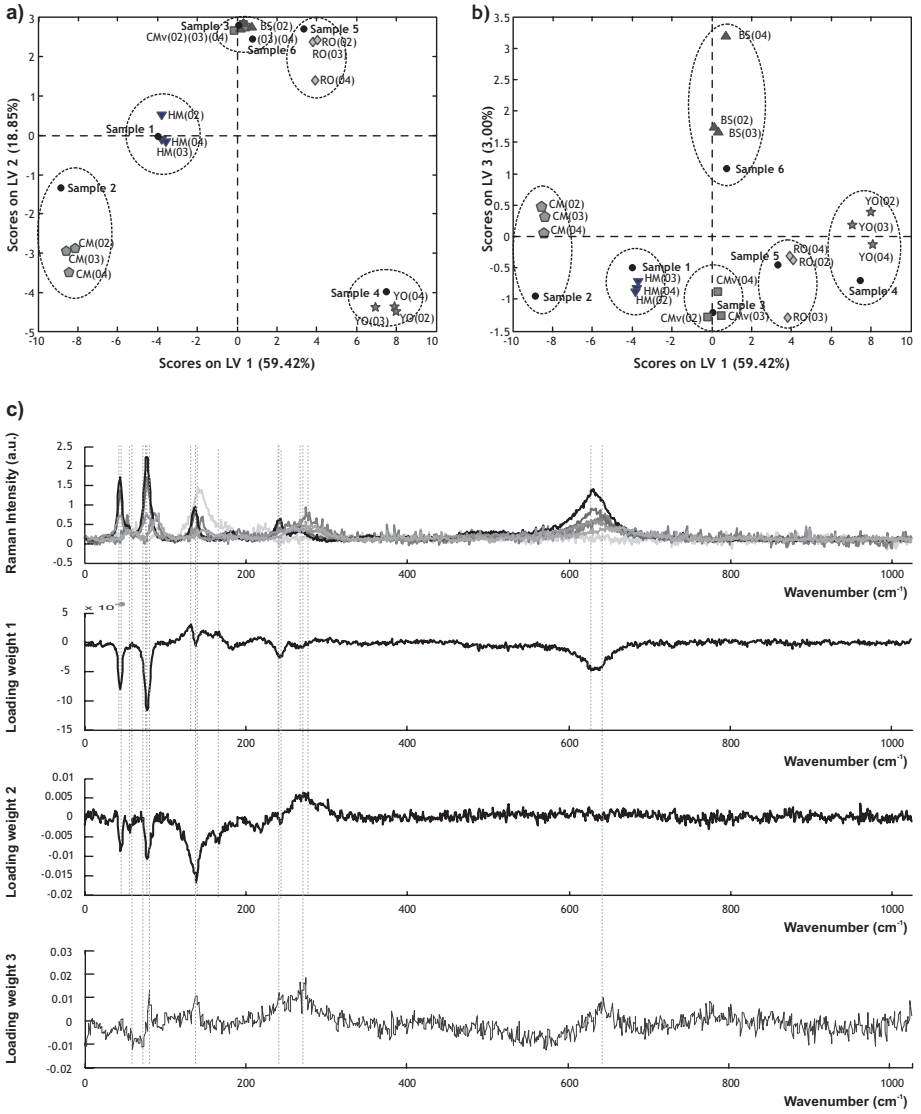

Figure 4. PLS-DA on Raman spectra. a) LV1 – LV2 score plot, b) LV1 – LV3 score plot and c) projection of maximum (positive and negative) values from loading weights 1, 2 and 3 on original variables from Raman spectra.

SAMPLE	PLS-DA CLASS ASSIGNMENT C(1)	C(2)	C(3)	C(4)	C(5)	C(6)	THRESHOLD	Q(red)	T^2(red)	PREDICTED PROBABILITY P(1)	P(2)	P(3)	P(4)	P(5)	P(6)
Hematite	0.21	0.17	0.00	-0.20	-0.04	-0.14	**0.13**	0.27	0.04	1.00	0.00	0.00	0.00	0.00	0.00
Caput mortum	0.39	0.42	0.19	-0.26	-0.43	-0.32	**0.35**	0.75	0.21	1.00	1.00	0.00	0.00	0.00	0.00
Caput mortum violet	-0.07	-0.19	0.70	-0.19	-0.09	-0.16	**0.49**	0.12	0.19	0.02	0.00	1.00	0.00	0.00	0.00
Red ochre	-0.11	-0.16	-0.17	0.70	0.15	-0.40	**0.22**	1.47	0.21	0.01	0.00	0.00	1.00	0.90	0.00
Yellow ochre	-0.30	-0.15	0.05	-0.19	0.63	-0.04	**0.11**	0.49	0.17	0.02	0.00	0.00	0.00	1.00	0.00
Burnt Sienna	-0.20	-0.11	0.04	-0.16	0.02	0.42	**0.10**	1.20	0.08	0.01	0.00	0.00	0.00	0.01	1.00

Table 1. Raman PLS-DA prediction values of unknown samples.

XRF classification

Following the same structure of analysis performed on Raman data, the set of pigments was studied by means of micro-XRF spectrometry so classification of ochre pigments is done using the qualitative information extracted from spectra.

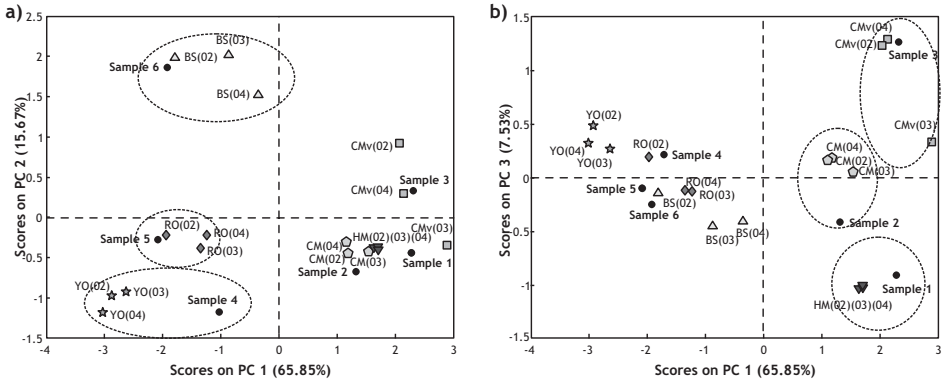

Figure 5. PCA on XRF spectra. a) PC1 – PC2 score plot; and b) PC1 – PC3 score plot.

The PCA plot of data projected on PC1 – PC2 axes (Figure 5a), presents 3 groups which are easily identified: YO, RO and BS samples. And the PC1 – PC3 score plot (Figure 5b), allows to visually discriminate the other three classes (HM, CM and CMv). So, as with the Raman analysis, it is possible to observe a satisfactory separation for the six classes of ochre pigments and also for the unknown samples from each class cluster together.

Classification and prediction of new samples was performed by PLS-DA. This model used six latent variables determined after a leave-one-out cross-validation analysis. In Figure 6 a-b) the score plots of LV1 – LV2 and LV1 – LV3 are showed. Both plots are needed in order to observe the group distribution previously visualized by the PCA processing.

The loading weights of the PLS-DA model were inspected in order to determine the variables responsible for the discrimination between classes. In Figure 6c) the loading weights for LV1, LV2 and LV3 are plotted and the highest (positive and

negative) values are marked with their corresponding variable in the XRF spectra. We can observe that classification of ochre samples is done principally by the minor peaks present in the spectra and also by the differences in intensity observed in the major peaks located between 6 and 7 keV, which correspond to the amount of iron.

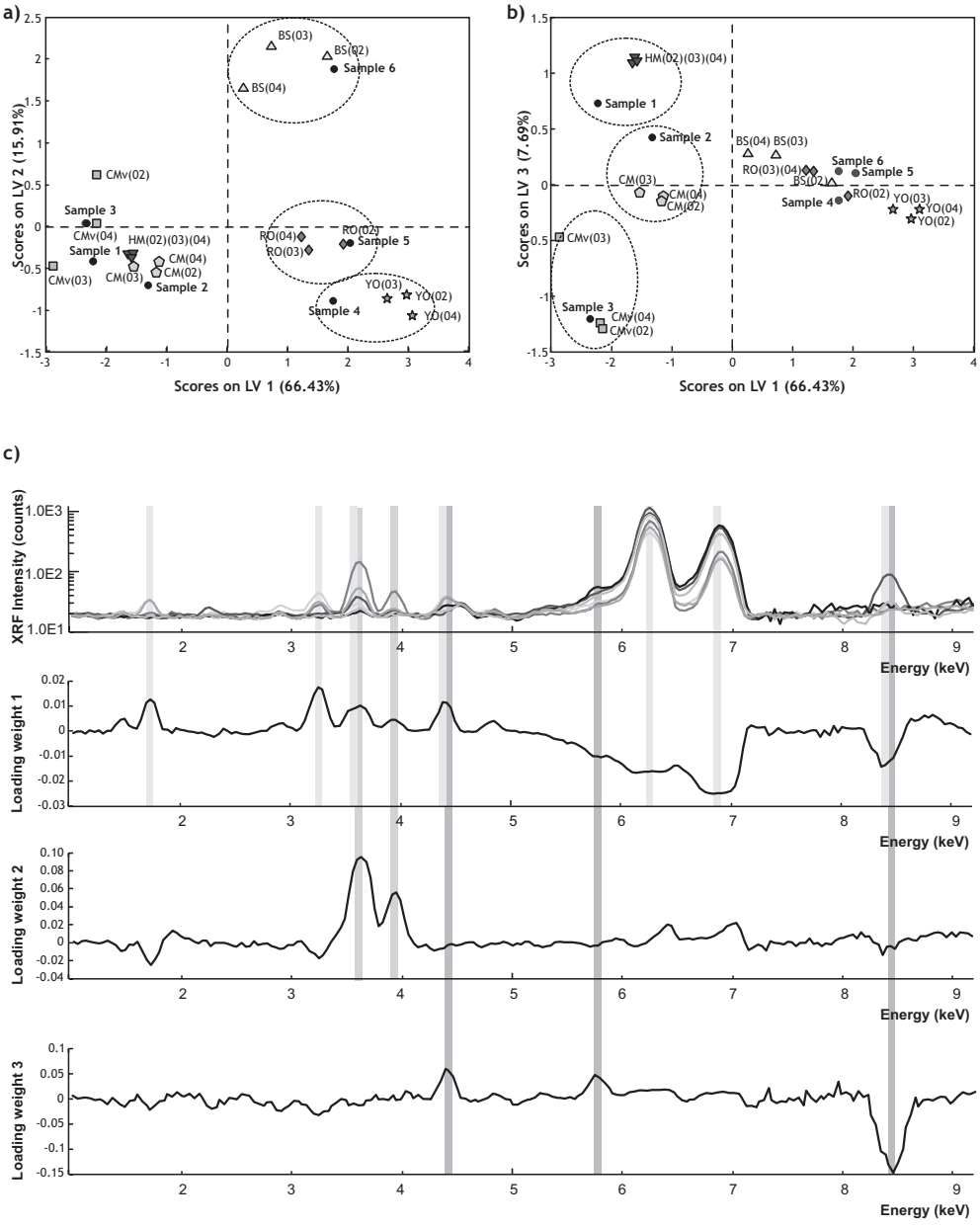

Figure 6. PLS-DA on XRF spectra. a) LV1 – LV2 plot, b) LV1 – LV3 plot and c) projection of maximum (positive and negative) values from loading weights 1, 2 and 3 on original variables from Raman spectra.

SAMPLE	PLS-DA CLASS ASSIGNMENT						THRESHOLD			PREDICTED PROBABILITY					
	C(1)	C(2)	C(3)	C(4)	C(5)	C(6)		Q(red)	T^2(red)	P(1)	P(2)	P(3)	P(4)	P(5)	P(6)
Hematite	0.43	-0.06	0.06	-0.22	-0.05	-0.15	**0.19**	0.91	0.13	1.00	0.00	0.00	0.00	0.00	0.00
Caput mortum	-0.01	0.14	0.16	-0.11	0.02	-0.20	**0.43**	0.76	0.11	0.00	0.00	0.00	0.00	0.00	0.00
Caput mortum violet	0.06	-0.04	0.47	-0.11	-0.29	-0.09	**0.45**	1.08	0.11	0.00	0.01	1.00	0.00	0.00	0.00
Red ochre	0.00	-0.15	-0.06	0.35	0.00	-0.14	**0.14**	0.95	0.08	0.00	0.00	0.00	0.97	0.17	0.00
Yellow ochre	-0.20	-0.06	-0.20	0.17	0.58	0.04	**0.26**	0.87	0.14	0.00	0.00	0.00	0.00	1.00	0.00
Burnt Sienna	-0.02	-0.28	-0.23	0.13	-0.07	0.77	**0.27**	0.82	0.11	0.00	0.00	0.00	0.00	0.00	1.00

Table 2. XRF prediction for samples not included in the PLS-DA model.

The samples used to be predicted by the model are listed in Table 2 along with their corresponding result. In this case only one sample could not be predicted by the model, it was the caput mortum sample. The predicted probability given by the model for this class was 0, showing that future samples of this class are difficult to predict. The rest of the samples were correctly classified and predicted, also the reduced values of Q_{red} and T^2_{red} show that all the samples are within the 95% limits of the classes (Table 2).

Low-level Raman and XRF data fusion

The Raman and XRF spectra were concatenated according to the methodology described in the theory section, and the Raman-XRF meta-spectra obtained was processed by the PLS-DA. The model was performed using six latent variables and they were determined by the leave-one-out cross-validation method. Fused data projected on the first latent variables of the PLS-DA model are showed in Figure 7a) and b) with the score plots of the three first latent variables: LV1-LV2 and LV1-LV3 respectively. The six classes are easily discriminated using both plots and better distribution of classes is achieved compared with the individual models.

The inspection of loading weights of the PLS-DA model (Figure 7c) reveals that the variables responsible for the discrimination between classes are mostly those which were used in the individual Raman and XRF models.

The prediction results for the unknown samples are presented in Table 3. The predicted probabilities for each corresponding class are 1 and 0 for the rest of the classes, asserting that all future samples from each class can be correctly identified. The discrimination of HM and CM unknown samples is improved with this methodology; however the PLS-DA class assignment (0.35) obtained for class 1 (HM) is close to the threshold value obtained from the calibration model. The reduced values of Q_{red} and T^2_{red} show that not all the samples are within the 95% limits of the classes (Table 3) and values corresponding to red ochre (1.26) and burnt sienna (1.23) are out of the interval confidence given for the PLS-DA model.

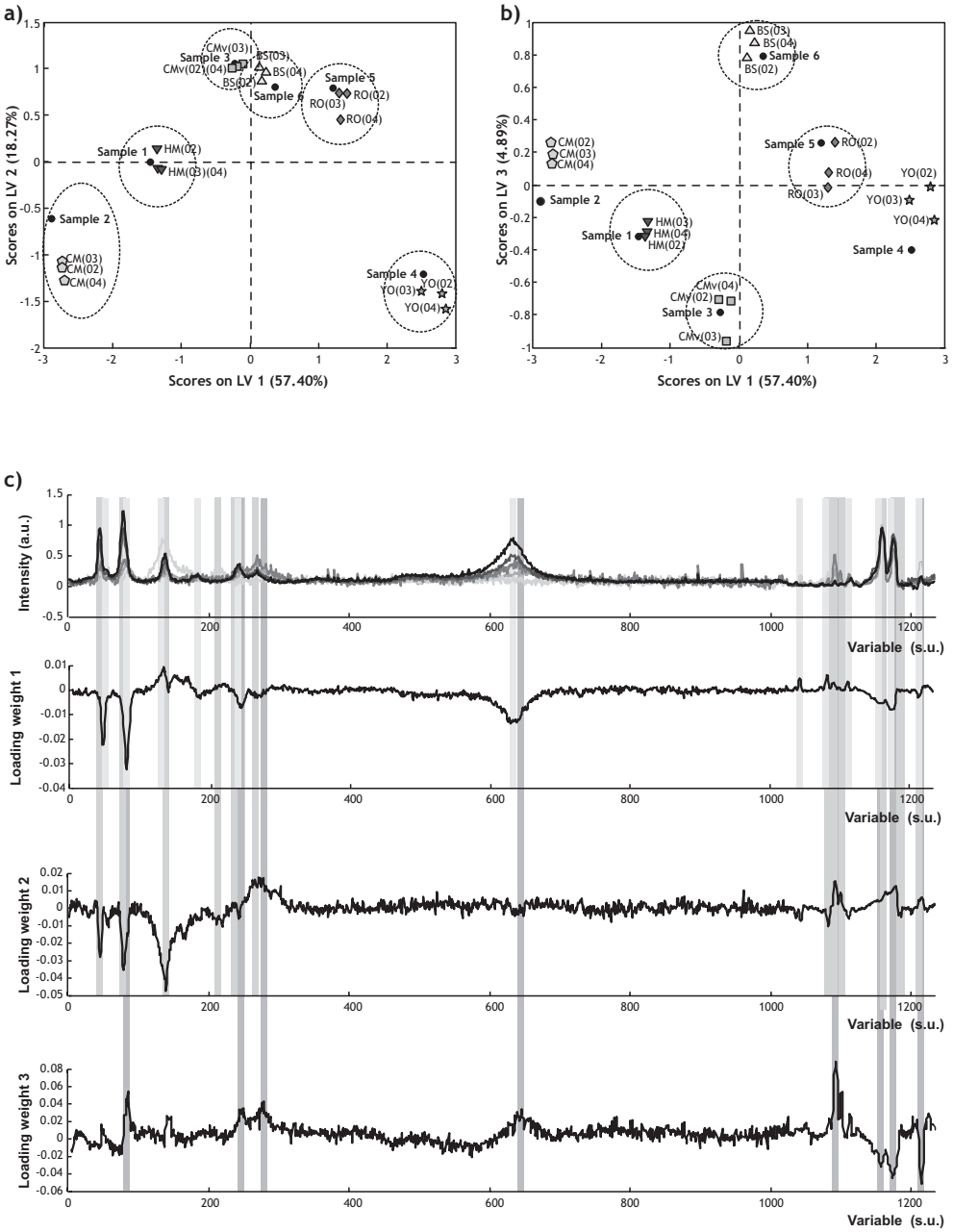

Figure 7. PLS DA on Raman-XRF meta-spectra from a low-level data fusion model. a) LV1 – LV2 score plot, b) LV1 – LV3 score plot and c) projection of maximum (positive and negative) values from loading weights on variables from Raman-XRF meta-spectra.

SAMPLE	PLS-DA CLASS ASSIGNMENT						THRESHOLD			PREDICTED PROBABILITY					
	C(1)	C(2)	C(3)	C(4)	C(5)	C(6)		Q(red)	T^2(red)	P(1)	P(2)	P(3)	P(4)	P(5)	P(6)
Hematite	0.35	0.08	0.01	-0.20	-0.07	-0.16	**0.18**	0.61	0.08	1.00	0.00	0.00	0.00	0.00	0.00
Caput mortum	0.16	0.54	0.02	-0.26	-0.23	-0.20	**0.23**	0.94	0.22	0.00	1.00	0.00	0.00	0.00	0.00
Caput mortum violet	0.01	-0.21	0.80	-0.19	-0.10	-0.12	**0.41**	0.64	0.18	0.00	0.00	1.00	0.00	0.00	0.00
Red ochre	-0.03	-0.23	-0.06	0.69	0.01	-0.36	**0.20**	1.26	0.17	0.00	0.00	0.00	1.00	0.00	0.00
Yellow ochre	-0.23	-0.18	-0.09	-0.13	0.75	0.07	**0.13**	0.74	0.17	0.00	0.00	0.00	0.00	1.00	0.00
Burnt Sienna	-0.08	-0.17	-0.19	-0.12	0.08	0.63	**0.24**	1.23	0.15	0.00	0.00	0.00	0.00	0.00	1.00

Table 3. Raman-XRF prediction obtained from a low-level data fusion system.

Mid-level Raman and XRF data fusion

Raman and XRF extracted features are used to set up the Raman-XRF meta-spectra used for discrimination of ochre pigments. These features are those variables which denote the maximum discrimination power between classes as it was explained in the theory section.

Following the same scheme of methodologies as in the low-level sensor fusion study, classification and prediction of new samples (Raman-XRF) was performed by a PLS-DA model. The model was performed using five latent variables and it was determined by the leave-one-out cross-validation analysis.

In Figure 8 score plots LV1-LV2 and LV1-LV3 are showed; the score plot of the two first latent variables can be used to visually discriminate all the classes, also known and unknown samples are better clustered in their corresponding classes. The distribution of classes is better than those obtained with the low-level Raman-XRF fusion and the Raman and XRF individual models.

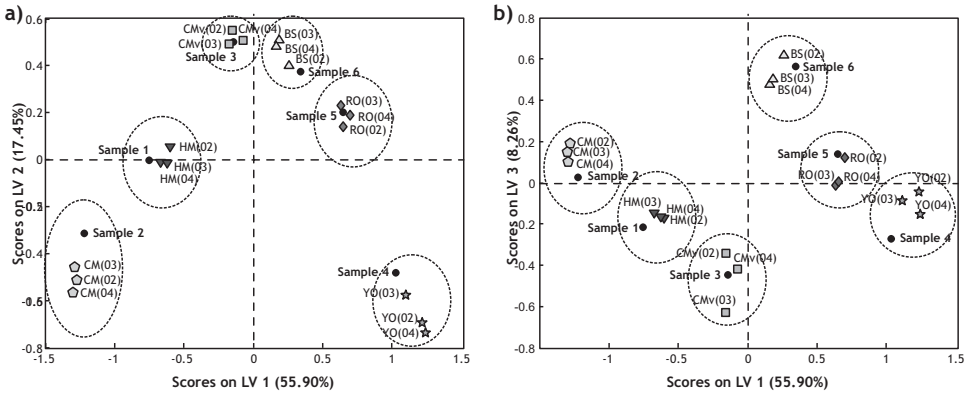

Figure 8. PLS DA on Raman-XRF meta-spectra from a mid-level data fusion model. a) LV1 – LV2 score plot, and b) LV1 – LV3 score plot.

The prediction results for unknown samples obtained by this model are presented in Table 4. The discrimination of HM and CM samples is also improved with this methodology and the rest of the samples are correctly predicted. The predicted probabilities for each corresponding class are 1 and 0 for the rest of the classes, asserting that all

classes can be correctly identified. The reduced values of Q_{red} and T^2_{red} show that all the samples are mostly within the 95% limits of the classes (Table 3).

SAMPLE	PLS-DA CLASS ASSIGNMENT						THRESHOLD			PREDICTED PROBABILITY					
	C(1)	C(2)	C(3)	C(4)	C(5)	C(6)		Q(red)	T^2(red)	P(1)	P(2)	P(3)	P(4)	P(5)	P(6)
Hematite	0.47	0.15	0.05	-0.20	-0.03	-0.25	**0.34**	0.66	0.08	1.00	0.00	0.00	0.00	0.00	0.00
Caput mortum	0.03	0.55	-0.02	-0.22	-0.16	-0.23	**0.30**	0.91	0.12	0.00	1.00	0.00	0.00	0.00	0.00
Caput mortum violet	0.09	-0.12	0.82	-0.17	-0.18	-0.18	**0.41**	0.83	0.12	0.00	0.00	1.00	0.00	0.00	0.00
Red ochre	0.03	-0.22	-0.03	0.62	0.05	-0.35	**0.20**	1.16	0.15	0.00	0.00	0.00	1.00	0.00	0.00
Yellow ochre	-0.19	-0.12	-0.08	-0.07	0.81	-0.06	**0.20**	0.84	0.08	0.00	0.00	0.00	0.00	1.00	0.00
Burnt Sienna	-0.04	-0.13	-0.19	-0.16	0.06	0.72	**0.31**	1.06	0.10	0.00	0.00	0.00	0.00	0.00	1.00

Table 4. Raman-XRF prediction obtained from a mid-level data fusion system.

High-level Raman and XRF data fusion

Results obtained from the individual classification models were fused by means of the four fuzzy aggregation connective operators and majority vote rule, as described in the theory section. The results obtained for maximum, average, minimum and product aggregations are presented in Table 5 a-d), and the decisiveness of these operators increases in that order [10].

Fusion results by maximum aggregation give a correct prediction for samples in all pigment classes. However, sample 1 (hematite) and sample 2 (caput mortum) could be misclassified by this aggregation operator. Sample 2 has a score of 0.54 for the hematite class and 0.56 for the caput mortum class. These values are too close to one another to obtain an accurate assignment of the pigment class.

Average aggregation also gives a correct prediction for all samples in each class. This fuzzy aggregation operator gives a global result of the predictions given by the Raman and XRF analysis. This operator reflects the potential of the sensor fusion process in the study of ochre pigments. The identification of hematite and caput mortum samples is successfully achieved; the level of decisiveness is not the optimal one for the caput mortum samples but its classification is really improved by the fusion process.

Using the minimum aggregation operator the sample of caput mortum pigment could not be correctly predicted due to the fact that this operator uses the minimum score given by the sensors. In this case, this score corresponds to the XRF analysis in which sample 2 (caput mortum) was incorrectly assigned to the class caput mortum violet. The rest of the samples were correctly identified in their corresponding classes.

Finally, with product aggregation we obtained a correct assignment for all the samples. As we could observe in the average aggregation, the caput mortum sample was well predicted but the certainty of this result is bad influenced by the results obtained for hematite and caput mortum violet samples. This is due to the close similarities observed in their Raman spectra and the poor prediction obtained from the individual models.

Applied Spectroscopy, submitted.

a) MAXIMUM AGGREGATION

SAMPLE	CLASS ASSIGNMENT						MAJORITY VOTE
	C(1)	C(2)	C(3)	C(4)	C(5)	C(6)	
1 (Hematite)	0.58	0.39	0.29	0.15	0.26	0.19	Hematite
2 (Caput mortum)	0.54	0.56	0.41	0.15	0.26	0.08	Caput mortum
3 (Caput mortum violet)	0.29	0.21	0.74	0.16	0.22	0.18	Caput mortum violet
4 (Red ochre)	0.24	0.17	0.19	0.73	0.38	0.13	Red ochre
5 (Yellow ochre)	0.08	0.19	0.31	0.38	0.69	0.27	Yellow ochre
6 (Burnt Sienna)	0.23	0.21	0.31	0.34	0.29	0.60	Burnt Sienna

b) AVERAGE AGGREGATION

SAMPLE	CLASS ASSIGNMENT						MAJORITY VOTE
	C(1)	C(2)	C(3)	C(4)	C(5)	C(6)	
1 (Hematite)	0.50	0.29	0.28	0.11	0.23	0.16	Hematite
2 (Caput mortum)	0.39	0.45	0.39	0.13	0.13	0.08	Hematite - Caput mortum
3 (Caput mortum violet)	0.26	0.18	0.68	0.15	0.12	0.17	Caput mortum violet
4 (Red ochre)	0.23	0.15	0.18	0.63	0.31	0.07	Red ochre
5 (Yellow ochre)	0.08	0.19	0.20	0.27	0.56	0.26	Yellow ochre
6 (Burnt Sienna)	0.19	0.11	0.18	0.26	0.24	0.58	Burnt Sienna

c) MINIMUM AGGREGATION

SAMPLE	CLASS ASSIGNMENT						MAJORITY VOTE
	C(1)	C(2)	C(3)	C(4)	C(5)	C(6)	
1 (Hematite)	0.42	0.19	0.28	0.06	0.20	0.12	Hematite
2 (Caput mortum)	0.24	0.35	0.37	0.11	0.00	0.07	Caput mortum
3 (Caput mortum violet)	0.23	0.16	0.61	0.15	0.01	0.16	Caput mortum violet
4 (Red ochre)	0.21	0.12	0.17	0.52	0.24	0.02	Red ochre
5 (Yellow ochre)	0.08	0.18	0.08	0.16	0.43	0.26	Yellow ochre
6 (Burnt Sienna)	0.15	0.02	0.06	0.17	0.19	0.56	Burnt Sienna

d) PRODUCT AGGREGATION

SAMPLE	CLASS ASSIGNMENT						MAJORITY VOTE
	C(1)	C(2)	C(3)	C(4)	C(5)	C(6)	
1 (Hematite)	0.24	0.07	0.08	0.01	0.05	0.02	Hematite
2 (Caput mortum)	0.13	0.20	0.15	0.02	0.00	0.01	Caput mortum
3 (Caput mortum violet)	0.07	0.03	0.45	0.02	0.00	0.03	Caput mortum violet
4 (Red ochre)	0.05	0.02	0.03	0.38	0.09	0.00	Red ochre
5 (Yellow ochre)	0.01	0.04	0.03	0.06	0.30	0.07	Yellow ochre
6 (Burnt Sienna)	0.03	0.00	0.02	0.06	0.06	0.34	Burnt Sienna

Table 5. High-level Raman-XRF data fusion system results by means of fuzzy aggregation connectives. a) Maximum aggregation, b) Average aggregation, c) Minimum aggregation, and d) Product aggregation.

Conclusions

The combination of micro-Raman spectroscopy and micro-X-ray fluorescence spectrometry offers a powerful tool for the characterization of pigments in works of art. This combination implemented in a portable instrument needs to be complemented with robust methodologies for data processing. Three strategies to perform data-fusion followed by classification analysis were presented in this work and successful results were obtained for the classification of ochre pigments; their benefits and drawbacks are discussed below.

Low-level fusion is the simplest way to perform data fusion. However, signal processing must be performed after concatenation of raw spectra, especially to remove background signal components from both types of spectral data in order to apply chemometric tools on the fused data. Redundancies in data and different types of noise could convey a poor performance of the classification method. In spite of this, classification of ochre pigments was improved using low-level fusion. PCA and PLS-DA models performed with the fused data are more robust for prediction of new samples and visual discrimination from class distributions is better with respect to those results obtained by individual classification.

Mid-level fusion implements another step in which features from each type of signals are extracted and fused. The main advantage of this methodology is the possibility of discarding irrelevant data. The extra computation needed for variable selection is compensated with the rapid processing of only a few set of variables fused instead of the full spectra concatenated. These benefits are obtained by the reduction of the reduced values of Q_{red} and T^2_{red} to values closer or smaller than one. Also, a better distribution of classes in the multivariate space given by PCA and PLS-DA is obtained. In that way, each group could be easily identified in PCs plots.

High-level fusion improves ochre classification with respect to individual classifications. It is simple to implement for classification purposes, and fuzzy aggregation connectives are a good tool for the inference and combining stage. More information is needed in order to increment the certainty in the discrimination of hematite and caput mortum classes. This is related to the fact that the only significant difference between these two pigments is in the amount of Silicon.

This methodology permits the fusion of different types of data. To that end, in a further study, quantification results obtained by XRF analysis may also be incorporated to the Raman-XRF data-fusion model in order to improve classification results.

Acknowledgments

The authors acknowledge financial support from the European Community Project, Competitive and Sustainable growth program (G6RD-CT2001-00602).

References

[1] P. Vandenabeele, A. von Bohlen, L. Moens, R. Klockenkamper, F. Joukes and G. Dewispelaere, Analytical Letters 33, (2000), 3315-3332.

[2] P. Moioli and C. Seccaroni, X Ray Spectrometry 29, (2000), 48-52.

[3] K. H. A. Janssens, F. C. V. Adams and A. Rindby, Microscopic X-ray Fluorescence Analysis; John Wiley & Sons, LTD, (2000).

[4] P. Vandenabeele, T. L. Weis, E. R. Grant and L. J. Moens, Analytical and Bioanalytical Chemistry 379, (2004), 137-142.

[5] K. Andrikopoulos, S. Daniilia, B. Roussel and K. Janssens, Journal of Raman Spectroscopy submitted, (2006).

[6] J. Esteban, A. Starr, R. Willetts, P. Hannah and P. Bryanston-Cross, Neural Computing & Applications 14, (2005), 273 - 281.

[7] V. Steinmetz, F. Sevila and V. Bellon-Maurel, Journal of Agricultural Engineering Research 74, (1999), 21-31.

[8] P. Boilot, E. L. Hines, M. A. Gongora and R. S. Folland, Sensors and Actuators B: Chemical 88, (2003), 80-88.

[9] S. Roussel, W. Bellon-Maurel, J. M. Roger and P. Grenier, Journal of Food Engineering 60, (2003), 407-419.

[10] I. Bloch, Systems, Man and Cybernetics, Part A, IEEE Transactions on 26, (1996), 52-67.

[11] D. L. Hall and J. Llinas, Proceedings of the IEEE 85, (1997), 6-23.

[12] U. Indahl and T. Naes, Journal of Chemometrics 18, (2004), 53-61.

[13] H. Nocairi, E. Mostafa Qannari, E. Vigneau and D. Bertrand, Computational Statistics & Data Analysis 48, (2005), 139-147.

[14] F. Delmotte and P. Smets, Ieee Transactions on Systems Man and Cybernetics Part a-Systems and Humans 34, (2004), 457-471.

[15] P. Geladi and B. R. Kowalski, Analytica Chimica Acta 185, (1986), 1-17.

[16] M. Barker and W. Rayens, Journal of Chemometrics 17, (2003), 166-173.

[17] L. A. Zadeh, Information and Control 12, (1968), 94-102.

[18] L. A. Zadeh, Computer 21, (1998), 83-93.

[19] M. Otto, Chemometrics and Intelligent Laboratory Systems 4, (1988), 101-120.

[20] D. Dubois and H. Prade, Information Sciences 36, (1985), 85-121.

[21] Z. S. Xu and Q. L. Da, International Journal of Intelligent Systems 18, (2003), 953-969.

[22] L. Lam and S. Y. Suen, Systems, Man and Cybernetics, Part A, IEEE Transactions on 27, (1997), 553-568.

[23] D. Bikiaris, S. X. Daniilia, S. Sotiropoulou, O. Katsimbiri, E. Pavlidou, A. P. Moutsatsou and Y. Chryssoulakis, Spectrochimica Acta Part a-Molecular and Biomolecular Spectroscopy 56, (2000), 3-18.

[24] D. L. A. deFaria, S. V. Silva and M. T. deOliveira, Journal of Raman Spectroscopy 28, (1997), 873-878.

[25] L. F. C. de Oliveira, H. G. M. Edwards, R. L. Frost, J. T. Kloprogge and P. S. Middleton, Analyst 127, (2002), 536-541.

6

Chapter 6: Data-fusion and dual-domain classification

This chapter describes two dual-domain fusion models based on multiresolution, one of the main advantages of wavelet transform. The first model is intended to perform mid-level fusion in the wavelet domain and its performance as a new tool to fuse Raman and XRF data is presented in the paper: *Data fusion and dual-domain classification analysis of pigments studied in works of art*.

The second model performs high-level fusion in the wavelet domain and the class assignments are combined by means of fuzzy aggregation connectives operators. The performance of this model is presented in the paper: *Data fusion in the wavelet domain by means of fuzzy aggregation connectives.*

6.1. DUAL-DOMAIN ANALYSIS

6.1.1. Introduction

The idea of performing classification at different levels of resolution is founded on the fact that in spectroscopy different phenomena occur at different frequencies; for example, detector noise, spikes, instrumental disturbances, peaks, drifts, all of them in different forms. The spectral variations related to the properties of interest appear mostly in the middle range of frequencies.

The benefits of the multiscale representation may also be used to extract empirical models from measured data that are multiscale in nature. Since most data contain contributions at multiple scales, multiscale methods are expected to result in better empirical models than those obtained by existing methods.

Latent variables regression methods have the inherent ability of reducing errors by retaining only those latent variables that capture the relationship between the variables. Unfortunately, this approach can never eliminate the errors completely, since the scores and loadings retained will still be contaminated by these errors. PLS-DA decrease the contribution of errors in data matrix, but it is impossible to eliminate the entire error while capturing the underlying relationship between the variables.

Multiscale or dual-domain PLS-DA combines the properties of wavelet analysis and PLS-DA. The relationship between the variables is de-correlated by PLS-DA, while the relationship between the stochastic measurements is approximately de-correlated by the wavelet decomposition. By applying multiresolution analysis, the signal can be scrutinized at different scales. However, it is also possible to manipulate the signals in different ways depending on the objectives. For example, to clean up the data, one can apply thresholding techniques in order to reduce or eliminate small coefficients. Unwanted features, such as low frequency signal components can be eliminated as was described in chapter 3. Another possibility explored in this chapter is to perform fusion on features scales of data from different sensors. This idea is analysed in the following sections of this chapter.

6.1.2. Data fusion and dual-domain classification analysis of pigments studied in works of art.

Pablo M Ramos and Itziar Ruisánchez.

Analytica Chimica Acta 558, 2006, 274-282.

Analytica Chimica Acta 558 (2006), 274-282

DATA FUSION AND DUAL-DOMAIN CLASSIFICATION ANALYSIS OF PIGMENTS STUDIED IN WORKS OF ART

Pablo Manuel Ramos and Itziar Ruisánchez

Department of Analytical Chemistry and Organic Chemistry. Universitat Rovira i Virgili. Campus Sescelades, C/. Marcel·lí Domingo, s/n 43007 Tarragona, SPAIN

Abstract

We propose a new mid-level data-fusion system to process, as a unique signal, the Raman and X-ray fluorescence (XRF) spectra obtained from the first micro-Raman-XRF instrument. The system is based on the main advantage of the wavelet transform, which is multiresolution. First, each spectrum set is split into blocks according to their frequency. The blocks which contains background and noise signals are removed and variable selection is performed on the remaining blocks to extract those variables with the most power of classification. These variables are concatenated and form a Raman-XRF meta-signal ensemble. Finally, dual-domain signal ensembles from references and samples are classified using partial least squares discriminant analysis (PLS-DA). Our results show that this system is suitable for rapidly and automatically classifying ancient pigments using the complementary information provided by both techniques. Classification with different levels of difficulty can be handled and no prior knowledge of the sample composition is required. This system has been applied to real spectra of ancient pigments and can also be applied to combinations of other spectral signals.

Keywords: Data fusion; Wavelet transform; Dual-domain partial least squares discriminant analysis (DDPLS-DA); micro Raman spectroscopy; micro X-ray fluorescence spectrometry; Ancient pigments.

Introduction

Micro Raman spectroscopy (Raman) and micro X-ray fluorescence (XRF) microscopy are particularly well suited to identifying ancient pigments in cultural heritage studies. Raman provides a fingerprint of the material being analysed while XRF provides the qualitative and quantitative elementary composition [1-8]. Both have the attributes of high reproducibility and high sensitivity and are non-destructive techniques [5, 6, 9]. Their ever-increasing contribution to the study of

works of art can be partially ascribed to major improvements in the configuration of new instrumentation [10-13]. The development of portable instruments for *in situ* measurements and for gathering suitable information in a non-destructive way have played an particularly important role in these improvements, since the main objective of art analysis is to acquire the maximum amount of information on an object while keeping the risk of damage as low as possible.

Complementary methods maximise the amount of information obtained. Raman and XRF techniques are a good combination because they provide complementary information. Both techniques have so far been used independently, in the sense that the spectra are obtained and processed independently from their respective instruments and single conclusions are obtained, by expert analysts, considering both results. Since the beginning of this century, a new generation of analytical instruments is being developed. The first prototype of an instrument that combines Raman and XRF techniques in a single instrument and contains all the attributes of both techniques is currently being tested in art and archaeological studies.

This improvement in analytical instrumentation provides micro Raman and XRF spectra from the same spot in the sample. In this sense, a new perspective for data processing is needed in order to find tools to quickly and easily process large amounts of data from several sources (complementary techniques) and obtain, by data fusion, a single result. Data fusion is a formal framework that expresses the means and tools to integrate data from several sources. It has been widely used in robotics, remote sensing, image analysis and, in the last years, in analytical chemistry [14-17].

The aim of this paper is to show the ability of a mid-level data fusion system to combine Raman and XRF spectra for classifying pigments studied in cultural heritage. Classification is further done by Partial Least Square Discriminant Analysis (PLS-DA), the input for which is the single output obtained from the data fusion. Additionally, classification prediction is done by minimizing the number of false positives and negatives using Bayes theorem.

Data fusion is performed on the dual-domain spectra obtained from the wavelet transform. Since analytical signals are essentially multiscale signals, noise is usually located in high frequency ranges while background components are located at low frequency ranges. In wavelet transform, an original signal is decomposed into multiple scales in the frequency domain. This multiresolution property of the wavelet transform provides significant advantages for solving modern multivariate regression problems. In dual-domain regression analysis, the raw signals (time domain signals) are first transformed into the wavelet domain (frequency domain) and then information from both domains is incorporated into the regression model. Liu and Brown made an excellent study of the connection of multiresolution representation of the original signal in wavelet regression using the concept of data fusion [18].

Data processing

Dual-domain spectra

The wavelet transform [19, 20] provides multiresolution. The term *dual-domain* is used because the spectra possess local features in the time domain and also reflect local aspects in the frequency domain. Tan and Brown propose the dual-domain spectra [21-23] by means of the pyramid algorithm developed by Mallat [24] coupled with wavelet reconstruction. As a result, a time-domain signal is separated into a set of multifrequency scales, each of which retains the original length of the signal. Approximation and details components are reconstructed separately; they are mutually orthogonal and contribute to the original signal from different frequency ranges and have the same resolution as the original signal. So, baseline-like information can be found in the lowest frequency approximation component whereas noise-like information is mostly located in high frequency detail components. Figure 1 shows a scheme in which, from the Raman raw data matrix each spectrum is decomposed by means of the wavelet transform and its approximation and details are reconstructed and stored separately. This results in a group of matrices or blocks containing all the spectral information grouped by particular frequencies.

The main advantage of using this decomposition over those often reported in chemometrics is that here there is no wavelength compression as the scale increases, so it is possible to examine and selectively remove certain local features with restricted frequency characteristics.

Tan and Brown proposed modelling separately, at different frequency scales, each block with the frequency components in the dual-domain obtained by the wavelet prism (Figure 1). They successfully demonstrated the capacity of this method for regression analysis [21]. Here, we perform classification analysis on the dual-domain spectra produced from a wavelet prism decomposition of two spectroscopic data sets. In addition to this and based on this method, we perform a data fusion procedure in dual-domain classification.

Mid-level data fusion

As a first step in mid-level fusion, variable selection is performed in each data source (sensor) and the selected variables are then concatenated to be processed as a single signal [18]. As we said, in this paper we use the blocks obtained from the respective wavelet prism of Raman and XRF data as the sensors to be fused. From each data source, first we select, from the wavelet prism, those blocks with details that are free of noise and background contributions. Variable selection is then

performed on these blocks using the method proposed by Indahl and Naes, which identifies the local positive maxima and negative minima of the loading weights which defines the directions in the variable space with good classification power [25, 26]. In our application, we use the loading weights obtained from the standard PLS-DA algorithm and select a small set of wavelengths around each selected point to provide more stable models. In the next step, the selected variables from the blocks of the two wavelet prisms (Raman and XRF) are concatenated to form a single matrix containing singular features from the bands and peaks of the Raman and XRF spectra. The resulting matrix is called meta-spectra since it contains the extracted features which characterize each pigment. Finally, the meta-spectra matrix is processed using Partial least squares for discriminant analysis (PLS-DA) to perform pigment classification.

PLS-DA

As its name implies, in PLS-DA a PLS model is developed to predict the class assignment of each sample. We will not go into details of PLS theory, which has largely been described elsewhere [27]. PLS-DA is carried out using an exclusive binary coding scheme with one bit per class [28]. For example, if ones want to discriminate between six classes, a response encoded {0,0,0,1,0,0} means that the sample belongs to class 4. During the calibration process, the PLS-DA method is trained to compute the six membership values one for each class. The sample is then assigned to the class that shows the highest membership value. The class assignment result is expressed in terms of a value from 0 to 1, but these values are the projected results in the multidimensional space defined by the factors selected. So, really these values are normally distributed around 0 when the prediction is not being in a class and around 1 when the prediction is to being in a class. For that reason is possible to obtain prediction values below 0 (negative values) and also above 1.

In addition to the PLS-DA class assignment, we have implemented the Bayes theorem to obtain a threshold value for each class, the purpose is to obtain a discrete class assignment for the continuous values obtained from the PLS-DA. More specifically, Bayes theorem is used to calculated a threshold value to assume that a sample belongs or not to a determinate class of pigments [29]. For instance, a sample will be classified in the class for which the PLS-DA class assignment value is greater than the threshold value. The Bayesian threshold calculation assumes that the predicted *y* values follow a distribution similar to that which will be observed for future samples. Using these estimated distributions, a threshold is selected at the point where the two estimated distributions cross. This is the value at which the number of false positives and false negatives should be minimized for future predictions.

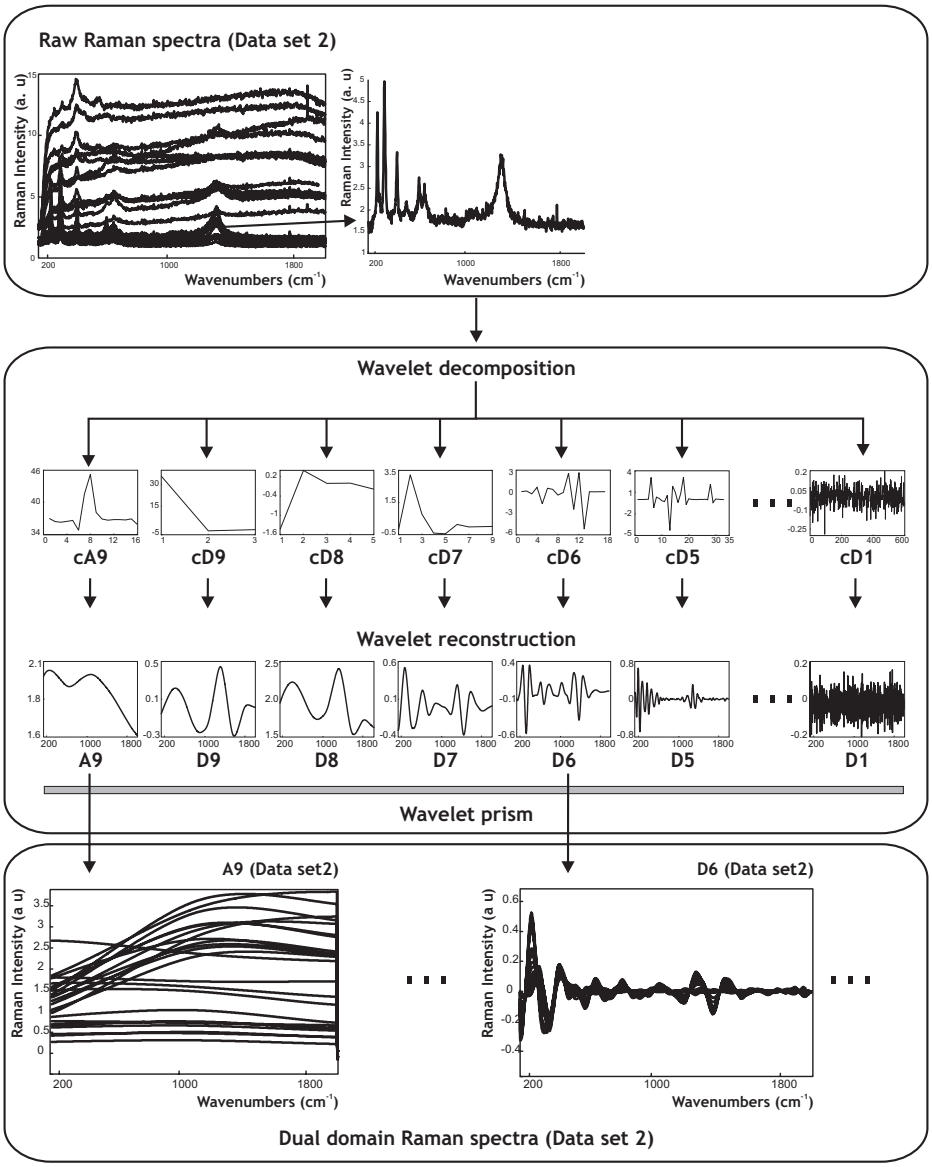

Figure 1. Procedure for obtaining the dual-domain spectra from raw Raman spectra of the pigments from data set 2.

To study the robustness of the models, prediction probability is obtained with the references samples used to build the PLS-DA model. The purpose of the implemented algorithm is to discriminate probabilities of discrete classes for continuous predicted values. The actual PLS-DA class assignments at the model y-value predictions are used to obtain a probability that the given value belongs to each of the original classes [30].

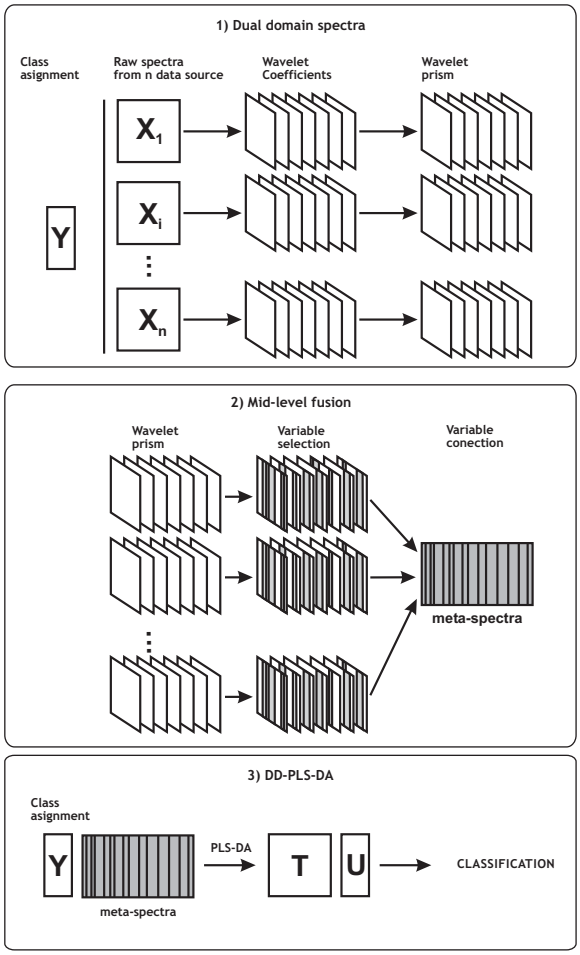

Figure 2. Scheme of the proposed method: mid-level data fusion and dual-domain classification.

The residual *Q* and the Hotelling T^2 values are calculated in order to obtain the lack of fit for the PLS-DA model. The *Q* statistic indicates how well each sample conforms to the PLS-DA model. It is a measure of the difference, or residual between a sample and its projection into the five latent variables retained in the model. The T^2 statistic is a measure of the variation in each sample within the PLS-DA model. The tables 1, 2 and 3 contains the reduced *Q* and T^2 values which are the original *Q* and T^2 values divided by respective *Q* and T^2 values at the 95% confidence interval. Inspection of the reduced *Q* and T^2 reveals how many samples are not within the 95% limits of the classes.

One important aspect of this general PLS-DA approach is that we get access to very useful score-plots of the X-space (samples space), showing disposition of all objects and classes reflecting the PLS-DA derived discrimination.

Experimental

Samples and instruments

Reference spectra are pigments from one of the most well-known collections of artists' pigments, the Kremer's collection. Two data sets of pigments were selected. Data set 1 constitutes an easy identification problem in which the samples can be identified using only one of the two techniques. The pigments studied are: minium (Pb_3O_4), cinnabar (HgS), cadmium red (CdS), ultramarine blue ($Na_{6-10}Al_6Si_6O_{24}S_{2-4}$), lead white ($2PbCO_3.Pb(OH)_2$) and hematite ($Fe_2O_3$). The data set 2, comprises ochre pigments whose main component is iron oxide (III) (Fe_2O_3). The pigments studied are: hematite, caput mortum, caput mortum violet; yellow ochre, red ochre and burnt sienna. These pigments are usually characterised by investigating the presence of minor components, which normally requires the use of complementary techniques. It is important to study iron (III) oxide pigments and ochre differentiation when studying ancient pigments [31-33].

In both cases, for each pigment, four Raman and XRF spectra are obtained at different spots of the pigment. Three of these are used to build the PLS-DA model and one is to be predicted. The reference and samples are selected randomly.

The instrument used is a prototype of a combined micro-Raman/micro-XRF instrument comprising a remote measuring head attached to an easily transportable base unit [34]. The Raman-XRF microprobe has a camera to select different grains and measure in the middle of them. So, with this instrument we measure on a pure pigment grain, then is possible to manage the problem of mixtures of pigments.

Software

The algorithms for data-fusion methodology were programmed with Matlab software version 6.5. The wavelet transform applications belonged to the wavelet toolbox from Matlab software and PLS-DA applications belonged to the PLS toolbox 3.5 from Eigenvector Research Incorporated.

Methodology

Our scheme for pigment classification based on DDPLS-DA is shown in Figure 2. In the first step, the X_i data spectra from references and samples are decomposed by means of the wavelet transform and the wavelet prism is then obtained. In our application, the optimal wavelet used was Symmlet 8 until a level of decomposition of 9 was reached. This wavelet was used because we have found that it is a very good wavelet for modelling spectra. The Symmlet 8 basis resembles to some extent the shape of peaks found in Raman and XRF spectra. The Symmlet wavelets are a

modification version of Daubechies wavelet family with more symmetry but retaining great simplicity. Another reason is that the wavelet Symmlet 8 has 8 vanishing moments. From the theory of wavelet transform we have that a wavelet with *k +1* vanishing moments is suitable to suppress long term evolution signals which can be represented by a polynomial of degree *k*. With this combination of properties we can optimize the frequency discrimination of the split signal in the wavelet prism.

In the second step, the blocks and variables are selected, since when studying ancient pigments with Raman spectroscopy, it is very common to encounter low frequency signals from the fluorescence effect of the sample. Therefore, the detailed components containing frequency components from the signals of interest are selected. Following the guidelines of Tan and Brown, we calculated the Shannon entropy to select these detail components [22]. The details from level 3 to 7 were selected and, from each level, variable selection is performed using the strategy for supervised classification developed by Indahl and Naes [25]. The selected variables from each detail component are concatenated and, according to Liu and Brown [18], this process is actually very much related to the concept of data fusion. To balance the different scaling of data coming from both techniques in the fused data, we normalized them dividing each wavelet prism by the maximal intensity observed in the detail blocks. So, data is balanced by the maximal intensity of the peaks in the respective techniques avoiding the influence of the respective backgrounds signals and keeping the relative band intensities within a group.

Finally, the Raman-XRF concatenated data is used to build the PLS-DA model. The number of latent variables retained in each PLS-DA model was five and the length of the Raman-XRF meta-spectra was 1599 points. To see which variables from the original spectra have more classification power, local positive maximum (or negative minimum) values of the loading weights from the first two latent variables in the dual-domain are projected onto the corresponding variables of the original spectra in the single-domain. This allows us to see which Raman bands or XRF peaks from the original spectra the model uses to discriminate. Note that this method can be applied for one or more data source.

Results and discussion

As we have already mentioned, our proposed method can be divided into three steps:

1. Dual domain spectra are obtained by means of the wavelet transform and variable selection is performed on them.
2. Mid-level fusion on the wavelet dual-domain is applied to data provided by the Raman-XRF instrument.

3. Classification is done by means of PLS-DA. The scores from the two first latent variables of the PLS-DA model are projected in order to determine which groups can be identified, and the sample is therefore classified.

The proposed method is tested in two ways. First we present the results obtained using only the data provided by each technique (individual classification). Then we present the results provided by the Raman and XRF data fusion. In this way we will show the potential of using mid-level data-fusion in the wavelet domain and properly compare the results obtained in both cases.

Raman classification

Classification results for the two data sets of pigments are presented in Table 1. For data set 1, the 6 samples are easily and well classified since all are given a correct class assignment by the DDPLS-DA method; class assignments are around 0.8 and above of the corresponding threshold. No pigments are misclassified and the model has a prediction probability value of 1 of belonging to the proper class while the prediction probabilities values of the other classes are 0. The reduced values of Q_{red} and T^2_{red} show that all the samples in data set 1 are within the 95% limits of the classes (Table 1a).

For the samples included in data set 2, four pigments are misclassified (Table 1b). Two of these are hematite and caput mortum, since they have DDPLS-DA class assignment very close to the estimated threshold (Table 1b). Also, the prediction probability shows that the model cannot predict very well since although the prediction probability for the correct class assignment is close to 1, they have also a prediction probability value above zero for the wrong class assignment (0.31 and 0.45 respectively). These two pigments are usually very difficult to characterize using Raman spectroscopy alone [33]. The other two misclassified pigments are caput mortum violet and burnt sienna. Burnt sienna has two DDPLS-DA class assignments above the threshold value and the prediction probability shows that for caput mortum violet sample, the model cannot distinguish between class 3 (caput mortum violet) and class 6 (burnt sienna).

Iron (III) oxide pigments presents very similar Raman spectra and can be discriminated, by expert analysts, due to the presence of minor differences in the shape and height of the Raman bands.

In both sets we can observe that some DD PLS-DA predictions are projected below zero values and the corresponding threshold values are small and close to zero. This is due to the unequal dispersion of the classes and samples within a class.

a)

SAMPLE	PREDICTION PROBABILITY						DD PLS-DA CLASS ASSIGNMENT								
	P(1)	P(2)	P(3)	P(4)	P(5)	P(6)	C(1)	C(2)	C(3)	C(4)	C(5)	C(6)	Q(red)	T^2(red)	THRESHOLD
Minium	**1.00**	0.00	0.00	0.00	0.00	0.00	**0.82**	-0.18	-0.16	-0.16	-0.18	-0.17	0.0610	0.2386	**0.71**
Cinnabar	0.00	**1.00**	0.00	0.00	0.00	0.00	-0.16	**0.86**	-0.18	-0.17	-0.17	-0.17	0.0100	0.2536	**0.19**
Cadmium red	0.00	0.00	**1.00**	0.00	0.00	0.00	-0.24	-0.14	**0.88**	-0.17	-0.13	-0.19	0.7270	0.2716	**0.06**
Ultramarine blue	0.00	0.00	0.00	**1.00**	0.00	0.00	-0.12	-0.15	-0.16	**0.78**	-0.18	-0.17	0.3471	0.2112	**0.33**
Lead white	0.00	0.00	0.00	0.00	**1.00**	0.00	-0.19	-0.18	-0.13	-0.14	**0.80**	-0.15	0.1958	0.2222	**0.16**
Hematite	0.00	0.00	0.00	0.00	0.00	**1.00**	-0.12	-0.17	-0.12	-0.19	-0.18	**0.78**	0.4580	0.2120	**0.08**

b)

SAMPLE	PREDICTION PROBABILITY						DD PLS-DA CLASS ASSIGNMENT								
	P(1)	P(2)	P(3)	P(4)	P(5)	P(6)	C(1)	C(2)	C(3)	C(4)	C(5)	C(6)	Q(red)	T^2(red)	THRESHOLD
Hematite	**0.96**	**0.31**	0.00	0.00	0.00	0.00	**0.28**	**0.11**	-0.05	-0.28	-0.26	-0.04	0.2671	0.0765	**0.13**
Caput mortum	**0.45**	**1.00**	0.00	0.00	0.00	0.00	**0.24**	**0.59**	-0.23	-0.20	-0.23	-0.26	0.4077	0.1675	**0.27**
Caput mortum violet	0.11	0.00	**1.00**	0.00	0.00	**1.00**	0.01	-0.19	**0.54**	-0.19	-0.21	-0.22	0.6592	0.1414	**0.31**
Red ochre	0.11	0.00	0.00	**1.00**	0.00	**0.47**	-0.24	-0.07	-0.18	**0.34**	-0.13	0.00	0.9579	0.1000	**0.15**
Yellow ochre	0.09	0.00	0.00	0.00	**1.00**	0.02	-0.04	-0.25	-0.25	0.23	**0.77**	-0.03	0.6064	0.2587	**0.48**
Burnt Sienna	0.12	0.00	0.00	0.02	0.00	**1.00**	-0.25	-0.19	**0.17**	0.10	0.05	**0.55**	1.1174	0.1326	**0.10**

Table 1. Raman classification. a) Data set 1 Class assignment; C(1): minio, C(2): cinnabar, C(3): cadmium red; C(4): ultramarine blue, C(5): lead white and C(6): hematite. Data set 1 Prediction probability; P(1): minio, P(2): cinnabar, P(3): cadmium red; P(4): ultramarine blue, P(5): lead white and P(6): hematite. b) Data set 2 Class assignment; C(1): hematite, C(2): caput mortum, C(3), caput mortum violet, C(4): red ochre, C(5): yellow ochre and C(6): burnt sienna. Data set 2 Prediction probability; P(1): hematite, P(2): caput mortum, P(3), caput mortum violet, P(4): red ochre, P(5): yellow ochre and P(6): burnt sienna.

XRF classification

The classification results are presented in Table 2. For data set 1, all samples are easily and well identified since all are given a correct class assignment by the DDPLS-DA method. No pigments are misclassified and the model has a DDPLS-DA prediction probability of 1 of belonging to the proper class, while the prediction probabilities of the other classes are 0. The reduced values Q_{red} and T^2_{red} show that all the samples in set 1 are within the 95% limits of the classes (Table 2a).

For the samples included in data set 2, four pigments (caput mortum, red ochre, burnt sienna and hematite) are partially misclassified since their prediction values for class assignment are very close to the estimated threshold and caput mortum and red ochre have two possible class assignments. Red ochre, yellow ochre and burnt sienna cannot be predicted since the model shows very low prediction probability values. Finally, for caput mortum, the model cannot distinguish between class 2 and class 4 (Table 2b).

In both sets we can observe that some predictions are projected below zero values and the corresponding threshold values are small or below zero. This is due to the unequal dispersion of the classes and samples within a class.

a)

SAMPLE	PREDICTION PROBABILITY						DD PLS-DA CLASS ASSIGNMENT								
	P(1)	P(2)	P(3)	P(4)	P(5)	P(6)	C(1)	C(2)	C(3)	C(4)	C(5)	C(6)	Q(red)	T^2(red)	THRESHOLD
Minium	**1.00**	0.00	0.00	0.00	0.00	0.00	**0.94**	-0.17	-0.19	-0.07	-0.38	-0.14	0.6159	0.3496	**0.21**
Cinnabar	0.00	**1.00**	0.00	0.00	0.00	0.00	-0.11	**0.78**	-0.09	-0.19	-0.26	-0.14	0.0259	0.2161	**-0.12**
Cadmium red	0.00	0.00	**1.00**	0.00	0.00	0.00	-0.09	-0.17	**0.89**	-0.20	-0.25	-0.17	0.0593	0.2919	**-0.07**
Ultramarine blue	0.00	0.00	0.00	**1.00**	0.00	0.00	-0.13	-0.16	-0.13	**0.54**	0.05	-0.17	0.0345	0.1601	**0.50**
Lead white	0.00	0.00	0.00	0.00	**1.00**	0.00	-0.16	-0.17	-0.17	-0.21	**0.86**	-0.16	0.0777	0.3365	**0.15**
Hematite	0.00	0.00	0.00	0.00	0.00	**1.00**	-0.16	-0.17	-0.17	-0.16	-0.18	**0.84**	0.0027	0.2404	**-0.22**

b)

SAMPLE	PREDICTION PROBABILITY						DD PLS-DA CLASS ASSIGNMENT								
	P(1)	P(2)	P(3)	P(4)	P(5)	P(6)	C(1)	C(2)	C(3)	C(4)	C(5)	C(6)	Q(red)	T^2(red)	THRESHOLD
Hematite	**1.00**	0.00	0.00	0.00	0.00	0.00	**0.40**	-0.10	-0.03	-0.20	-0.05	-0.02	0.4694	0.0863	**0.27**
Caput mortum	0.00	**0.97**	0.00	**0.89**	0.00	0.00	-0.23	**0.36**	-0.01	**0.30**	-0.30	-0.13	0.8251	0.1832	**0.31**
Caput mortum violet	0.00	0.00	**1.00**	0.00	0.00	0.00	-0.12	0.10	**0.45**	-0.12	-0.25	-0.06	0.6313	0.1204	**0.32**
Red ochre	0.12	0.00	0.00	0.00	0.00	0.00	**0.24**	-0.23	-0.13	-0.16	**0.22**	0.07	0.4611	0.0902	**0.17**
Yellow ochre	0.00	0.00	0.00	0.03	**0.01**	0.00	-0.02	-0.03	-0.21	0.01	**0.37**	-0.11	0.5044	0.0839	**0.43**
Burnt Sienna	0.00	0.00	0.00	**0.18**	0.00	**0.44**	-0.17	-0.25	0.05	0.10	-0.03	**0.41**	0.7427	0.1063	**0.41**

Table 2. XRF classification. a) Data set 1 Class assignment; C(1): minio, C(2): cinnabar, C(3): cadmium red; C(4): ultramarine blue, C(5): lead white and C(6): hematite. Data set 1 Prediction probability; P(1): minio, P(2): cinnabar, P(3): cadmium red; P(4): ultramarine blue, P(5): lead white and P(6): hematite. b) Data set 2 Class assignment; C(1): hematite, C(2): caput mortum, C(3), caput mortum violet, C(4): red ochre, C(5): yellow ochre and C(6): burnt sienna. Data set 2 Prediction probability; P(1): hematite, P(2): caput mortum, P(3), caput mortum violet, P(4): red ochre, P(5): yellow ochre and P(6): burnt sienna.

Raman-XRF classification

Classification results for the two data sets of pigments are presented in Table 3. For data set 1 and 2, all the samples are easily and well identified since all are given a correct class assignment by the DDPLS-DA method. No pigments are misclassified and the model has a prediction probability of 1 of belonging to the proper class, while the prediction probabilities of the other classes are 0. We observed that when a single spectroscopic technique (Raman or XRF) is used to analyse the ochre samples, the sum of these probabilities are above one.

a)

SAMPLE	PREDICTION PROBABILITY						DD PLS-DA CLASS ASSIGNMENT								
	P(1)	P(2)	P(3)	P(4)	P(5)	P(6)	C(1)	C(2)	C(3)	C(4)	C(5)	C(6)	Q(red)	T^2(red)	THRESHOLD
Minium	**1.00**	0.00	0.00	0.00	0.00	0.00	**0.84**	-0.16	-0.16	-0.16	-0.18	-0.17	0.1575	0.1870	**0.03**
Cinnabar	0.00	**1.00**	0.00	0.00	0.00	0.00	-0.16	**0.81**	-0.17	-0.15	-0.16	-0.16	0.8961	0.1812	**0.08**
Cadmium red	0.00	0.00	**1.00**	0.00	0.00	0.00	-0.19	-0.16	**0.77**	-0.09	-0.13	-0.20	0.6384	0.2148	**0.08**
Ultramarine blue	0.00	0.00	0.00	**1.00**	0.00	0.00	-0.11	-0.15	-0.17	**0.78**	-0.18	-0.17	0.3067	0.1708	**0.61**
Lead white	0.00	0.00	0.00	0.00	**1.00**	0.00	-0.46	-0.07	-0.19	-0.10	**0.73**	-0.11	0.1797	0.2547	**0.50**
Hematite	0.00	0.00	0.00	0.00	0.00	**1.00**	-0.14	-0.17	-0.14	-0.17	-0.18	**0.80**	0.4052	0.1734	**0.28**

b)

SAMPLE	PREDICTION PROBABILITY						DD PLS-DA CLASS ASSIGNMENT								
	P(1)	P(2)	P(3)	P(4)	P(5)	P(6)	C(1)	C(2)	C(3)	C(4)	C(5)	C(6)	Q(red)	T^2(red)	THRESHOLD
Hematite	**1.00**	0.00	0.00	0.00	0.00	0.00	**0.58**	-0.04	-0.23	-0.07	-0.18	-0.01	0.3764	0.1306	**0.35**
Caput mortum	0.00	**1.00**	0.00	0.00	0.00	0.00	0.01	**0.69**	-0.08	-0.37	-0.26	-0.30	0.5455	0.1912	**0.16**
Caput mortum violet	0.00	0.00	**1.00**	0.00	0.00	0.00	-0.13	-0.17	**0.71**	-0.12	-0.16	-0.15	0.7647	0.1826	**0.21**
Red ochre	0.00	0.00	0.00	**1.00**	0.00	0.00	-0.24	-0.02	-0.10	**0.34**	-0.04	-0.02	0.8991	0.1041	**0.19**
Yellow ochre	0.00	0.00	0.00	0.00	**1.00**	0.00	-0.07	-0.29	-0.22	0.28	**0.78**	-0.03	0.5766	0.2287	**0.49**
Burnt Sienna	0.00	0.00	0.00	0.00	0.00	**1.00**	-0.14	-0.17	-0.07	-0.05	-0.14	**0.51**	1.0597	0.1079	**0.34**

Table 3. Raman-XRF data-fusion classification. a) Data set 1 Class assignment; C(1): minio, C(2): cinnabar, C(3): cadmium red; C(4): ultramarine blue, C(5): lead white and C(6): hematite. Data set 1 Prediction probability; P(1): minio, P(2): cinnabar, P(3): cadmium red; P(4): ultramarine blue, P(5): lead white and P(6): hematite. b) Data set 2 Class assignment; C(1): hematite, C(2): caput mortum, C(3), caput mortum violet, C(4): red ochre, C(5): yellow ochre and C(6): burnt sienna. Data set 2 Prediction probability; P(1): hematite, P(2): caput mortum, P(3), caput mortum violet, P(4): red ochre, P(5): yellow ochre and P(6): burnt sienna.

The meaning of this is that a sample can be (or there are some probability of be) categorized in more than one class. For example, in Table 1 b); the sample caput mortum could be well discriminated using only the Raman data in the Dual Domain PLS-DA, because the only predicted value above the threshold value is for the class 2 that correspond to the caput mortum class. But, looking the prediction probability values we observe that misclassification of future samples is possible using only this information, because there some probability of put the caput mortum sample in class 1 which corresponds to hematite class. When we use the Raman-XRF data in the Dual Domain PLS-DA, the probability values shows that the power of classification is improved and the probabilities of pigment misclassification are minimized or cancelled.

The reduced values Q_{red} and T^2_{red} show that all the samples in data set 1 are within the 95% limits of the classes (Table 3a), so samples are inside of the 95% limits of the classes.

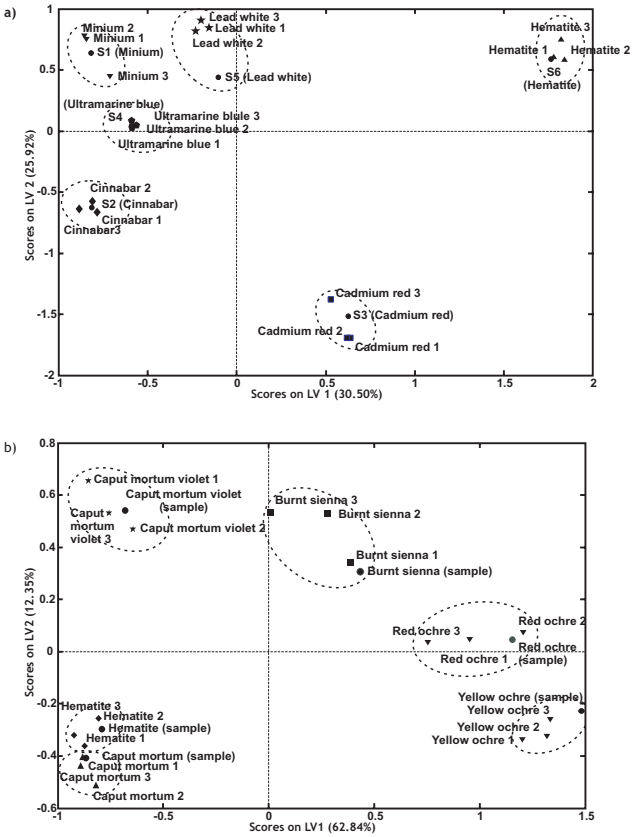

Figure 3. Projection of PLS-DA scores from the Raman-XRF meta-spectra onto latent variables 1 and 2 (LV1 and LV2). a) Classification of pigments from different families, data set 1: minio, cinnabar, cadmium red, ultramarine blue, lead white and hematite. b) Classification of pigments within a family, data set 2: hematite, caput mortum, caput mortum violet, red ochre, yellow ochre and burnt sienna.

Figures 3a and 3b show, respectively, the projection of both data sets onto each model, where each group can be easily grouped using the two first latent variables. The loading weights of the first two latent variables from the PLS-DA models are studied in order to establish which variables have the most power of classification and to relate them to the original variables of the raw Raman and XRF spectra.

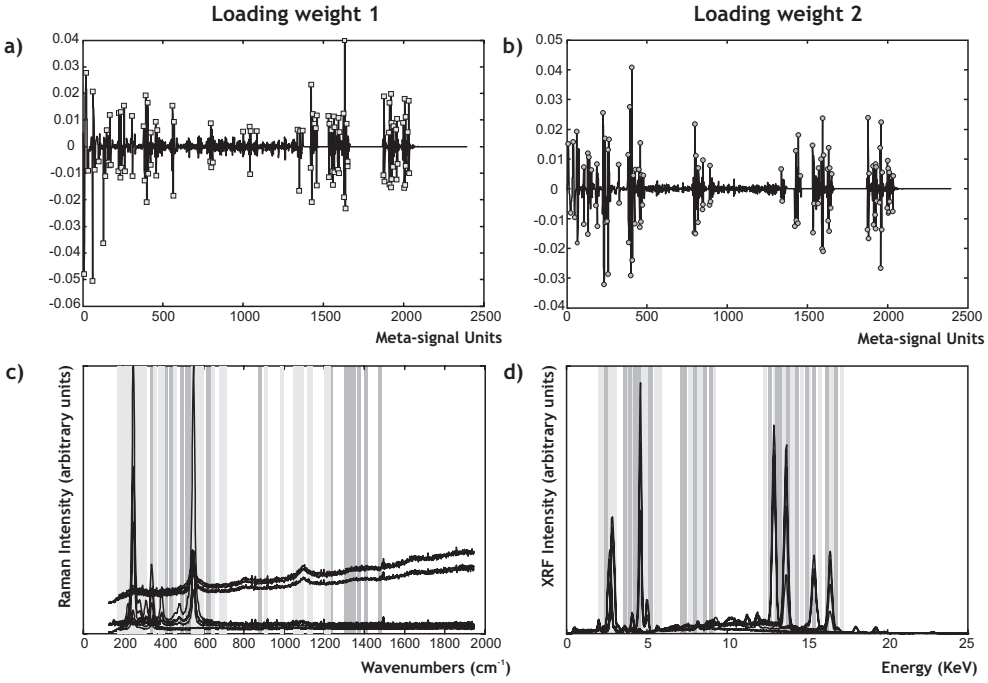

Figure 4. Local positive maxima and negative minima of the first two loading weights from the PLS-DA model (Raman-XRF meta-spectra classification) projected onto the corresponding original variables of Raman and XRF raw spectra. For data set 1: a) loading weights 1, b) loading weights 2, c) Raman raw spectra from data set 1, and d) XRF raw spectra from data set 1.

Figure 4 for data set 1 identifies the local positive maxima and negative minima with values above half the maximum loading weight and links them with the corresponding Raman bands and XRF peaks. For this data set, the major peaks from each type of spectra are those with the most classification power. Classification is performed by looking for the more intensity signals in XRF analysis and the same happens for the Raman contribution. The principal Raman bands are those used to discriminate between families of pigments. For data set 2, Figure 5 shows that the variables involved in the classification are not those that correspond to the more intense bands or major peaks. Classification is done by observing differences in the shapes and heights of the Raman bands and, in the case of the XRF spectra, the variables with the most classification power are those corresponding to peaks of

the minor elements present in these pigments, e.g. Potassium, Calcium, Titanium, Manganese and Zinc. In fact, this is the method usually applied by the expert analyst to discriminate these types of samples.

Again, we can observe that some predictions are projected below zero values and the corresponding threshold values are small and close to zero. This is due to the unequal dispersion of the classes and samples within a class.

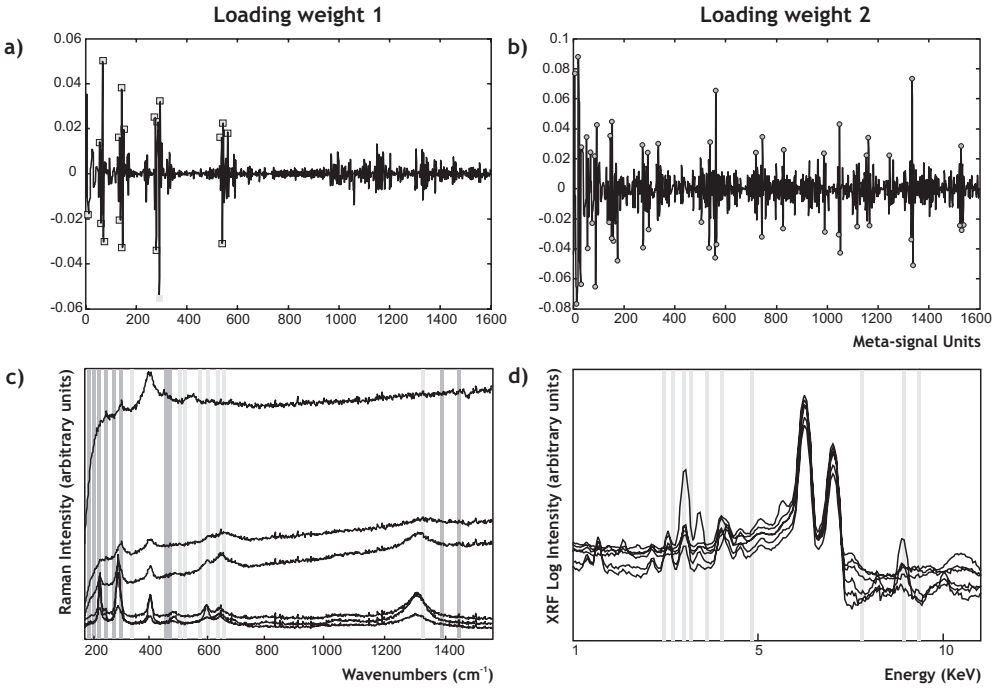

Figure 5. Local positive maxima and negative minima of the first two loading weights from the PLS-DA model (Raman-XRF meta-spectra classification) projected onto the corresponding original variables of Raman and XRF raw spectra. For data set 2: a) loading weights 1, b) loading weights 2, c) Raman raw spectra from data set 2, and d) XRF raw spectra from data set 2 (mean spectrum from each group).

Conclusions

The main aim of this work was to describe a data-fusion system to be implemented in a new micro Raman-XRF instrument. A preliminary study was performed in two groups of pigments representing the different levels of classification usually found in the study of ancient pigments. The first challenge

was to perform an automatic classification of pigments with different compositions that therefore present different features in the Raman and XRF spectra obtained from them. The second challenge was to increase the difficulty of the classification problem, so we selected a group of iron (III) oxide pigments and studied them with this system. Both challenges were well accomplished in this preliminary study using mid-level data-fusion in the dual-domain and the advantages of using non-destructive complementary techniques to study pigments in works of art have once more been demonstrated.

We want to emphasize that to properly validate the results obtained in the ochre pigments case study, it is necessary a bigger set of ochre references and samples.

This methodology follows the expert analyst strategy for pigments identification, it is simple to apply and the process is not time consuming. It is suitable for processing large amounts of data automatically and can be applied to an individual data source or *n* data sources to achieve data fusion.

The system uses the wavelet transform technique by means of wavelet multiscale analysis. A great advantage is that, as local features of spectra signals in terms of time and frequency domain are considered, predictions are improved. Mid-level data fusion enables us to generate a unique signal to be processed in a classification model and then obtain a single result. Here we have used PLS-DA because it has a proven robustness for discrimination but, clearly, other classification tools can also be used.

Acknowledgement

This work was supported by the European Community Project, Competitive and Sustainable growth program (G6RD-CT2001-00602). The authors gratefully acknowledge Koen Janssens at University of Antwerp and Konstantinos S. Andrikopoulos of Ormylia Arts Diagnostic Centre for providing reference samples and helpful comments.

References

[1] P. Vandenabeele, Journal of Raman Spectroscopy 35, (2004), 607-609.

[2] R. J. H. Clark, Comptes Rendus Chimie 5, (2002), 7-20.

[3] H. G. M. Edwards, S. E. J. Villar and K. A. Eremin, Journal of Raman Spectroscopy 35, (2004), 786-795.

[4] K. L. Brown and R. J. H. Clark, Journal of Raman Spectroscopy 35, (2004), 217-223.

[5] L. Burgio, R. J. H. Clark and K. Theodoraki, Spectrochimica Acta Part a-Molecular and Biomolecular Spectroscopy 59, (2003), 2371-2389.

[6] P. Vandenabeele, A. von Bohlen, L. Moens, R. Klockenkamper, F. Joukes and G. Dewispelaere, Analytical Letters 33, (2000), 3315-3332.

[7] R. Klockenkamper, A. von Bohlen and L. Moens, X Ray Spectrometry 29, (2000), 119-129.

[8] M. Mantler and M. Schreiner, X Ray Spectrometry 29, (2000), 3-17.

[9] G. VanHooydonk, M. DeReu, L. Moens, J. VanAelst and L. Milis, European Journal of Inorganic Chemistry, (1998), 639-644.

[10] P. Moioli and C. Seccaroni, X Ray Spectrometry 29, (2000), 48-52.

[11] J. L. Ferrero, C. Roldan, D. Juanes, E. Rollano and C. Morera, X-Ray Spectrometry 31, (2002), 441-447.

[12] A. Perardi, L. Appolonia and P. Mirti, Analytica Chimica Acta 480, (2003), 317-325.

[13] M. Perez-Alonso, K. Castro, I. Martinez-Arkarazo, M. Angulo, M. A. Olazabal and J. M. Madariaga, Analytical and Bioanalytical Chemistry 379, (2004), 42-50.

[14] J. Esteban, A. Starr, R. Willetts, P. Hannah and P. Bryanston-Cross, Neural Computing & Applications 14, (2005), 273 - 281.

[15] V. Steinmetz, F. Sevila and V. Bellon-Maurel, Journal of Agricultural Engineering Research 74, (1999), 21-31.

[16] P. Boilot, E. L. Hines, M. A. Gongora and R. S. Folland, Sensors and Actuators B: Chemical 88, (2003), 80-88.

[17] S. Roussel, W. Bellon-Maurel, J. M. Roger and P. Grenier, Journal of Food Engineering 60, (2003), 407-419.

[18] Y. Liu and S. D. Brown, Analytical and Bioanalytical Chemistry 380, (2004), 445-452.

[19] B. K. Alsberg, A. M. Woodward and D. B. Kell, Chemometrics and Intelligent Laboratory Systems 37, (1997), 215-239.

[20] B. Walczak, Wavelets in Chemistry; Elsevier, (2000)

[21] H. Tan and S. D. Brown, Analytica Chimica Acta 490, (2003), 291-301.

[22] H. W. Tan and S. D. Brown, Journal of Chemometrics 16, (2002), 228-240.

[23] H. W. Tan and S. D. Brown, Journal of Chemometrics 17, (2003), 111-122.

[24] S. G. Mallat, Pattern Analysis and Machine Intelligence, IEEE Transactions on 11, (1989), 674-693.

[25] U. Indahl and T. Naes, Journal of Chemometrics 18, (2004), 53-61.

[26] H. Nocairi, E. Mostafa Qannari, E. Vigneau and D. Bertrand, Computational Statistics & Data Analysis 48, (2005), 139-147.

[27] P. Geladi and B. R. Kowalski, Analytica Chimica Acta 185, (1986), 1-17.

[28] M. Barker and W. Rayens, Journal of Chemometrics 17, (2003), 166-173.

[29] D. L. Massart, B. G. M. Vandeginste, L. M. C. Buydens, S. d. Jong, P. J. Lewi and J. Smeyers-Verbeke, Handbook of chemometrics and qualimetrics: Part A; Elsevier science B.V., 1997

[30] B. M. Wise, N. B. Gallagher, R. Bro, J. M. Shaver, W. Windig and R. Scott Koch, PLS_Toolbox Version 3.5 for use with MATLAB™; Eigenvector Research, Inc., (2005).

[31] D. Bikiaris, S. X. Daniilia, S. Sotiropoulou, O. Katsimbiri, E. Pavlidou, A. P. Moutsatsou and Y. Chryssoulakis, Spectrochimica Acta Part a-Molecular and Biomolecular Spectroscopy 56, (2000), 3-18.

[32] D. L. A. deFaria, S. V. Silva and M. T. deOliveira, Journal of Raman Spectroscopy 28, (1997), 873-878.

[33] L. F. C. de Oliveira, H. G. M. Edwards, R. L. Frost, J. T. Kloprogge and P. S. Middleton, Analyst 127, (2002), 536-541.

[34] K. Janssens, Z. Jia, M. V. Gysel and P. V. Espen, PRAXIS: A Combined micro-Raman –micro-XRF Instrument, Euroanalysis XIII, Salamanca, Spain, 6-10 September. (2004).

6.1.3. Data fusion in the wavelet domain by means of fuzzy aggregation connectives.

Pablo M Ramos and Itziar Ruisánchez.

Chemometrics and Intelligent Laboratories, submitted.

Chemometrics and Intelligent Laboratories, submitted.

DATA FUSION IN THE WAVELET DOMAIN BY MEANS OF FUZZY AGGREGATION CONNECTIVES

Pablo Manuel Ramos and Itziar Ruisánchez

Department of Analytical Chemistry and Organic Chemistry. Rovira i Virgili University. Campus Sescelades, C/. Marcel·lí Domingo, s/n 43007 Tarragona, SPAIN

Abstract

Dual-domain classification analysis is proposed to identify pigments used in works of art studied by Raman spectroscopy and X-ray fluorescence spectrometry. By means of this methodology, Raman and X-ray fluorescence data obtained from a prototype of a micro Raman/XRF instrument are jointly processed by a high-level fusion approach. The system proposed aims to avoid the pre-processing stage and directly process raw data obtained from the instrument. The system was tested with spectra contaminated with background components of different shapes and intensities and the results were good. The benefits of the approach were well demonstrated in a study of an ochre pigment classification.

The approach is based on the main advantage of wavelet transform, which is multiresolution. Each spectrum is split into blocks, according to a specific frequency, to form a wavelet prism. Partial Least Squares Discriminant Analysis (PLS-DA) is then applied to those blocks which contain the deterministic part of the signal and are not influenced by noise and background signal components. From fuzzy set theory, a group of fuzzy aggregation connective operators are used to perform a high-level data fusion with the decision levels obtained from PLS-DA analysis. Our study showed that fuzzy aggregation may be suitable for performing high-level data fusion on dual-domain data. This method can be automated so that classification can be rapid. It can handle classifications with different levels of difficulty and requires no prior knowledge of sample composition.

Keywords: Data fusion; Wavelet transform; Fuzzy aggregation connectives; micro Raman spectroscopy; micro X-ray spectrometry; Ancient pigments

Introduction

At times, specific problems can only be solved by the use of an additional

analytical technique to maximize and optimize the amount of information. In this respect, Raman spectroscopy and X-ray fluorescence spectrometry (XRF) are a very good combination because they provide complementary information: Raman spectroscopy provides information about the molecular structure while XRF analysis provides a qualitative and quantitative elementary composition. Since the turn of the century a new generation of analytical instruments has been developed. The first prototype of a single instrument combining Raman and XRF techniques, with all the attributes of both, is currently being tested in art and archaeological studies [1-3].

Thanks to this improvement in analytical instrumentation we can now not only obtain micro Raman and XRF spectra from the same spot in the sample, but also perform one and two dimensional scanning. So, a new perspective on data processing is therefore needed if tools are to be found to process large amounts of data from more than one source (complementary techniques) quickly and easily and, by means of data fusion, obtain a single result. Data fusion is a formal framework in which the means and tools for combining data from several sources are expressed. It has been widely applied to robotics, remote sensing, image analysis and analytical chemistry [4-7]. In most data fusion systems, the information extracted from each sensor is represented as a degree of belief in an event with real values. These degrees of belief are combined through numerical fusion operators. Fuzzy set theory has predominantly been used at the combination stage [8]. Aggregation operations can be applied by simple fuzzy aggregation connective operators.

The aim of this paper is to create a system based on dual-domain regression with fuzzy aggregation connectives for classifying pigments in works of art. The system is evaluated in Raman and XRF studies of ancient pigments. It is shown that it can improve the classification of pigments and process raw data with featured noise and background interferences. Finally, we show how this system can perform Raman and XRF data fusion and therefore improve the classification results of the techniques when they are applied individually.

The concept of dual-domain is given by wavelet transform theory. In wavelet transform, an original signal is decomposed into multiple scales in the frequency domain. This multiresolution property of wavelet transformation is an important feature that provides significant advantages for solving modern multivariate regression problems. In dual-domain regression analysis, the raw signals (time domain signals) are first transformed into the wavelet domain (frequency domain) and then information from both domains is incorporated into a classification model [9-12].

The aim of many recent studies in the field of cultural heritage, performed by conservation scientists, is to identify pigments in works of art. Micro Raman spectroscopy (Raman) and micro X-ray fluorescence (XRF) microscopy are particularly well suited to this field [13]. Both techniques are highly reproducible, highly sensitive and non-destructive. Their ever increasing contribution to the study

of works of art is partly due to recent major improvements in the configuration of new instrumentation [14, 15], in which the development of portable instruments for taking *in situ* measurements and collecting suitable information in a non-destructive way has played a significant role, since the main objective of art analysis is to acquire the maximum amount of information about an object while minimizing the risk of damage.

Theory

Dual-domain spectra

Multiresolution is achieved by wavelet transform [16]. Using the pyramid algorithm developed by Mallat [17] coupled with wavelet reconstruction, Tan and Brown proposed the dual-domain spectra, in which a time-domain signal is separated into a set of multifrequency scales, each of which retains the original length of the signal. The term *dual-domain* is used because the spectra possess local features in the time (wavelength) domain and reflect local aspects (a limited bandwidth) in the frequency domain. This application is described in several studies by Tan and Brown [9, 12, 18].

The idea is to decompose a set of spectra using the wavelet transform and then reconstruct them separately. As a result, a time-domain signal is separated into a set of multifrequency scales, each of which retains the original length of the signal. These components are better known as approximation (A) and detail (D) components. They are mutually orthogonal, contribute to the original signal from different frequency ranges and have the same resolution as the original signal. The total sum of these contributions gives the original signal; therefore, all the original information from the signal is stored. The main advantage of using this decomposition is that there is no wavelength compression as the scale increases, so it is possible to examine and selectively remove certain local features with restricted frequency characteristics. As a novelty, we propose modelling separately, at different frequency scales, each block with the frequency components in the dual-domain obtained by wavelet prism (Figure 1).

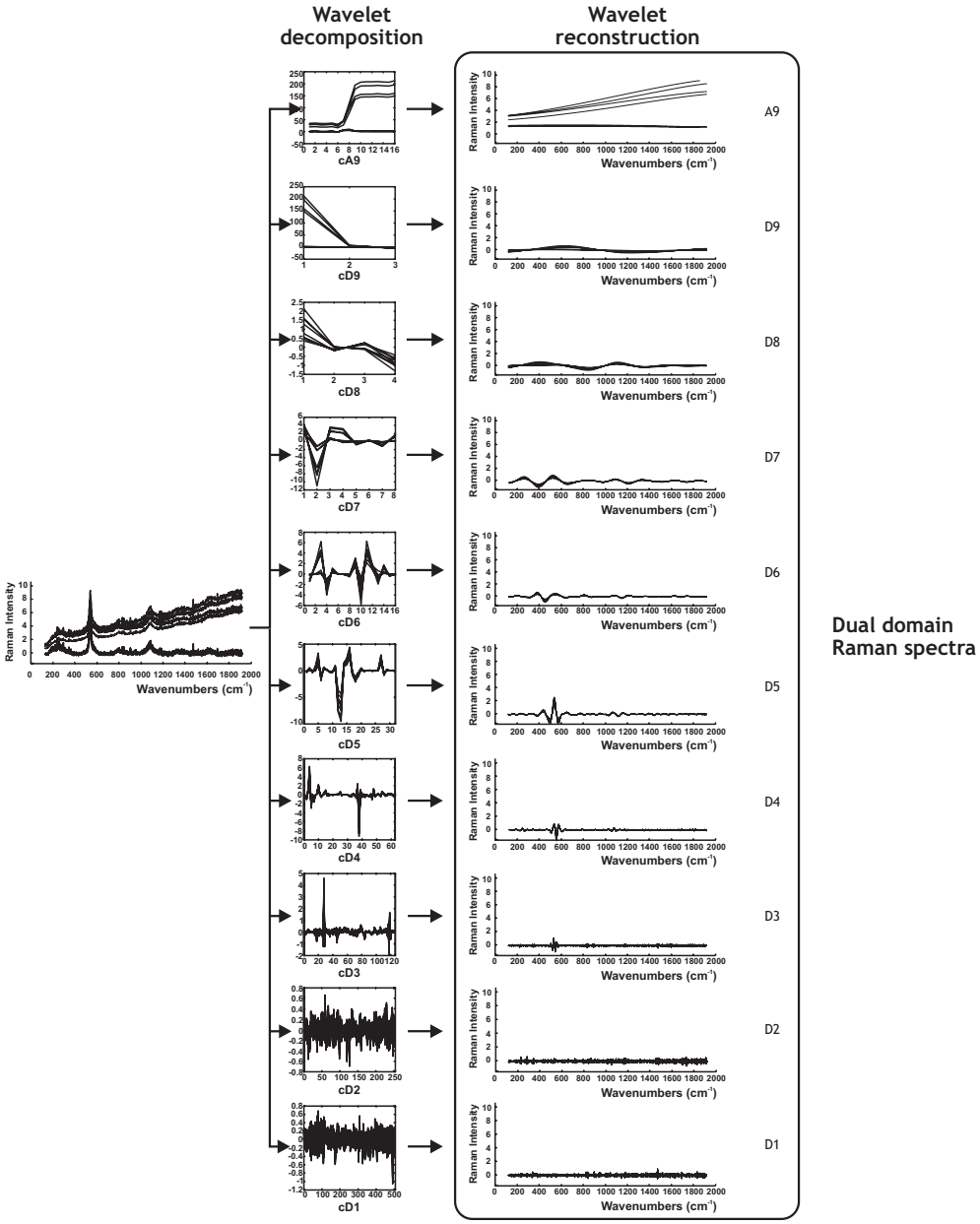

Figure 1. A Scheme of the procedure for obtaining dual-domain spectra from a Raman spectra data set of several ultramarine blue pigments. The spectra are decomposed at level 9 with one approximation coefficient (A9) and nine detail coefficients (D1….D9)

PLS-DA

As its name implies, in PLS-DA (Partial least squares – Discriminant analysis) a PLS model is used to predict the class to which each sample has been assigned. We will not go into details here about the theory of PLS and PLS-DA since it has largely been described elsewhere [19, 20]. PLS-DA uses an exclusive binary coding scheme with one bit per class. For example, if one wants to discriminate between four classes, a response encoded {0, 0, 1, 0} means that the sample belongs to class 3. During the calibration process, the PLS-DA method is trained to compute the four membership values one for each class. The sample is then assigned to the class that shows the highest membership value. The result of the class assignment is expressed in terms of a value between 0 and 1, but these values are the projected results in the multidimensional space defined by the factors selected. In fact, these values are normally distributed around 0 when the prediction is "not being in a class" and around 1 when the prediction is "being in a class". For this reason prediction values can be below 0 (negative values) and also above 1.

High-level data fusion

Data fusion combines information from several sources to produce a single model or decision. Data fusion models are presented in several published works [5, 7, 11, 21, 22]. High-level fusion is performed by using the identity declaration. In our particular case this is the classification result provided by each source. The classification results can be fused with heuristic techniques, Bayesian techniques, or the Defter-Shafer method. In this paper, we implemented soft computing solutions: from fuzzy set theory, we applied fuzzy aggregation connective operators to combine the classifiers. In high-level fusion wavelet regression, the predictors are outputs of individual models performed on each frequency scale and the same idea is applied here for a dual-domain classification analysis, where the classifiers are the outputs of the individual PLS-DA models performed on each frequency scale.

An appropriate weighting strategy or multiresolution block must be selected in order to combine the information from frequency components that contains the deterministic part of the signals and to avoid those components whose main components are noise (high frequency components) and background signals (low frequency components). In this study, we used the rate of change of the relative entropy of each frequency block with respect to the entropy in the original signal. This parameter is scaled to a value between 0 and 1, and we define a threshold value so that those blocks whose entropy values are above this threshold are kept (blocks with the deterministic part of the signal) and the rest are discarded (blocks with the interference components).

Fuzzy sets and fuzzy aggregation connectives

Fuzzy theory, introduced by Zadeh [23], is a powerful and general technology for processing information. It has numerous applications in areas such as control systems, pattern recognition, and signal processing. One reason for the success of fuzzy set theory in instrumentation and control is its flexible representation of human decision making.

A fuzzy set, say *A*, defined in the domain *U*, is described by a membership function m_A which maps the real interval [0,1]. For each $u \in U$, $m_A(u)$ gives the degree of membership of *u* to the set *A*, where 1 denotes full membership, 0 denotes no membership and any other value is partial membership.

We choose simple rescaling to devise the membership functions from PLS-DA predicted values. Let $x_{i,k}(c_j)$ be the predicted value obtained from the *ith* sample for the *kth* class when block c_j from the multiscale representation is processed. So:

$$m_{A_{i,k}}(c_j) = \frac{x_{i,k}(c_j) - \min(x_{i,k}(c_j))}{\max(x_{i,k}(c_j)) - \min(x_{i,k}(c_j))} \quad (1)$$

Hence, the information extracted from the multiscale classification analysis is represented as measures or degrees of belief in an event, which will belong or not to a class. Its representation as numerical degrees leads to a quantification of its characteristics (uncertain, imprecise, and incomplete) which have to be taken into account in a fusion process. Fuzzy aggregation connectives will be used to combine them.

An aggregation operator *F* is defined as: $F:[0:1]^n \rightarrow [0,1]$, which satisfies the following properties.

1. Limit conditions:

   $F(0,0,\ldots,0) = 0 \quad F(1,1,\ldots,1)=1$

2. Commutativity:

   $F(a_1,a_2,\ldots,a_n) = F(b_1,b_2,\ldots,b_n)$, where $b_1,b_2,\ldots,b_n$ is any permutation of $a_1,a_2,\ldots,a_n$ $a_i \in [0,1]$, $i=1,\ldots,n$

3. Monotonicity:

   $F(a_1,a_2,\ldots,a_n) \geq F(b_1,b_2,\ldots,b_n)$ for any $a_1,a_2,\ldots,a_n$, $b_1,b_2,\ldots,b_n \in [0,1]$, such that $a_i \geq b_i$, $\forall\ i = 1,\ldots,n$.

There is a wide range of fuzzy connectives and aggregation operators [24, 25]. For our study, we chose five fuzzy aggregation connective operators which belong to the class of context independent constant behaviour (CICB) operators [8]. This class consists of operators which behave in the same way whatever values of information have to be combined, and which are computed without any contextual or external information.

Let a_1 and a_2 denote two real variables representing the degrees of belief to be combined with values in the interval *I*, which is [0,1]. The extreme values of *I* play particular roles. The value 0 means that, for a prediction, the processed block provides a null measure, because it considers that this sample does not belong to the class under study. On the other hand, the value 1 means that the processed block considers that the sample belongs to the class under study and that the certainty is total. Values between 0 and 1 represent degrees of uncertainty or partial knowledge about the information. They can also be interpreted as imprecision, or as a quantity of information available about the event. An aggregation connective is consider to be a function *F* acting on a_1 and a_2, defining the combination or fusion operator. Under the closure property assumption, $F(a_1,a_2)$ also has values in *I*.

Simple aggregation operators

1. Pessimistic-type aggregation:

   Product: $F_1(a_1,a_2,\ldots,a_n) = a_1 \times a_2 \times \ldots \times a_n$

   Minimum: $F_2(a_1,a_2,\ldots,a_n) = min\ \{a_1,a_2,\ldots,a_n\}$

2. Optimistic-type aggregation:

   Maximum: $F_3(a_1,a_2,\ldots,a_n) = max\ \{a_1,a_2,\ldots,a_n\}$

3. Indifferent-type aggregation:

   Arithmetic average, (AA): $F_4(a_1,a_2,\ldots,a_n) = \frac{1}{n}(a_1 + a_2 + \ldots + a_n)$

Pessimistic aggregation reduces the less certain information and at most has confidence in the sensor which gives the smallest measure. It searches for a simultaneous satisfaction of criteria or objectives. Optimistic aggregation, on the other hand, increases the certainty we have about information and at least has confidence in the block which gives the greatest or the most certain prediction, or the most information. It expresses redundancy between criteria. An indifferent type of aggregation provides a global prediction, somewhere between the partial predictions provided by each block.

If a_i is replaced with $m_{A_{i,k}}(c_j)$, each of these aggregation operators defines a unique membership value for each class. Therefore, classification models performed on each scale can be fused to obtain a unique result from the multiresolution classification process.

The *majority vote rule* is implemented at a decision rule to obtain the ensemble decision [26]. This method is simple and it does not assume prior knowledge of the behavior of the individual classifiers. The majority vote assigns sample x to the most represented class label among the classifiers and connective outputs.

The following notations will be used:

$\mu_j^k(x)$ denotes the information (confidence or belief) about the membership of sample *x* to the class *j (j = 1…n)*.

$\mu_j(x)$ denotes the combination of each $\mu_j^k(x)$ by the operator *F* (i.e. overall information on class j resulting from the individual information provided by PLS-DA analysis in each block).

$$\mu_j(x) = F\left(\mu_j^k(x)\right), \quad k = 1...n \tag{2}$$

The decision rule is:

$$\mu_i(x) = \max_{j=1}^{C} \mu_j(x) \tag{3}$$

Where *i* denotes the class chosen by the decision process.

Experimental

Samples and instruments

The pigments studied here were from one of the best-known collections of artists' pigments: the Kremer's collection. A data set of eight pigments was selected: minio (Pb_3O_4), cinnabar (HgS), ultramarine blue ($Na_{6\text{-}10}Al_6Si_6O_{24}S_{2\text{-}4}$), lead white ($2PbCO_3.Pb(OH)_2$), caput mortum ($Fe_2O_3$), caput mortum violet ($Fe_2O_3$), yellow ochre ($Fe_2O_3.H_2O$, clay), red ochre ($Fe_2O_3$, clay). The data set consisted of 64 Raman and XRF spectra, which were obtained at different spots on the pigment. In order to test the robustness of the system developed, we removed the background component signals in half of the reference and sample spectra. So, each class had four spectra with background and four without background, identified with the index 1 and index 2, respectively. The PLS-DA model was built with a data set of 24 spectra which represented the whole analytical problem. This problem consisted of classifying pigments in one of four classes where the spectra had different background profiles between and within classes. The rest of the spectra were used as a test set.

The instrument used was a prototype of a micro Raman and micro XRF instrument which combines the excitation radiation from both techniques in a small sample area, which makes possible a position sensitive analysis with a spatial resolution of 5-50 microns [1-3]. It consists of an energy dispersive micro-beam X-ray fluorescence spectrometer with a fine focus X-ray tube (max. 50 kV, 30 W), a polycapillary optic with spot size of approximately 30 µm and a drift chamber detector with a sensitive area of 5 mm^2 and an energy resolution of < 140 eV.

The Raman spectrometer component (Jobin Yvon) has a two wavelength laser excitation (633 nm and 785 nm); a fiber optic connection of the measuring head to the spectrometer and a compact axial optical spectrometer for these two wavelength. The spectral range is: 130 cm^{-1} – 327 cm^{-1} for 633 nm, 130 cm^{-1} – 2240 cm^{-1} for 785 nm and the resolution: approx. 3 cm^{-1}/pixel for 633 nm and 2 cm^{-1}/pixel for 785 nm.

The Raman-XRF microprobe has a camera to select different grains of the pigment sample and it can measure in the middle of each one. So, with this instrument we measure on a pure grain, and then is possible to manage the problem of a mixture of pigments.

Software

The algorithms were programmed with Matlab software version 6.5. The wavelet transform applications belonged to the wavelet toolbox 2.0 from Matlab software, and PLS applications belonged to the PLS toolbox 3.5 from Eigenvector Research Incorporated.

Methodology

Our scheme for pigment classification based on dual domain PLS-DA is shown in Figure 3 and can be described in four stages.

In the first step, the spectra data are decomposed by means of the wavelet transform using the wavelet Symmlet 8 until a level of decomposition of 9. Details are reconstructed separately at each level in order to obtain the wavelet prism. The Symmlet 8 basis somewhat resembles the shape of the peaks found in Raman and XRF spectra and in a previous study we found it suitable for the wavelet processing of Raman data [27]. The Symmlet wavelets are a modified version of the Daubechies wavelet family: they have greater symmetry but at the same time are simpler. Another reason is that the wavelet Symmlet 8 has eight vanishing moments. The theory of wavelet transform [16] states that a wavelet with k+1 vanishing moments is suitable for suppressing long-term evolution signals which can be represented by a polynomial of degree k. With this combination of properties we can improve the frequency discrimination of the split signal in the wavelet prism. The original length of the data was 1024 points and the resulting wavelet prism generates 10 vectors of 1024 points.

The second step is to select those blocks whose frequency is in the range of the frequency of the signal of interest. Our criterion of selection is based on the change in the Shannon entropy of each block with respect to the original signal. The results obtained are shown in the examples in Figure 2 where it can be observed

that the middle frequencies of the wavelet prism have the highest values while the extremes frequencies have the lowest values. We normalized this parameter into a scale from 0 to 1 and defined a threshold value for selecting those blocks with entropy values above this threshold. In this study, a threshold value of 0.45 proved to be optimal, because blocks with lower entropies were mainly composed of noise and background signal components.

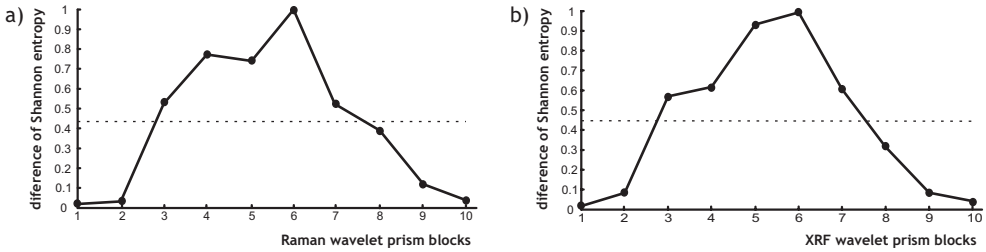

Figure 2. Rate of change of the Shannon entropy with respect to the original spectrum. a) Levels obtained for Raman data and b) Levels obtained for XRF data.

In the third step, classification was performed in each of the selected blocks. We chose PLS-DA as the classification methodology but, of course, other classification methodologies can be applied. The latent variables were selected after a cross validation study to define how many were required. Cross-validation was carried out by leave one out and this evaluation was then optimized by dividing the data into segments and removing the six spectra of each sample in each validation step.

The fourth and final step was the aggregation process. We fused the output results obtained from the PLS-DA models using the four fuzzy aggregation connective operators described above. As a result, the final classification was performed in terms of linguistic variables.

The methodology described was first applied to identify the samples studied by means of Raman spectroscopy. Then, we performed a single aggregation or fusion of all the outputs from the individual models obtained from the multiresolution analysis performed on Raman and XRF data. So we obtained a single classification result based on both spectroscopic analyses. A scheme of these processes is shown in Figure 3.

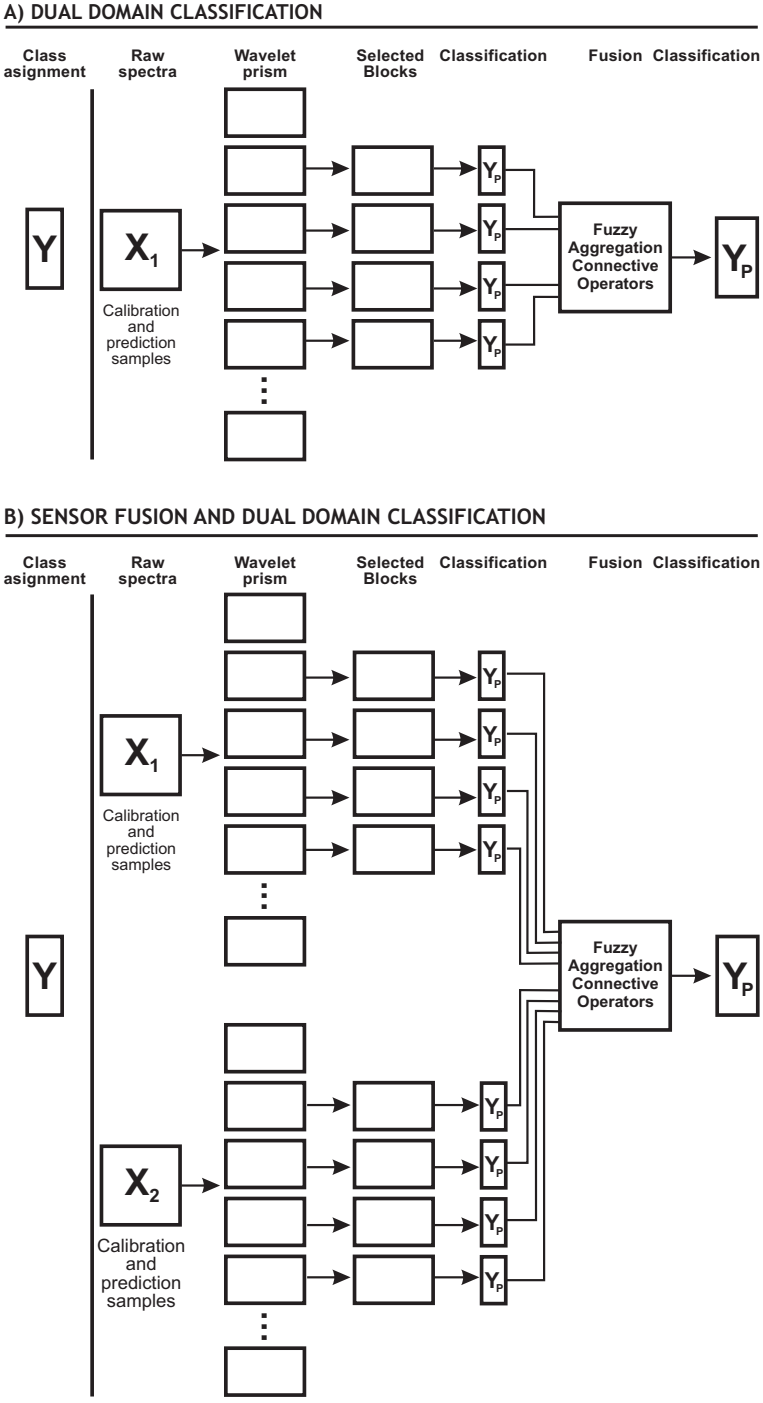

Figure 3. a) Dual-domain classification scheme for a single data source. **b)** Dual-domain classification and fusion of different data sources.

Results

The results obtained from applying the methodology described are discussed in two different situations. First, the methodology was applied to classify pigments based on Raman dual-domain. In this case, the possibility of using raw and pre-processed spectra as data input is shown. The processing of all aggregation operators is described using the example of the decision profile obtained for ultramarine blue sample 1 (spectra without pre-treatment).

Second, the methodology was applied to perform data fusion by means of Raman spectroscopy and XRF spectrometry. The capabilities of the methodology are shown by the improved classification results obtained for ochre pigments. The sensor fusion methodology is described with the analysis of the decision profile of yellow ochre sample 1 (spectra without pre-treatment), and the full classification results for all the ochre samples are presented.

In both cases, the classification results are presented first in the form of the overall prediction result given by indifferent aggregation fuzzy connectives, and then in the form of the full prediction given by the majority vote obtained from all fuzzy aggregation connective operators.

Raman dual-domain classification

Table 1 presents the overall classification results in terms of numerical values when indifferent aggregation fuzzy connectives are used. Prediction results were good for the minium, cinnabar, ultramarine blue and lead white pigments. For the other samples, prediction values were low and many of them were misclassified. This subset of samples corresponds to the family of ochre pigments and their classification will be described later.

The prediction results obtained demonstrate that the influence of background signal components, usually present in Raman raw spectra, can be minimized or even avoided in a classification analysis that uses this methodology. This is observed with the prediction values obtained for samples without (super-index 1) and with (super-index 2) pre-treatment; since both samples are well predicted and the corresponding prediction values are very close to each other. This result can be explained by the fact that the main background components of the signals are not included in the classification analysis. As an example, Figure 1 shows the spectra of ultramarine blue pigment used to build the calibration model and to predict. It also shows the spectra processed to obtain dual-domain spectra. We can see that the main background components of the signals are retained in block A9 of the dual-domain spectra, which is not included in the classification analysis.

Raman identification of new samples - Indifferent aggregation

	support for classes							
samples	minium	cinnabar	ultramarine blue	lead white	caput mortum	caput mortum violet	yellow ochre	red ochre
minium[1]	0.96	0.25	0.31	0.22	0.24	0.25	0.22	0.20
minium[2]	0.94	0.25	0.31	0.23	0.23	0.25	0.24	0.21
cinnabar[1]	0.19	0.89	0.28	0.28	0.29	0.23	0.30	0.28
cinnabar[2]	0.22	0.86	0.27	0.24	0.29	0.22	0.34	0.26
ultramarine blue[1]	0.36	0.36	0.69	0.36	0.37	0.34	0.36	0.35
ultramarine blue[2]	0.36	0.36	0.69	0.35	0.37	0.35	0.34	0.34
lead white[1]	0.38	0.39	0.39	0.81	0.39	0.43	0.43	0.44
lead white[2]	0.40	0.39	0.39	0.84	0.39	0.43	0.43	0.44
caput mortum[1]	0.40	0.39	0.38	0.28	0.48	0.45	0.42	0.43
caput mortum[2]	0.39	0.38	0.38	0.25	0.57	0.45	0.40	0.41
caput mortum violet[1]	0.36	0.39	0.38	0.27	0.45	0.45	0.43	0.44
caput mortum violet[2]	0.40	0.39	0.38	0.31	0.44	0.45	0.42	0.44
yellow ochre[1]	0.40	0.39	0.38	0.32	0.41	0.44	0.46	0.45
yellow ochre[2]	0.39	0.39	0.38	0.25	0.40	0.42	0.49	0.44
red ochre[1]	0.39	0.39	0.38	0.27	0.43	0.44	0.45	0.44
red ochre[2]	0.40	0.39	0.39	0.22	0.41	0.44	0.44	0.45

Table 1. Global classification results obtained by means of indifferent aggregation. Super-index 1 indicates raw spectra and super-index 2 indicates spectra without background.

Raman identification of new samples - Majority vote

samples	support for classes
minium[1]	minium
minium[2]	minium
cinnabar[1]	cinnabar
cinnabar[2]	cinnabar
ultramarine blue[1]	ultramarine blue
ultramarine blue[2]	ultramarine blue
lead white[1]	lead white
lead white[2]	lead white
caput mortum[1]	caput mortum – caput mortum violet
caput mortum[2]	caput mortum
caput mortum violet[1]	caput mortum violet
caput mortum violet[2]	caput mortum violet – caput mortum
yellow ochre[1]	yellow ochre – caput mortum
yellow ochre[2]	yellow ochre – caput mortum
red ochre[1]	red ochre
red ochre[2]	red ochre – yellow ochre

Table 2. Classification labels output obtained by the majority vote rule applied to all aggregation operators. Super-index 1 indicates raw spectra and number 2 spectra without background signal components.

In Table 2, the full prediction for all samples is presented by means of the majority vote applied to the results obtained with the four fuzzy aggregation operators. This table confirms the preliminary results given in Table 1. Prediction results were good in those pigments which present a proper and characteristic Raman spectrum: in other words, problems arise when classification needs to be performed on slight details present in the spectra. This is the case of the ochre pigments, which have similar Raman spectra because their main component is iron (III) oxide.

Table 3 summarizes how a class label output can be obtained for each sample by showing the analysis of the decision profile for sample number 1 (ultramarine blue pigment). In this table, the scaled outputs obtained from the PLS-DA performed in each selected block were organized in a 5 by 8 matrix, which was known as the decision profile for the sample. The overall support for each class was calculated using the majority vote rule on the five aggregation connective operators. For this sample, the label output obtained for all the operators and also for each block was ultramarine blue. The results were the same for the samples of minium, cinnabar and lead white pigments, in which identification was very good and final decisions were obtained without conflict between operators and blocks.

Raman dual-domain classification of ultramarine blue sample 1

	support for pigment classes								
blocks	**minium**	**cinnabar**	**ultramarine blue**	**lead white**	**caput mortum**	**caput mortum violet**	**yellow ochre**	**red ochre**	**label output**
D3	0.36	0.42	0.79	0.43	0.45	0.43	0.42	0.43	ultramarine blue
D4	0.32	0.35	0.60	0.35	0.36	0.30	0.30	0.30	ultramarine blue
D5	0.45	0.41	0.67	0.39	0.36	0.41	0.43	0.43	ultramarine blue
D6	0.38	0.28	0.59	0.23	0.29	0.26	0.31	0.26	ultramarine blue
D7	0.31	0.33	0.80	0.41	0.37	0.31	0.33	0.32	ultramarine blue
Minimum	0.31	0.28	0.59	0.23	0.29	0.26	0.30	0.26	ultramarine blue
Maximum	0.45	0.42	0.80	0.43	0.45	0.43	0.43	0.43	ultramarine blue
Average	0.36	0.36	0.69	0.36	0.37	0.34	0.36	0.35	ultramarine blue
Product	0.0061	0.0056	0.1538	0.0055	0.0064	0.0042	0.0055	0.0045	ultramarine blue
Majority	—	—	—	—	—	—	—	—	ultramarine blue

Table 3. Raman decision profile for ultramarine blue sample 1 (sample without pre-treatment).

As has been stated for the ochre pigments, new samples were not successfully classified and misclassification was high when this methodology and Raman data were used. Table 4 shows the decision profile for sample 1 of yellow ochre in which it can be seen that it is misclassified as caput mortum by two operators. Even when the rule of majority vote gives a label output of yellow ochre for this sample, the conflict between ochre samples is high and the ability of the system to cope with this discrimination problem is poor.

Raman dual-domain classification of yellow ochre sample 1

	support for pigment classes								
blocks	minium	cinnabar	ultramarine blue	lead white	caput mortum	caput mortum violet	yellow ochre	red ochre	label output
D3	0.47	0.43	0.43	0.31	0.49	0.48	0.48	0.48	caput mortum
D4	0.38	0.38	0.38	0.35	0.37	0.45	0.46	0.46	yellow ochre - red ochre
D5	0.40	0.45	0.44	0.27	0.46	0.48	0.49	0.48	yellow ochre
D6	0.34	0.32	0.31	0.32	0.37	0.36	0.37	0.36	yellow ochre - caput mortum
D7	0.40	0.39	0.36	0.36	0.37	0.41	0.48	0.45	yellow ochre
Minimum	0.34	0.32	0.31	0.27	0.37	0.36	0.37	0.36	yellow ochre - caput mortum
Maximum	0.47	0.45	0.44	0.36	0.49	0.48	0.49	0.48	yellow ochre - caput mortum
Average	0.40	0.39	0.38	0.32	0.41	0.44	0.46	0.45	yellow ochre
Product	0.0099	0.0091	0.0080	0.0034	0.0114	0.0153	0.0192	0.0172	yellow ochre
Majority	–	–	–	–	–	–	–	–	yellow ochre - caput mortum

Table 4. Raman decision profile for yellow ochre sample 1 (sample without pre-treatment).

Raman-XRF dual-domain classification

The identification of ochre samples was improved by adding information from dual-domain XRF analysis following the methodology proposed in Figure 3. Hence, Raman and XRF data were fused by means of aggregation operators in the same way that Raman data was processed in the section above. Table 5 presents the prediction results obtained for ochre samples using indifferent aggregation. As can be seen, the prediction was improved as the prediction values for the corresponding class are high and closer to 1 than the other classes and also it can be concluded that considering Raman and XRF spectral data, samples from the four ochre classes were well identified. Again, the prediction result is not influenced by the presence of background components in the input signals.

Raman - XRF: identification of new samples
Indiferent aggregation

	Support for classes			
samples	caput mortum	caput mortum violet	yellow ochre	red ochre
caput mortum[1]	0.60	0.37	0.26	0.28
caput mortum[2]	0.78	0.24	0.25	0.33
caput mortum violet[1]	0.29	0.70	0.30	0.17
caput mortum violet[2]	0.27	0.70	0.23	0.31
yellow ochre[1]	0.25	0.31	0.68	0.29
yellow ochre[2]	0.24	0.29	0.65	0.30
red ochre[1]	0.24	0.32	0.33	0.63
red ochre[2]	0.27	0.23	0.24	0.80

Table 5. Classification results obtained by means of indifferent aggregation on Raman-XRF fused data.

Table 6 shows the full prediction results obtained by the majority vote rule applied to the four aggregations. The results are similar to those previously discussed and obtained by indifferent aggregation. The discrimination of ochre samples was improved and this methodology demonstrates its ability to incorporate information that is useful for the classification process.

Raman - XRF: identification of new samples
Majority vote

samples	Support for classes
caput mortum[1]	caput mortum
caput mortum[2]	caput mortum
caput mortum violet[1]	caput mortum violet
caput mortum violet[2]	caput mortum violet
yellow ochre[1]	yellow ochre
yellow ochre[2]	yellow ochre
red ochre[1]	red ochre
red ochre[2]	red ochre

Table 6. Classification labels output obtained by the majority vote rule applied to all aggregation operators.

The new decision profile was now constructed with the predicted values obtained from Raman and XRF blocks and processed in the same way as for Raman dual-domain classification. The result was a new decision profile reorganized in an 8 by 4 matrix for each sample. This is shown in Table 7 for sample 1 of yellow ochre. All the aggregation operators unanimously gave the correct level output for this sample, and from the individual level outputs we can see that XRF classification annuls the conflict that arose when only Raman data were used.

Raman-XRF dual-domain classification of yellow ochre sample 1

		support for pigment classes				
Blocks		caput mortum	caput mortum violet	yellow ochre	red ochre	Label output
RAMAN	D3	0.18	0.36	0.45	0.29	yellow ochre
	D4	0.23	0.34	0.61	0.36	yellow ochre
	D5	0.18	0.56	0.41	0.36	caput mortum violet
	D6	0.15	0.45	0.43	0.45	red ochre – caput mortum violet
	D7	0.32	0.28	0.52	0.15	yellow ochre
XRF	D3	0.20	0.26	0.95	0.25	yellow ochre
	D4	0.07	0.00	0.83	0.15	yellow ochre
	D5	0.28	0.22	0.93	0.21	yellow ochre
	D6	0.57	0.00	0.76	0.31	yellow ochre
	D7	0.33	0.64	0.92	0.41	yellow ochre
Minimum		0.07	0.00	0.41	0.15	yellow ochre
Maximum		0.57	0.64	0.95	0.45	yellow ochre
Average		0.25	0.31	0.68	0.29	yellow ochre
Product		0.0000	0.0000	0.0128	0.0000	yellow ochre
Majority		–	–	–	–	yellow ochre

Table 7. Raman-XRF decision profile for yellow ochre sample 1 (without pre-treatment).

Conclusions

Dual-domain classification discriminated very well between pigments studied by micro-Raman spectroscopy and micro-XRF spectrometry. Its main advantage is that there is no need for a pre-processing stage and it can directly use raw spectroscopic data as input in the classification system. This was well demonstrated in this study after samples had been predicted with and without background signal components in their respective spectra. The influence of noise, which can affect PLS-DA modelling, is also avoided. This is a great advantage when large amounts of data are to be processed automatically (for example in a 2D mapping of a work of art). In fact the proposed methodology is flexible and can be modified so that it is easier to operate. In this respect, the classification stage need not always use the same classification method: for example, Mahalanobis distance can be used instead of PLS-DA.

Fuzzy aggregation connectives are definitively the best way of performing high level fusion of the output classification from dual-domain data. The decision profiles make it possible to confirm that the ability of each operator to discriminate decreases in the following order: product, minimum, average and maximum. The majority vote rule can be used to obtain common criteria for processing the information provided by the operators.

High level fusion of dual-domain Raman and XRF data was successfully performed and is very well suited to combining outputs from different sources. The classification of four ochre pigments by means of micro-Raman spectroscopy was improved by applying this methodology to perform high level fusion of the decision levels obtained by means of micro-Raman spectroscopy and micro-XRF spectrometry.

Acknowledgement

This work was supported by the European Community Project, Competitive and Sustainable growth program (G6RD-CT2001-00602), PRAXIS "A portable Raman X-ray instrument". The authors gratefully acknowledge Koen Janssens at University of Antwerp and Konstantinos S. Andrikopoulos of Ormylia Arts Diagnostic Centre for providing reference samples and helpful comments.

References

[1] K. Janssens, Z. Jia, M. V. Gysel and P. V. Espen, PRAXIS: A Combined micro-Raman – micro-XRF Instrument, Euroanalysis XIII, Salamanca, Spain, 6-10 September (2004).

[2] K. Janssens, J. Sekula, M. Becucci, E. Castellucci, B. Roussel, J. Ostwald, J. Schmalz, A. Bjeoumikhov, N. Langhoff, P. Ramos, I. Ruisánchez and K. Andrikopoulos, Design Of A Combined Micro-Xrf/Micro-Raman Spectrometer, 2nd international conference on the application of Raman spectroscopy in art and archaeology, Ghent, Belgium (2003).

[3] K. Janssens, W. D. Nolf, O. Schalm, B. Vekemans, E. Castellucci, B. Roussel, S. Charonov, J. Schmalz, J. Tilgner, M. Haschke, N. Langhoff, P. Ramos, I. Ruisánchez and K. Andrikopoulos, Praxis: A Combined µ-Xrf/µ-Raman Spectrometer For Use In The Cultural-Heritage Area, 2005 Denver X-ray conference, Colorado Springs, Colorado, USA (2005).

[4] J. Esteban, A. Starr, R. Willetts, P. Hannah and P. Bryanston-Cross, Neural Computing & Applications 14, (2005), 273 - 281.

[5] V. Steinmetz, F. Sevila and V. Bellon-Maurel, Journal of Agricultural Engineering Research 74, (1999), 21-31.

[6] P. Boilot, E. L. Hines, M. A. Gongora and R. S. Folland, Sensors and Actuators B: Chemical 88, (2003), 80-88.

[7] S. Roussel, W. Bellon-Maurel, J. M. Roger and P. Grenier, Journal of Food Engineering 60, (2003), 407-419.

[8] I. Bloch, Systems, Man and Cybernetics, Part A, IEEE Transactions on 26, (1996), 52-67.

[9] H. W. Tan and S. D. Brown, Journal of Chemometrics 17, (2003), 111-122.

[10] P. M. Ramos and I. Ruisanchez, Analytica Chimica Acta 558, (2006), 274-282.

[11] Y. Liu and S. D. Brown, Analytical and Bioanalytical Chemistry 380, (2004), 445-452.

[12] H. Tan and S. D. Brown, Analytica Chimica Acta 490, (2003), 291-301.

[13] P. Vandenabeele, A. von Bohlen, L. Moens, R. Klockenkamper, F. Joukes and G. Dewispelaere, Analytical Letters 33, (2000), 3315-3332.

[14] P. Moioli and C. Seccaroni, X Ray Spectrometry 29, (2000), 48-52.

[15] P. Vandenabeele, T. L. Weis, E. R. Grant and L. J. Moens, Analytical and Bioanalytical Chemistry 379, (2004), 137-142.

[16] B. Walczak, Wavelets in Chemistry; Elsevier, (2000).

[17] S. G. Mallat, Pattern Analysis and Machine Intelligence, IEEE Transactions on 11, (1989), 674-693.

[18] H. W. Tan and S. D. Brown, Journal of Chemometrics 16, (2002), 228-240.

[19] P. Geladi and B. R. Kowalski, Analytica Chimica Acta 185, (1986), 1-17.

[20] M. Barker and W. Rayens, Journal of Chemometrics 17, (2003), 166-173.

[21] S. Roussel, V. Bellon-Maurel, J. M. Roger and P. Grenier, Chemometrics and Intelligent Laboratory Systems 65, (2003), 209-219.

[22] Steinmetz V., Crochon M., Bellon Maurel V., Garcia Ferhnandez J. L., Barreiro Elorza P. and Verstreken L., Journal of Agricultural Engineering Research 64, (1996), 15-27.

[23] L. A. Zadeh, Information and Control 12, (1968), 94-102.

[24] D. Dubois and H. Prade, Information Sciences 36, (1985), 85-121.

[25] Z. S. Xu and Q. L. Da, International Journal of Intelligent Systems 18, (2003), 953-969.

[26] L. Lam and S. Y. Suen, Systems, Man and Cybernetics, Part A, IEEE Transactions on 27, (1997), 553-568.

[27] P. M. Ramos and I. Ruisánchez, Journal of Raman Spectroscopy 36, (2005), 848-856.

7

Chapter 7: A methodology for data-fusion design

This chapter summarizes the different aspects that should be considered whenever a fusion of data from different spectroscopic instruments is required.

A METHODOLOGY FOR DATA-FUSION DESIGN

7.1. INTRODUCTION

As it has been shown, data-fusion exploits the synergy given by the information originated from various sources. The operation of data-fusion by itself is not new in any domain of application. For example, meteorologists predict the weather using information extracted from different analyses performed on the atmosphere. Data-fusion allows formalizing the combination of a set of measurements, as well as monitoring the quality of information in the course of the fusion process. The emerging of new instruments and advanced processing techniques make real-time fusion of data increasingly possible [1, 2].

Data fusion first appeared in the literature in the 1960s, as mathematical models for data manipulation. It was implemented in the United States (US) in the 1970s in the fields of robotics and defence. In 1986 the US Department of Defence established the Data Fusion Sub-Panel of the Joint Directors of Laboratories (JDL) to address some of the main issues in data fusion and chart the new field in an effort to unify both terminology and procedures.

The use of different types of spectroscopic techniques may increase the accuracy with which a property can be observed and characterized. In this thesis, this is exemplified with the characterization of pigments from works of art, analyzed by micro-Raman and micro-XRF spectroscopy.

7.2. STATE OF THE ART: APPLICATIONS

Applications of data fusion are widespread and include maintenance engineering [3], remote sensing [4], robotics [5], automated target recognition and other military applications [6-8], traffic control [9], aerospace systems [8, 10], medical applications [11], pattern recognition [12], and quality assessment of commodities [12-17].

Scientific research works conducted with the aim of obtaining the fusion of spectroscopic data in chemical analysis are limited. Roussel et al (2003), [18, 19] present two works of data fusion for the classification of grape varieties in the food industry. They combine aroma sensors with Fourier transform infrared (FTIR) and ultraviolet (UV) spectrometry by means of low-level and high-level fusion methodologies. Mazerolles et al (2002) propose a chemometrics method for coupling infrared (IR) and fluorescence data for the study of the modifications in proteins of foods [20].

In the field of cultural heritage, as in many fields in which spectroscopic techniques are applied, complementary analyses have been done in order to maximize the data retrieved from a sample, in this case a work of art. The fusion is performed at the level of the identity declaration extracted from each single-technique and it is inferred by expert analysts from the conclusions obtained from each single analysis [21-27]. The first data-fusion approaches applied in this field and designed for a new Raman-XRF instrument are presented in this thesis [28-30].

7.3. ASPECTS THAT SHOULD BE CONSIDERED BEFORE THE DATA FUSION PROCESS

The actual combination of sensors (techniques) depends upon the requirements of the system. However, a number of things need to be considered when defining the type of fusion algorithm and the level at which the fusion will occur.

Some of these things are: the type and accuracy of the collected data, the nature and the resolution of the techniques and the available methodologies to process the fused data.

7.3.1. Complementary or redundancy in both type of spectra

Before performing data-fusion, it is important to check whether or not the spectroscopic analyses provide the same kind of information. When the analyses

provide different information from the sample, they are complementary. In the opposite case, the analyses may be redundant. Generally speaking, data fusion improves the classification analysis in the former case.

Raman and XRF are a good example of complementary analyses; however, the level of complementarity or redundancy can vary depending on the analytical problem under study. For instance, in the classification study of ochre pigments, XRF analysis information from major elements can be redundant while XRF information obtained from minor elements is complementary to the Raman analysis.

Multivariate techniques like PCA and PLS-DA try to separate that information which makes the objects unique from the information the objects have in common. Therefore, redundancy is not a serious problem in this context but it is important in order to minimize computation and not to process irrelevant data.

Redundancy between techniques can be evaluated by statistical indices such as the correlation coefficient or the similarity index. Descriptive approaches, like the principal components analysis (PCA), also allow the detection of the linear relationship existing between techniques. This descriptive process enables the elimination of the redundant techniques and consequently of the useless data, or on the contrary, the improvement of the robustness of the system with respect to the analyses failures when some techniques are redundant.

7.3.2. Signal processing

An initial process allocates data to appropriate process in the data fusion system. This processing also makes the data fusion system focus on the deterministic information present in data. In spectroscopic data, extensive signal processing is necessary in order to allocate spectra properly in a data-fusion system. It often includes smoothing and de-noising procedures, normalisation, trend analysis and detection and elimination of outliers.

In Raman and XRF data-fusion this stage is highly required due to the presence of noise and background signal components in the raw spectra obtained from both techniques. Data alignment is also necessary to achieve a common spatial reference.

Signal de-noising

The reduction of noise in spectroscopic data was discussed in chapter 1. The level of noise in the data can be reduced by smoothing and de-noising procedures. Optimal smoothing procedures can be: Fourier analysis, Savitzky-Golay, least-squares and digital smoothing polynomial filters. De-noising procedures based

on the orthogonal wavelet transform were developed in chapter 3 of this thesis. Thresholding and/or attenuation can be applied to wavelet coefficients in order to remove the noise from the data.

Background removal

Another processing objective is to remove of unwanted features from the data. As in the case of de-noising, background removal was investigated. The most common methodologies used to eliminate background signal components were presented in chapter 1 of this thesis. An innovative methodology based on wavelet transform was developed in chapter 3, to achieve de-noising and background removal in Raman spectra simultaneously.

Data alignment

When data to be fused come from different techniques, they may be in different scales, so before applying the fusion process they have to be formatted into a common form and aligned in the time domain. Normalisation is usually applied to achieve this as it identifies relationships between measurements and features. It is also an attempt to correct the systematic bias in data and it permits to balance data before it enters the data-fusion system.

7.4. DATA FUSION PROCESS

The application of a data fusion process implies several steps. A data fusion level must be selected depending on the problem to be addressed. Once the fusion has been done, it must be evaluated. And finally, as in any other process, it must be properly validated.

7.4.1. Selection of the data-fusion level

The methologies mostly used for data-fusion, classified in three different levels: a low-level, a mid-level, and a high-level are presented in chapter 1. It is important to accentuate that all three levels use feature extraction, transforming the raw signal provided by instrumental techniques into a reduced vector of selected variables describing the original information, and an identity declaration that assigns a class to the given data, based on the feature extraction process.

The three levels include some practical limitations. Low level fusion implies high memory capacity and high-speed data processing. Mid and high-level fusion methodologies use less information with respect to the raw signal provided by each single instrumental technique; eventually, this transformation may include errors that will be transmitted to the fusion process. However, mid and high-level fusion techniques allow the fusion of different types of spectroscopic techniques and do not require too much computation. The choice of the fusion level is of course related to the choice of the techniques used to process the fused data.

The application of the fusion approach shows success with techniques such as expert systems, probabilistic techniques and multivariate analysis. Hence, there is no simple rule for selecting the proper fusion technique.

Providing advice for the optimal fusion technique is a difficult task, but there are some criteria considered relevant for spectroscopy data:

1) The nature of the instrumental techniques to be combined. For instance, combining dispersive Raman and XRF does not impose the same constraints as those of combining a 2D Raman imaging with a FTIR spectra.
2) The level of accuracy of the extracted features. For example: in-situ acquisition may imply noisy data.
3) The extracted features space dimension. High dimensional data may eliminate some options and may imply feature selection processing.

Selecting algorithms for data-fusion is a difficult task due to the fact that data analysis aims to combine data in a complex environment and in real time. Therefore, it involves specialists from the data processing area.

7.4.2. Evaluation of the data-fusion system

Model evaluation is relevant for the comparison of a single technique system to a multi-technique data-fusion system. The performance can be defined with index values which show the ability of the fusion model to provide a better prediction than those obtained by means of a single instrumental technique. Based on the results obtained, two decisions concerning the data-fusion approach can be taken: acceptance or rejection. In the latter case, it is important to review the reasons for this action, to identify the problems and eventually to correct actions made at various steps of the methodology in order to improve the data-fusion approach.

7.4.3. Validation

The information extracted from fused data analyses and data processed by conventional methodologies must be confirmed at the validation stage. In the case of the analysis of pigments in works of art, conventional methodologies involve the spectroscopic analyses, along with their interpretation, performed by conservation scientists.

Performance assessment of the data-fusion system can be obtained by evaluating the uncertainty associated to the result obtained. It is possible to estimate this by studying the prediction probabilities of the models, the accuracy in the results obtained and the performance parameters of the system.

A benchmark procedure can be implemented to improve the results obtained from the data-fusion systems, and to determine the optimal configuration appropriately.

7. 5. REFERENCES

[1] K. Janssens, W. D. Nolf, O. Schalm, B. Vekemans, E. Castellucci, B. Roussel, S. Charonov, J. Schmalz, J. Tilgner, M. Haschke, N. Langhoff, P. Ramos, I. Ruisánchez and K. Andrikopoulos, Praxis: A Combined µ-Xrf/µ-Raman Spectrometer For Use In The Cultural-Heritage Area, Denver X-ray conference, Colorado Springs, Colorado, USA , 1-5 August (2005).

[2] K. Janssens, Z. Jia, M. V. Gysel and P. V. Espen, PRAXIS: A Combined micro-Raman –micro-XRF Instrument, Euroanalysis XIII, Salamanca, Spain, 6-10 September (2004).

[3] A. N. Steinberg, Ieee Aerospace and Electronic Systems Magazine 16, (2001), 7-14.

[4] D. Moshou, C. Bravo, R. Oberti, J. West, L. Bodria, A. McCartney and H. Ramon, Real-Time Imaging 11, (2005), 75-83.

[5] K. C. Tan, Y. J. Chen, L. F. Wang and D. K. Liu, Applied Artificial Intelligence 19, (2005), 433-456.

[6] J. L. Paul, IEEE Aerospace and Electronic Systems Magazine 21, (2006), 13-20.

[7] I. Balajti, IEEE Aerospace and Electronic Systems Magazine 19, (2004), 15-29.

[8] C. J. Harris, A. Bailey and T. J. Dodd, Aeronautical Journal 102, (1998), 229-244.

[9] F. Logi and S. G. Ritchie, Transportation Research Part C-Emerging Technologies 9, (2001), 433-459.

[10] J. B. Zhu, Chinese Science Bulletin 46, (2001), 627-630.

[11] H. Kook, L. Gupta, D. Molfese and K. C. Fadem, Pattern Recognition 38, (2005), 2174-2184.

[12] X. H. Fan, Y. Y. Cheng, Z. L. Ye, R. C. Lin and Z. Z. Qian, Analytica Chimica Acta 555, (2006), 217-224.

[13] R. Nuray and F. Can, Information Processing & Management 42, (2006), 595-614.

[14] P. Boilot, E. L. Hines, M. A. Gongora and R. S. Folland, Sensors and Actuators B: Chemical 88, (2003), 80-88.

[15] C. Di Natale, M. Zude-Sasse, A. Macagnano, R. Paolesse, B. Herold and A. D'Amico, Analytica Chimica Acta 459, (2002), 107-117.

[16] C. Di Natale, R. Paolesse, A. Macagnano, A. Mantini, A. D'Amico, A. Legin, L.

Lvova, A. Rudnitskaya and Y. Vlasov, Sensors and Actuators B-Chemical 64, (2000), 15-21.

[17] V. Steinmetz, F. Sevila and V. Bellon-Maurel, Journal of Agricultural Engineering Research 74, (1999), 21-31.

[18] S. Roussel, V. Bellon-Maurel, J. M. Roger and P. Grenier, Chemometrics and Intelligent Laboratory Systems 65, (2003), 209-219.

[19] S. Roussel, W. Bellon-Maurel, J. M. Roger and P. Grenier, Journal of Food Engineering 60, (2003), 407-419.

[20] G. Mazerolles, M. F. Devaux, E. Dufour, E. M. Qannari and P. Courcoux, Chemometrics and Intelligent Laboratory Systems 63, (2002), 57-68.

[21] M. Castillejo, M. Martin, D. Silva, T. Stratoudaki, D. Anglos, L. Burgio and R. J. H. Clark, Journal of Cultural Heritage 1, (2000), S297-S302.

[22] L. Burgio, R. J. H. Clark, T. Stratoudaki, M. Doulgeridis and D. Anglos, Applied Spectroscopy 54, (2000), 463-469.

[23] G. Paternoster, R. Rinzivillo, F. Nunziata, E. M. Castellucci, C. Lofrumento, A. Zoppi, A. C. Felici, G. Fronterotta, C. Nicolais and M. Piacentini, Journal of Cultural Heritage 6, (2005), 21-28.

[24] N. Civici, O. Demko and R. J. H. Clark, Journal of Cultural Heritage 6, (2005), 157-164.

[25] L. Burgio, R. J. H. Clark and K. Theodoraki, Spectrochimica Acta Part a-Molecular and Biomolecular Spectroscopy 59, (2003), 2371-2389.

[26] G. VanHooydonk, M. DeReu, L. Moens, J. VanAelst and L. Milis, European Journal of Inorganic Chemistry, (1998), 639-644.

[27] P. Vandenabeele, A. von Bohlen, L. Moens, R. Klockenkamper, F. Joukes and G. Dewispelaere, Analytical Letters 33, (2000), 3315-3332.

[28] P. M. Ramos and I. Ruisanchez, Analytica Chimica Acta 558, (2006), 274-282.

[29] P. M. Ramos and I. Ruisanchez, Chemometrics and Intelligent Laboratories, submitted.

[30] P. M. Ramos, I. Ruisanchez, K. S. Andrikopoulos and K. Janssens, Applied Spectroscopy, submitted.

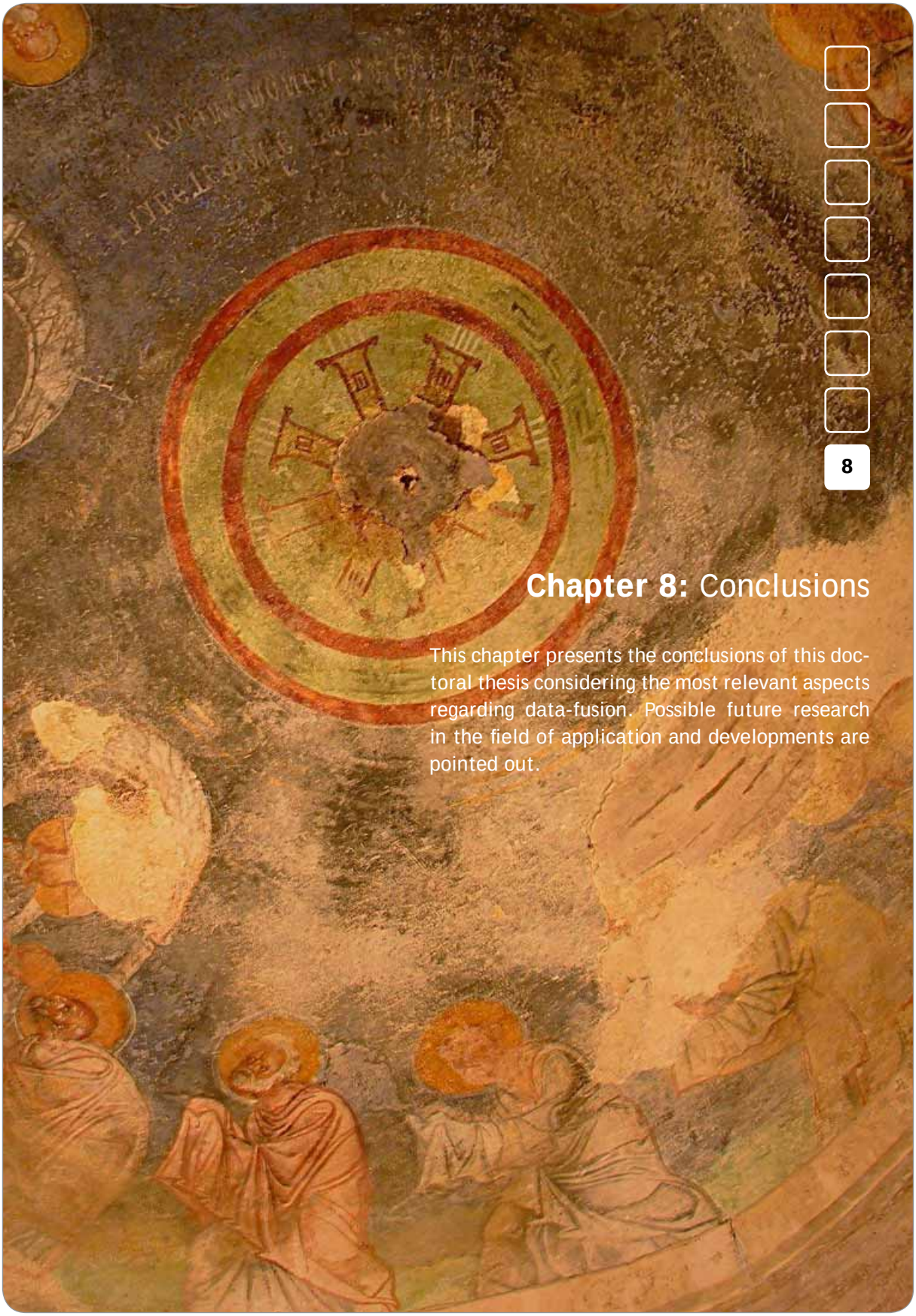

8

Chapter 8: Conclusions

This chapter presents the conclusions of this doctoral thesis considering the most relevant aspects regarding data-fusion. Possible future research in the field of application and developments are pointed out.

CONCLUSIONS

8.1. SUMMARY

Micro-Raman spectroscopy is a highly specific method of molecular analysis and is well established as a key technique for the identification of pigments in works of art. This is due to its spatial and spectral resolution, high sensitivity and specificity, and especially because it can be applied in situ.

Today, commercial Raman instruments are becoming increasingly accessible, along with easy software packages which make the instrumental setup easy to implement. Nowadays, an increasing number of well known museums own Raman instruments and have interdisciplinary research groups which include conservationist scientists specialized in Raman spectroscopy.

The panorama is similar with micro X-ray fluorescence spectroscopy; this technique is today a powerful and widely used tool, successfully applied to many analyses of objects in art and archaeology. XRF is also a non-destructive technique and in-situ XRF instrumentation is becoming available.

As in many areas of research, there is no unique and fail-safe method to tackle their respective analytical problems. In that sense, Raman and XRF have proved to be a suitable combination to characterize objects in the field of cultural heritage. Raman spectroscopy is more specific regarding the chemical form of the compounds constituting the pigments and XRF yields qualitative and quantitative information on major, minor and trace elements present in the pigments.

The design and construction of the first innovative hybrid Raman-XRF instrument, which incorporate chemometrics algorithms for the analysis of Raman-XRF patterns, is the start up of a new generation of instruments developed to improve metrological infrastructure in different fields.

This doctoral thesis shapes the research performed to achieve this goal through the design of a highly-specific Raman-XRF fingerprint analysis system for the characterization of pigments in the field of cultural heritage.

8.2. CONCLUSIONS

1. Wavelet transform (WT) is studied as a tool to improve classification results in Raman and XRF spectroscopy. The study is focused on the application of WT to the following methodologies: de-noising, background correction and multiresolution analysis.

   1.1. De-noising applied to spectra is important in any kind of multivariate process. The potential of wavelet de-noising of Raman and XRF spectra is investigated and very good results are obtained.

   Block thresholding methodology is successfully implemented to remove heteroscedastic noise present in Raman data. It is important to remove heteroscedastic noise when the location of smaller peaks is relevant. It is shown that this situation is usually present in the characterization of pigments in works of art using Raman spectroscopy.

   1.2. Simultaneous wavelet de-noising and baseline correction method is achieved. This methodology allows a better multivariate processing and, therefore, improves the results of classification analysis.

   1.3. The multiscale approach provides a way to explore important regions in both the wavenumber and frequency domains.

2. Fuzzy logic represents a significant change in both the methodology and the outcome of pigments classification analysis. The key advantage of fuzzy methods is how they reflect the human mind in its remarkable ability to store and process information that is consistently imprecise, uncertain, and resistant to classification.

   2.1. Self-learning fuzzy systems are suitable to perform automatic classification of pigments studied by Raman spectroscopy.

   2.2. These systems can be upgraded to a data-fusion system.

   2.3. Considering the rapid increase of applications and developments of new fuzzy systems, it is expected that fuzzy logic will be a highly valuable contribution to the design of any advanced instrumentation system.

3. The most widely used architectures for the implementation of data-fusion in chemical analysis are reviewed (chapter 5). The methodology behind successful implementation of the data-fusion architectures is investigated and the main conclusions are:

   3.1. The architecture chosen (level of the data fusion) is critical in order to achieve successful data fusion.

3.2. Tailoring the methodology is also important to obtain an optimal solution. To that end, data must be balanced and correctly aligned.

3.3. High level fusion can be applied to all types of analytical measurements capable of providing identity declarations.

4. Data-fusion in combination with multiresolution analysis (dual domain) is presented in chapter 6. Dual-domain given by wavelet transform is introduced to improve data-fusion methodologies and the main conclusions are:

4.1. Using a multiscale approach, it is possible to locate spatial features which exist at different spectral-resolution levels.

4.2. Dual-domain low-level fusion is not a suitable combination due to the need of too much computation and the unnecessary fusion of irrelevant data.

4.3. Fusion performed in the dual-domain enable the modelling of signals in both domains simultaneously. This provides a methodology for isolating the non-interesting variation in spectra, making the system and analysis method more robust against variations in instrument and environmental conditions.

5. Implementation of data-fusion systems requires an understanding of basic terminology, data-fusion processing models, and architectures. The purpose of this thesis is to assess the capability of different strategies of data-fusion systems for Raman and XRF spectral data. The developed methodologies can be extended to the application to other types of spectroscopic data.

8.3. FUTURE RESEARCH

The results presented are just the first stage of improvements and achievements which can be obtained by means of data-fusion systems in spectroscopic analysis of works of art. Based on the successful results obtained and discussed in this doctoral thesis, and considering the improvements achieved in instrumentation, there are several new issues that have not been dealt with here and which could be the subject of future research:

1. The possibility of performing two-dimensional mapping and imaging analysis is feasible nowadays. These instrumental improvements permit to obtain more information about the distribution of the pigments or particular elements in the

masterpiece. New challenges for spectroscopic data-fusion systems will appear in order to process different types of input data as images, spectra and even processed data. In that sense high-level fusion has great potential and is worth exploring further.

2. Another field which has similar requirements to the study of materials in art of works, is forensic science. Although the aim of both disciplines is quite different, their basic problems and operational limitations show a striking parallelism:

   - Authentication of a variety of materials (i.e. inks and paper in documents)
   - Matching of *unknown* samples to a series of library materials.
   - Non-destructive investigations are preferred.

Consequently, the contributions that data-fusion systems can make to the forensic field merit further exploration.

Appendix

This section presents the list of papers and meeting contributions performed during the elaboration of this doctoral thesis.

1. Fuzzy Logic for Identifying Pigments Studied by Raman Spectroscopy.

Pablo M Ramos[1], Joan Ferré[1], Itziar Ruisánchez[1] and Konstantinos S. Andrikopoulos[2].

Applied Spectrocopy 58, (2004), 848-854.

1. *Department of Analytical Chemistry and Organic Chemistry. Rovira i Virgili University. Campus Sescelades, C/. Marcel·lí Domingo, s/n 43007 Tarragona, Spain*

2. *"Ormylia" Art Diagnosis Center, Sacred Convent of the Annunciation IMSP Ormylia-Chalkidiki, EL-63071 Ormylia, Greece*

2. Noise and Background Removal in Raman Spectra of Ancient Pigments Using Wavelet Transform.

Pablo M Ramos and Itziar Ruisánchez.

Journal of Raman Spectroscopy 36, (2005), 848-856.

3. Data Fusion and Dual-domain Classification Analysis of Pigments Studied in Works of Art.

Pablo M Ramos and Itziar Ruisánchez.

Analytica Chimica Acta 558, (2006), 274-282.

4. Data Fusion in the Wavelet Domain by Means of Fuzzy Aggregation Connectives.

Pablo M Ramos and Itziar Ruisánchez.

Chemometrics and Intelligent Laboratories, submitted.

5. Micro Raman and X-ray Fluorescence Spectroscopy Data Fusion for the Classification of Ochre Pigments.

Pablo. M. Ramos[1], Itziar Ruisánchez[1], Konstantinos S. Andrikopoulos[2], and Koen Janssens[3]

Applied Spectroscopy, submitted.

1. *Department of Analytical Chemistry and Organic Chemistry. Rovira i Virgili University. Campus Sescelades, C/. Marcel·lí Domingo, s/n 43007 Tarragona, Spain*

2. *"Ormylia" Art Diagnosis Center, Sacred Convent of the Annunciation IMSP Ormylia-Chalkidiki, EL-63071 Ormylia, Greece*

3. *Micro and Trace Analysis Center, University of Antwerp, Belgium*

Automated Pigment Identification Algorithm For A Raman-XRF Instrument.

P. Ramos, S. Macho, A. Maroto, J. Ferré and I. Ruisánchez.

V Colloquium Chemiometricum Mediterraneum.
Ustica, Italy, June 25 – 27, (2003).

Poster communication.

Design of a Combined Micro-XRF / Micro-Raman Spectrometer.

K. Janssens, J. Sekula, M. Becucci, E. Castellucci, B. Roussel, J. Ostwald, J. Schmalz, A. Bjeoumikhov, N. Langhoff, **P. Ramos**, I. Ruisánchez and K. Andrikopoulos.

2nd International Conference on the Application of Raman Spectroscopy in Art and Archaeology.
Ghent, Belgium, September 3 – 6, (2003).

Poster communication.

Automated Pigment Identification Algorithm for a Raman-XRF Instrument.

P. Ramos, S. Macho, A. Maroto, J. Ferré and I. Ruisánchez.

2nd International Conference on the Application of Raman Spectroscopy in Art and Archaeology.
Ghent, Belgium, September 3 – 6, (2003).

Poster communication.

Multivariate Classification of Art Pigments Studied by Raman Spectroscopy and X-Ray Fluorescence Spectrometry.

P. Ramos, S. Macho and I. Ruisánchez.

Euroanalysis XIII, European Conference on Analytical Chemistry.
Salamanca, Spain, September 5 – 10, (2004).

Poster communication.
Euroanalysis Prize: Second Best Presentation Poster

PRAXIS: A Combined Micro-Raman – Micro-XRF Instrument.

K. Janssens, E. Castellucci, B. Roussel, J. Oswalt, J. Schmalz, J. Tilgner, A. Bjeoumikhov, N. Langhoff, **P.Ramos**, I. Ruisánchez, K. Andrikopoulos, E. Bulska, J. Zieba-Palus.

Eu-ARTECH Workshop on "Non destructive analysis of cultural heritage artefacts". Instituut Collectie Nederland, Amsterdam.
Netherlands, January 13, (2005).

Poster communication.

PRAXIS: A Combined μ-XRF / μ-Raman Spectrometer for use in the Cultural-Heritage Area.

K. Janssens, W. De Nolf, O. Schalm, B. Vekemans, E. Castellucci, B. Roussel, S. Charonov, J. Schmalz, J. Tilgner, M. Haschke, N. Langhoff, **P. Ramos**, I. Ruisánchez and K. Andrikopoulos.

2005 Denver X-Ray Conference.
Colorado Springs, Colorado, USA, August 1 – 5, (2005).

Poster communication.

Dual-Domain Raman-XRF Data Fusion for Classification Analysis of Art Pigments.

Pablo M Ramos and Itziar Ruisánchez.

3rd International Conference on the Application of Raman Spectroscopy in Art and Archaeology.
Paris, France, August 31 - September 3, (2005).

Poster communication.

Data Fusion for Classification Analysis of Art Pigments.

Pablo M Ramos and Itziar Ruisánchez.

1st Workshop of the Chemometric Catalan Net (xarxa catalana de quimiometria).
Barcelona, Spain, September 8, (2005).

Oral communication.

Graphic design and layout: Valeria Russo | **Print:** Medius Koloro | **Linguistic assistance:** Isabel Badaracco and Celia Nieto. Tarragona, May 2006

Chemometrics, Qualimetrics
and Nanosensors Group

Universitat
Rovira i Virgili

Department of Analytical Chemistry
and Organic Chemistry